NASA CR- 139033

FINAL REPORT

ATS-5 RANGING RECEIVER AND L-BAND EXPERIMENT

VOLUME II
DATA REDUCTION AND ANALYSIS

APPLICATIONS TECHNOLOGY SATELLITE PROGRAM
CONTRACT NAS 5-21598

DECEMBER 1971

PREPARED FOR

NATIONAL AERONAUTICS AND SPACE ADMINISTRATION
GODDARD SPACE FLIGHT CENTER
GREENBELT, MARYLAND

NASA CR- 139033

GODDARD SPACE FLIGHT CENTER

DOCUMENT RELEASE FORM

NAS 5-21598 Mr. G. Patterson, Code 951 (March 19, 1974)

REFER TO GHB 2200.1A, TECHNICAL INFORMATION AND GRAPHIC ARTS HANDBOOK, FOR DETAILED INSTRUCTIONS

Document Title: ATS-5 Ranging Receiver and L-Band Experiment - Volume II - Data Reduction and Analysis Final Report

Document Number	Document Date	Contractor Name/Contract No. (if contract report)
	Dec. 1971	Westinghouse Electric Corp - Balt., MD

Author(s): H.S. Fitshugh, L.V. Hartle, G. Vaughan, L. Riddle (all with Westinghouse)

Approved by: [signature]

ANNOUNCEMENT AND RELEASE OF THIS DOCUMENT ARE SUBJECT TO THE FOLLOWING RESTRICTIONS:

I. PREPRINTS & CONTRACT REPORTS

- [X] Announce in STAR (no limitations on availability)
- [ ] Release by Originating Office Only

Preprints will be subsequently published
- [ ] As a journal article
- [ ] As a formal NASA report
- [ ] Presented at a professional meeting

II. WORKING PAPERS (Operational Documents) & CONTRACT REPORTS

A. [ ] Announce in CSTAR (distribution limited as indicated)
   1. [ ] U. S. Government Agencies and Contractors Only
   2. [ ] U. S. Government Agencies Only
   3. [ ] NASA and NASA contractors Only

B. [ ] Release by Originating Office Only

III. PATENT COUNSEL REVIEW

A. GSFC Originated Documents

1. [ ] This document discloses potentially patentable subject matter (a new and useful process, product, mechancial and electrical arrangement of parts or composition of matter) and is to be reviewed by Patent Counsel.

   Patent Counsel Review: _____

2. [X] This document does not disclose potentially patentable subject matter.

B. Contract Reports (to the best of the T.O.'s knowledge)

1. [ ] This document should be reviewed by Patent Counsel.

   Patent Counsel Review: _____

2. [ ] The contractor has also published this material in _____

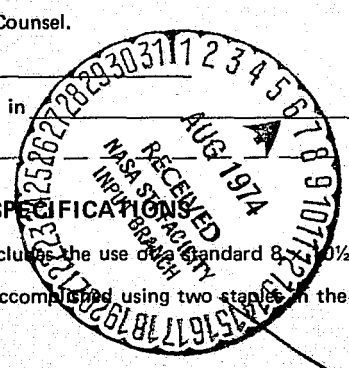

PRINTING SPECIFICATIONS

Normal X- and I-Document printing includes the use of a standard 8½ x 10½ cover, pages printed on both sides, with binding accomplished using two staples in the left margin.

Requester's Name			Job Order Number		
Code	Phone	Date of Request	Date Required	No. of Originals	No. of Copies

SPECIAL REQUIREMENTS (Subject to approval by Chief, Technical Information Division)

GSFC 25-13 (6/73)

GRAPHIC SERVICES BRANCH

1. Report No.	2. Government Accession No.	3. Recipient's Catalog No.
4. Title and Subtitle Final Report ATS-5 Ranging Receiver and L-Band Experiment, Volume II		5. Report Date 6. Performing Organization Code
7. Author(s)		8. Performing Organization Report No.
9. Performing Organization Name and Address Westinghouse Electric Corporation Defense and Electronic Systems Center Baltimore, Maryland 21203		10. Work Unit No. 11. Contract or Grant No. NAS5-21598
12. Sponsoring Agency Name and Address NASA/GSFC Greenbelt, Maryland		13. Type of Report and Period Covered Final 14. Sponsoring Agency Code

15. Supplementary Notes

16. Abstract

This volume contains the results of ranging and position location experiments which were performed at the NASA Application Technology Satellite ground station at Mojave California.

Four separate types of experiments are described and the results reported. The data handling and processing technique is also described. The four types of experiments performed are (1) Simultaneous C-band and L-band ranging to ATS-5, (2) Simultaneous C-band and VHF ranging, (3) Simultaneous 24-hour ranging and (4) Position location using ATS-1, ATS-3, and ATS-5.

Volume I of this report describes the ATS-5 Ranging Receiver which was used in performing the experiment, as well as some of the preliminary results.

17. Key Words (Selected by Author(s))	18. Distribution Statement
ATS-5 Ranging Receiver L-Band Ranging VHF Ranging Position Location	

19. Security Classif. (of this report)	20. Security Classif. (of this page)	21. No. of Pages	22. Price*
		127	

*For sale by the Clearinghouse for Federal Scientific and Technical Information, Springfield, Virginia 22151.

TABLE OF CONTENTS

TABLE OF CONTENTS (Continued)

TABLE OF CONTENTS (Continued)

LIST OF ILLUSTRATIONS

LIST OF ILLUSTRATIONS (Continued)

LIST OF ILLUSTRATIONS (Continued)

LIST OF TABLES

SECTION 1

INTRODUCTION

1.1 GENERAL

The National Aeronautics and Space Administration, Goddard Space Flight Center (NASA/GSFC) awarded the Westinghouse Electric Corporation, Baltimore, Md. a contract, early in 1971, to perform data reduction and analysis on L-band ranging and position location data. This volume (Volume II) presents the results of the data reduction and analysis of data obtained at the NASA Mojave, California, tracking station through June of 1971. Volume I of this publication covers the work performed on the L-band ranging and position location experiment equipment which was developed, designed, fabricated, and installed at the Mojave station. Volume I also includes some of the results of data collected during the initial phase of the experiment checkout at Mojave. The ranging equipment was installed at Mojave in January of 1971 preliminary ranging experiments were conducted over the next two months. These experiments included simultaneous C-band and L-band ranging to ATS-5, as well as L-band ranging to ATS-5 concurrent with C-band ranging to ATS-1. The two satellite rangings provided position location data.

Upon completion of the preliminary experiment checkout phase of the hardware under the previous contract, this data reduction and analysis contract was utilized to gather, reduce, and analyze the experimental data. All data collected, including that covered in Volume I, is included in Volume II.

Performed primarily on an individual experiment basis, the data reduction and analysis effort is presented in this document in like manner. There are four primary types of experiments performed: (1) Simultaneous C-band and L-band ranging to ATS-5, (2) Simultaneous C-band and VHF ranging to ATS-1 and ATS-3, (3) Simultaneous 24-hour ranging, and (4) Position location using ATS-5 and ATS-1 or ATS-3.

For the purpose of this report, the simultaneous C-band ranging data is used as the standard, in that it is the best range information available for the experiment. Thus, L-band and VHF measurements are compared to the C-band measurement to establish measurement accuracy.

The major objectives of the experiments are: (1) determine the ranging accuracy that could be achieved at L-band frequencies, (2) evaluate the propagation effects on L-band ranging signals, and (3) evaluate diurnal propagation effects on L-band ranging signals at different latitudes.

Data for this report was obtained at one latitude, that being 35^{o}N for the Mojave station. Only limited diurnal data has been obtained for the report.

ACKNOWLEDGMENTS

The authors wish to acknowledge those who have contributed to this program in various ways both at Westinghouse and the Goddard Space Flight Center.

Special thanks are extended to the Mojave ground station personnel and Mr. C. N. Smith, NASA/GSFC principal investigator, for his counsel and assistance throughout the experimental program and for his discerning review of this report.

SECTION 2

SUMMARY

The major objectives of the various experiments listed in Section 1 have been successfully carried out, except for the determination of L-band propagation effects at more than one latitude. The results of these experiments are briefly summarized in this section. Detailed descriptions and analyses are presented in Section 4 of this report.

L-band range measurements to ATS-5 from the Mojave station agreed quite well with simultaneous C-band measurements from the same station. When equipment biases and geometrical effects were taken into consideration, range measured by the L-band system differed from that measured by the C-band system on the order of ten meters for a transmitted L-band power level greater than eight watts. An extremely accurate and stable frequency source is required to reduce the range difference much further. Fluctuations in the L-band range data due to thermal noise and equipment jitter were comparable to those of the C-band data at the higher transmitted L-band power levels.

VHF range measurements to either ATS-1 or ATS-3 do not agree well with simultaneous C-band measurements. This is expected because the ionosphere has a large effect on VHF propagation. During local daylight, VHF range exceeded C-band range by as much as 1180 meters; while at night the difference dropped to around 100 meters, in accordance with the known diurnal variation in ionospheric electron density. For accurate VHF ranging and position location, therefore, it is necessary to correct the range data, which requires knowledge of the ionospheric electron density at the time range measurements are made.

Simultaneous L-and C-band range measurements to ATS-5 were performed over a 24-hour time interval to investigate diurnal propagation effects. Again, when equipment biases and geometrical effects were taken into consideration, the difference between L-band and C-band range was less than ten meters during the night-time low in electron density. However, during local daylight, when one would expect L-band range to exceed C-band range, the opposite was observed. No explanation for this

apparent anomaly has been advanced, to date. Nighttime measurements compared quite favorably, as expected. Several more such experiments should be performed to reach a definite conclusion.

The difference between measured L- or C-band range and calculated range extracted from satellite ephemeris exhibits a cyclic variation with a 24-hour period. This behavior seems to be characteristic of most results of the Goddard orbit determination and prediction program. It is believed to be due to the fact that not all orbit elements can be calculated with equal precision from range and range rate measurements alone. The difference between predicted and measured range depends on the elapsed time between the ephemeris epoch and the date on which range measurements are made, as well as the time of day measurements are made. When this elapsed time is less than about two weeks, the difference in range can be as much as one or two kilometers. This difference rapidly increases as the elapsed time increases beyond two weeks.

A capability for determining the location of a ground station by ranging from the station to two satellites has been demonstrated at C-band, L-band and VHF. Accuracy of position location is limited mainly by the existing orbit determination program. Distance between the actual station position and its calculated position is on the order of one kilometer when correctly updated versions of the present orbit program are used. The position location procedure is capable of accuracies on the order of tens of meters if more accurate satellite ephemeris can be obtained and when equipment biases and propagation effects are compensated. Accuracy of station location is only slightly sensitive to the random fluctuations that occur in the ranging data and to the geometrical arrangement of the station and two satellites.

The data gathered during three experiment periods were investigated to determine if L-band range measurement errors contained a periodic component at the spin rate of ATS-5, if range errors were being caused by propagation anomalies, and the statistical distributions of the errors. It was found that in each case errors at C-band were not correlated with errors at L-band, indicating that common propagation anomalies over a 3-minute period were not causing the range errors. There was no cyclic, unexplainable periodic component in either range error signal. This shows that the spinning of ATS-5 is not contributing a significant component to the range errors, at either ranging frequency. The statistical distributions of errors about the error biases are very nearly "normal" indicating that errors are probably being caused by sources such as thermal noise effects in the phase comparison sections of the ranging receivers.

The test intervals chosen for analysis are representative of three test conditions, one with a high signal to noise ratio at the spacecraft, one where the signal to noise ratio is low, and one for operation with independent ranging tone sources for the two separate ranging systems. The latter case is referred to as mode 1 in the body of this report. Aside from the increased standard deviation, reducing the signal to noise ratio at the spacecraft does not change the bias statistics or correlations of errors. However, Mode 1 operation does change the range bias without changing the error distributions or correlation functions. This shows that the change in range bias is probably caused by a deterministic source, such as the generation of false lanes or ambiguous zero set of the L-band ranging receiver.

SECTION 3

DATA PROCESSING

3.1 RECEIVED RANGING DATA

For this L-band experiment the ranging test results were automatically recorded on punched paper tapes at the Mojave ground station, using the ATS-5 ranging receiver which is discussed in detail in Volume I of this report. The L-band ranging data was placed on an ASCII coded eight-level paper tape by the ATS-5 ranging receiver while the C-band ranging data was placed on a standard five-level BAUDOT coded paper tape by the ATSR C-band ranging system. In addition, supporting data concerning system parameters and signal characteristics was simultaneously recorded on strip charts. After recording this data, the ground station did no additional processing of these paper tapes. The tapes in their raw data format were mailed to the Westinghouse Defense and Electronic Systems Center, Baltimore, Maryland for further processing.

The eight-level L-band paper tape is illustrated in figure 3.1 (A) and the format for placing the ranging data on the tape is shown in figure 3.1 (B). One line of data consists of 14 line characters. The first character is the line feed (L/F) or start character for this one line of data. Characters 2 through 7 are used to identify the time-of-day (TOD) in which this one ranging measurement was made. Character 8 identifies the tone frequency (T) used for this measurement (H is for the 20 kHz measuring frequency and L denotes the 4 kHz frequency). The characters 9 through 13 are the values for the range measurement. Character 9 is for 100 usec, character 10, for 10 usec, character 11 for 1 usec, character 12 for 0.1 usec (100 nsec) and character 13 for 0.01 usec (10 nsec). This gives a range reading of XXX.XX micro-seconds, which is a one-way range reading. For the 20 kHz (H) measuring frequency this reading will vary from 000.00 to 024.99 usec; while for the 4 kHz (L) measuring frequency the reading will vary from 000.00 to 124.99 usec. The 14th character in the data line is the carriage return (C/R) which resets the printout carriage for the next data line.

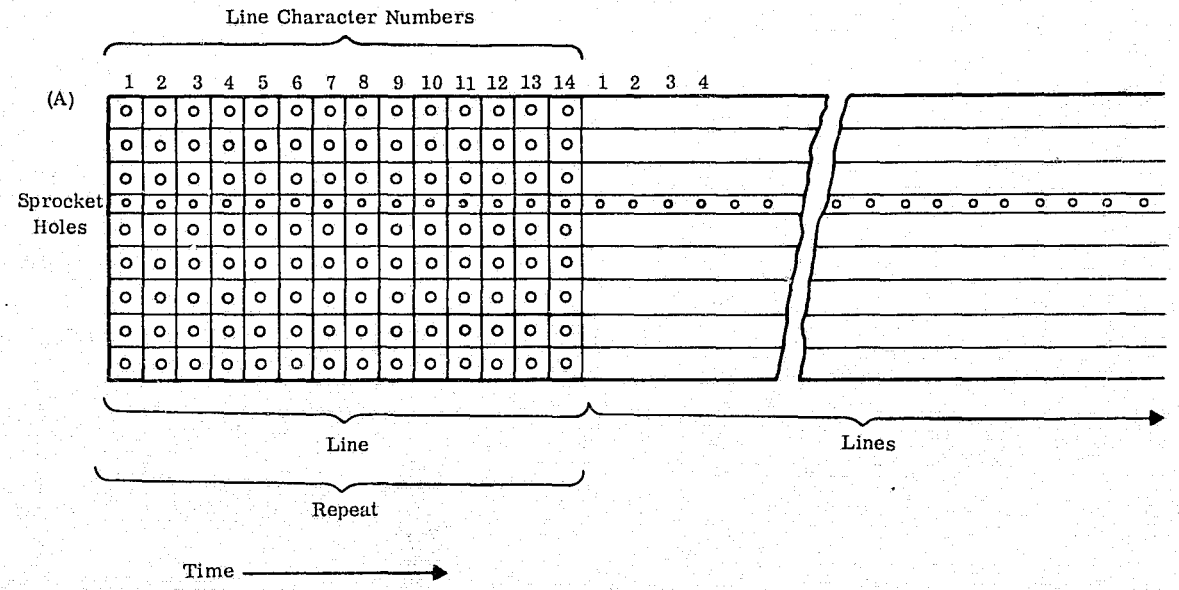

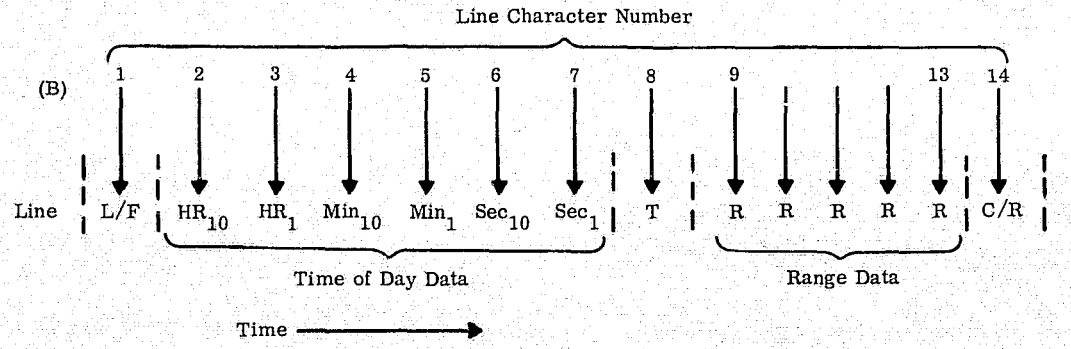

L/F	Line Feed (Start)	T	Tone Code (H = 20 kHz or L = 4 kHz)
HR	Hours (00-23)	R	Range (One-Way) (000.00 - 124.99 Microseconds)
Min	Minutes (00-59)	C/R	Carriage Return
	Seconds (00-59)		

NOTE: Data is punched in standard ACSII 8-level code.
There are 14 characters in each line to be transmitted serially.

Figure 3.1 L-Band Paper Tape Data Format

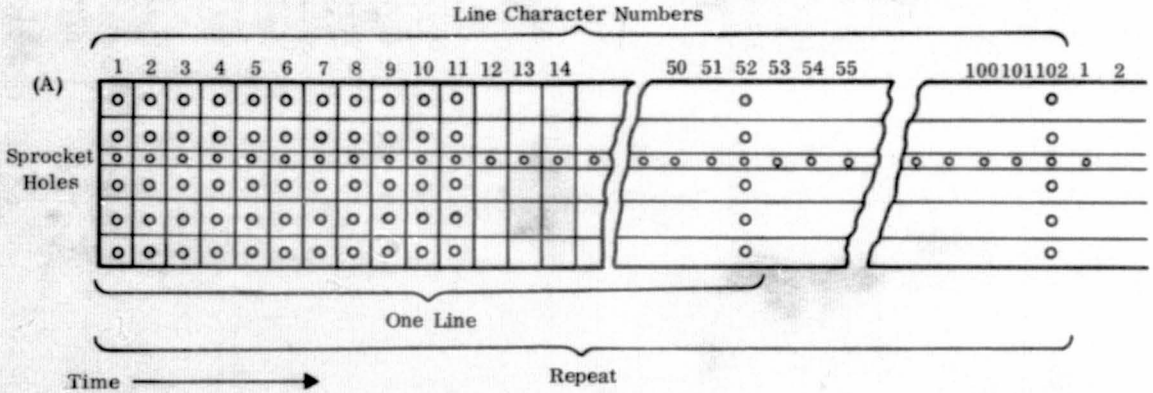

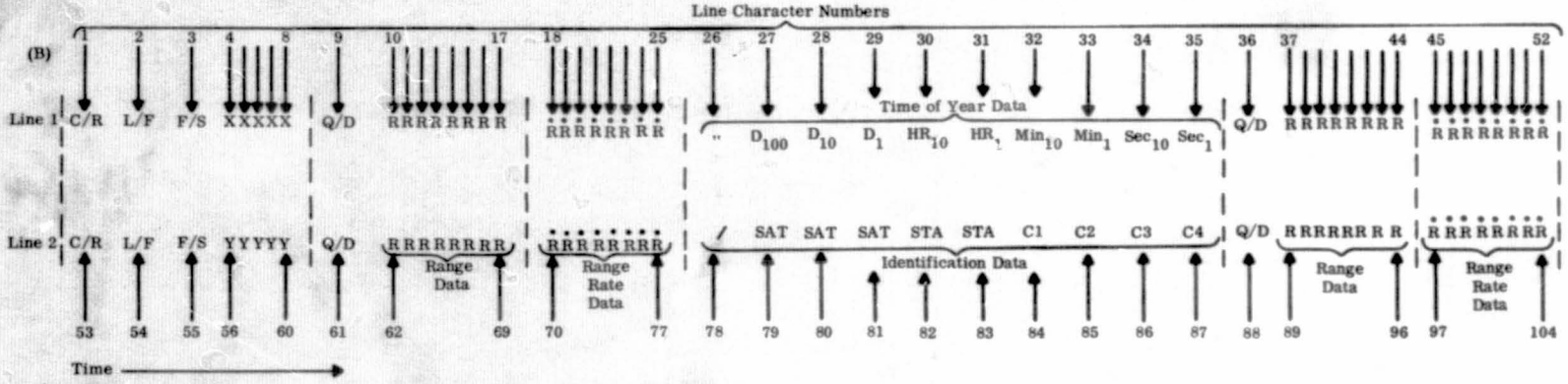

C/R Carriage Return
L/F Line Feed (Start)
F/S Figure Shift
X Antenna Position (Sign and Four Decimal Digits or Five Decimal Digits)
Q/D Quality Data (Space Indicates all Loops Locked)

R Range (Two-Way)
. (000000.00-124999.99 Micro Seconds)
R Range Rate
Sec. Seconds (00-59)
Min. Minutes (00-59)
C2 Sample Rate (0-4)
C3 Spare (0-9)
C4 Spare (0-9)

HR Hours (00-23)
D Days (000-365)
Y Antenna Position (Sign and Four Decimal Digits) Or Five Decimal Digits)
SAT Satellite Identification (000-999)
STA Station Identification (00-99)
C1 Ambiguity and resolution (1-9)

NOTE: Data is punched in standard BAUDOT 5-level code. There are 52 characters in each line, making a total of 104 characters to be transmitted serially before repeating.

Figure 3.2 C-Band Paper Tape Data Format

The C-band range measurements were made using the standard ATSR ranging system. The data output from this system is a five-level paper tape as illustrated in figure 3.2 (A) with the data format shown in figure 3.2 (B). Since this is the standard ATSR ranging format, there are many characters of information in this format in addition to the C-band range data which are not needed for this experiment. In the data format as shown, there are two lines of 52 characters each, in a complete set of data. There are two range measurements for each line of data and four range measurements for each TOD printout or repeat. The TOD data is placed on line characters 30 through 35, and the range data is placed on line characters 10 through 17, 37 through 44, 62 through 69, and 89 through 96. The range rate data shown in the format is not used in this experiment. The ATSR range readings are XXX,XXX.XX microseconds and will vary from 000,000.00 to 124,999.99 usec. This is a two-way range reading in contrast to the one-way range reading for the L-band system.

The C-band ranging measurements are taken at one-second intervals. However, the L-band ranging measurements are gated by the spin of the ATS-5 satellite which has a period of approximately 780 msec. One ranging reading is taken during each spin period providing four readings within three seconds. Thus, there will be two readings for the same second approximately every three seconds. As part of the data processing program, later these two readings are averaged for a single reading for that second.

In this discussion it was stated that the C-band data was placed on the 5-level paper tape and the L-band data was placed on the 8-level paper tape. This is the case for the major portion of this experiment which was measuring L-band and C-band ranging. However, for another part of the experiment, ranging measurements were made on C-band and VHF. In this instance the C-band measurements were switched from the ATSR ranging machine to the GSFC ranging machine, thereby, placing the C-band data on the 8-level paper tape. The VHF information was consequently placed on the 5-level paper tape. This change has been properly indicated in the data processing of these paper tapes.

3.2 DATA PROCESSING FLOW

3.2.1 Data Processing Step I - Paper Tape to Magnetic Tape

The first step in processing the field measurements is to transfer the data from the paper tapes to magnetic tapes. Figure 3.3 depicts step I of this data processing. As shown, the SDS-910 computer is used to store both the C-band and the L-band data on separate mag tapes. For either type of data a file record header is first generated containing: month, day, year of the test; the test transmitted power; and any pertinent test conditions. After the header, the data is then transferred to this tape. For the L-band measurements the data transferred is: the test tone used (H or L); the hour, minute, and second (TOD) of the data point, and the range data in nanoseconds. For the C-band measurements the data transferred is: the day, hour, minute, and second (TOD) for each data point, and the range data in nanoseconds. Since the C-band paper tape format contains only one TOD reference for every four range data points, the computer in this transfer process generates the three other missing TOD references and places them into the mag tape format with the appropriate data point. No other calculations or manipulations of the raw measured data is performed during this first processing step.

Before these separate mag tapes can be further processed, it is necessary to obtain a mag tape from NASA/GSFC containing per second ephemeris data over the measurement time intervals for the ATS-5 satellite in reference to the Mojave station. For the simultaneous L-band and C-band ranging (to ATS-5) portion of this experiment only the mag tape data for the ATS-5 satellite is required. For simultaneous C-band and VHF ranging (to either ATS-1 or ATS-3) magnetic tape data is required for only the particular spacecraft used. However, for the position location portion of this experiment since the C-band ranging was performed on the ATS-1 satellite and the L-band ranging used the ATS-5 satellite, ephemeris mag tapes for both satellites are required.

3.2.2 Data Processing Step II - Raw Data Magnetic Tape to Corrected Data Master Tape

This step in the range data processing converts the measured data points, in nanoseconds, to absolute one-way range values in meters. This corrected data of L-band ranging, C-band ranging and ephemeris is then time coordinated and simultaneously stored on a single master magnetic tape. This step II is shown in figure 3.4.

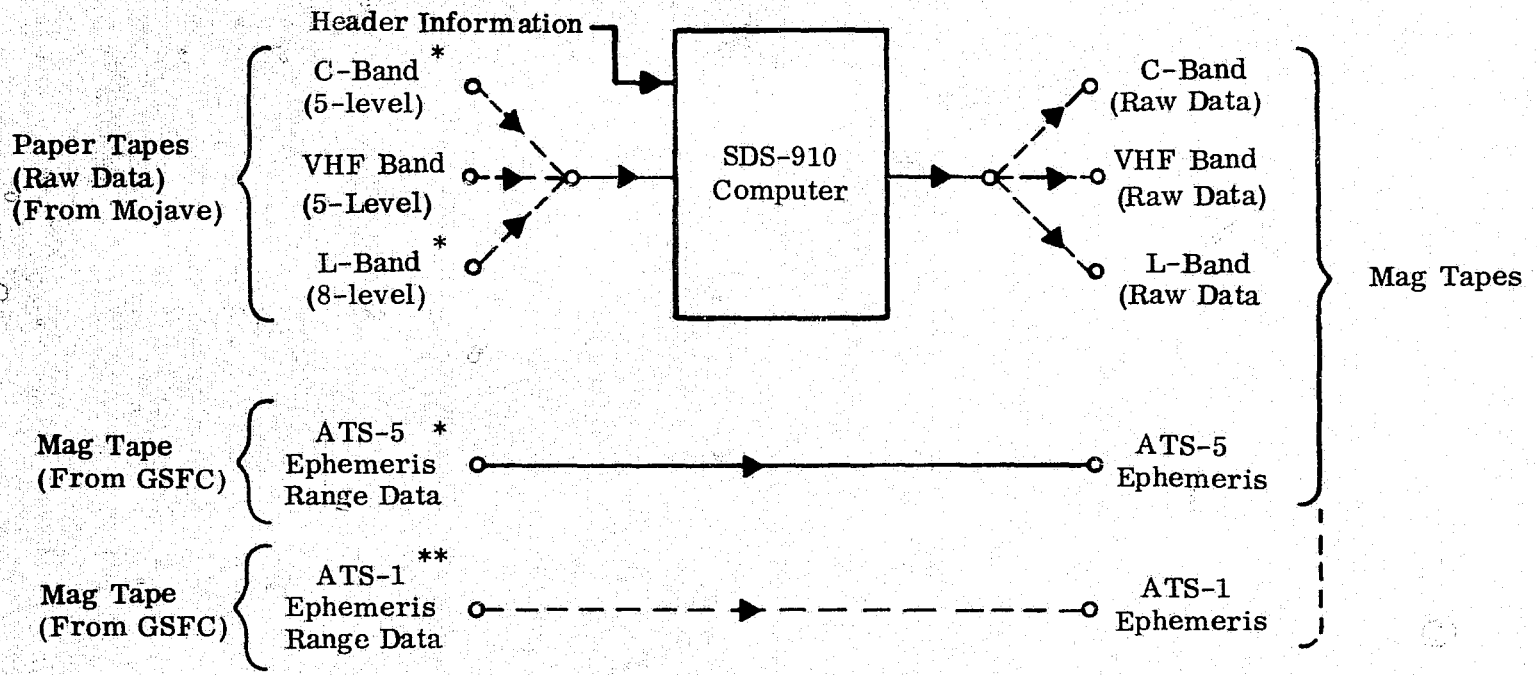

* For Ranging with C-Band and VHF:
a. VHF on 5-level paper tape
b. C-Band on 8-level paper tape
c. ATS-1 or ATS-3 Ephemeris Data instead of ATS-5

**Additional Ephemeris Range Data Required for Position Location Experiment

Figure 3.3 Data Processing Step I - Paper Tape to Magnetic Tape

The first operation by the Univac 1108 computer resolves the ambiguity* of the C-band ranging data and places this data reading in its proper lane. For the C-band measurements, this lane width is 125,000 usec, (approximately 20,200 N. miles) thereby placing the two way range reading in either the 2nd or 3rd lane. Next, this resultant two way range value in microseconds is used to compute the one-way corrected range output in meters.

In the L-band measurements, as previously stated, approximately every three seconds there will be two data readings for the same second. The first step in resolving the L-band data is to average these two readings when they occur to give a single reading for each second. The next step is the ambiguity resolution of the L-band data. Since the width of the lane for this L-band ranging system is only 50 usec, there will be approximately 5000 lanes to be added to the measured data. The correct number of lanes is determined from the previously corrected C-band range values. Since the L-band measurements are one-way readings, the one-way C-band calculation is used. After adding the ranging readings to the proper lane calculation, the one-way range is converted to meters.

At this point the L-band and C-band raw data has been corrected and is ready to be placed on the master magnetic tape, along with the appropriate ephemeris data. These three inputs are time coordinated and stored in the format shown in table 3.1. This magnetic tape may now be used to perform any of the computations of simultaneous ranging in the Data Processing Step III which follows.

The master magnetic tape for the position location experiment requires the same calculations and data as described above for L-band and C-band. However, in this case the L-band ambiguities have to be resolved against the ephemeris data since in this case the C-band ranging is to a different satellite. Also, as shown in figure 3.4, ephemeris data for both satellites must be fed in to be stored on the master magnetic tape.

3.2.3 Data Processing Step III - Master Magnetic Tape to Programmed Computation Outputs

This Step utilizes the master magnetic tape created from the raw data and ephemeris data to perform the analysis computations. Figure 3.5 shows Step III. The data processing programs were developed to provide an efficient method of processing the large amount of data obtained from these tests, and to aid the analyst in determining the validity of the test results. The main processing program contains a number of sub-programs which perform various computations. Data generated on the computer and plotter falls into one of two general classes:

*See Glossary

TABLE 3.1 MASTER MAGNETIC TAPE FORMAT

Word #	Contents	Digits or Char/Word	Format	Example
1	# Points,	3 digits	Binary	127
2	L-band tone freq. (kHz)	2 digits	Binary	20
3	Month	2 digits	Binary	2
4	Day (Test Date)	2 digits	Binary	17 (2/17/71)
5	Year	2 digits	Binary	71
6	C-band Xmtr pwr.	4 digits	Binary	1000 (1000.5 Watts)
7	C-band Xmtr pwr.	2 digits	Binary	5
8	L-band Xmtr pwr.	4 digits	Binary	52 (52.5 Watts)
9	L-band Xmtr pwr.	2 digits	Binary	5
10 ↓ 13	C-band Test Description, etc.	6 charac	BCD	ATS-5 Mode-5 Rec. in Man.
14 ↓ 17	L-band Test Description, etc.	6 charac	BCD	ATS-1 Mode 1 RTC locked
18	Hour	2 digits	Binary	19
19	Minute (Start Time)	2 digits	Binary	22 (19-22-01)
20	Second	2 digits	Binary	1
21	Hour	2 digits	Binary	19
22	Minute (End Time)	2 digits	Binary	25 (19-25-02)
23	Second	2 digits	Binary	2
24 ↓ 23 + # points	C-band Range in Meters	8 digits	Binary	37212319 meters
↓ + # points	L-band Range in Meters	8 digits	Binary	37212320 meters
↓ + # points	Ephemeris range predictions in meters	8 digits	Binary	37213320 meters
↓ 900	Zeroes			000000 ↓ 000000

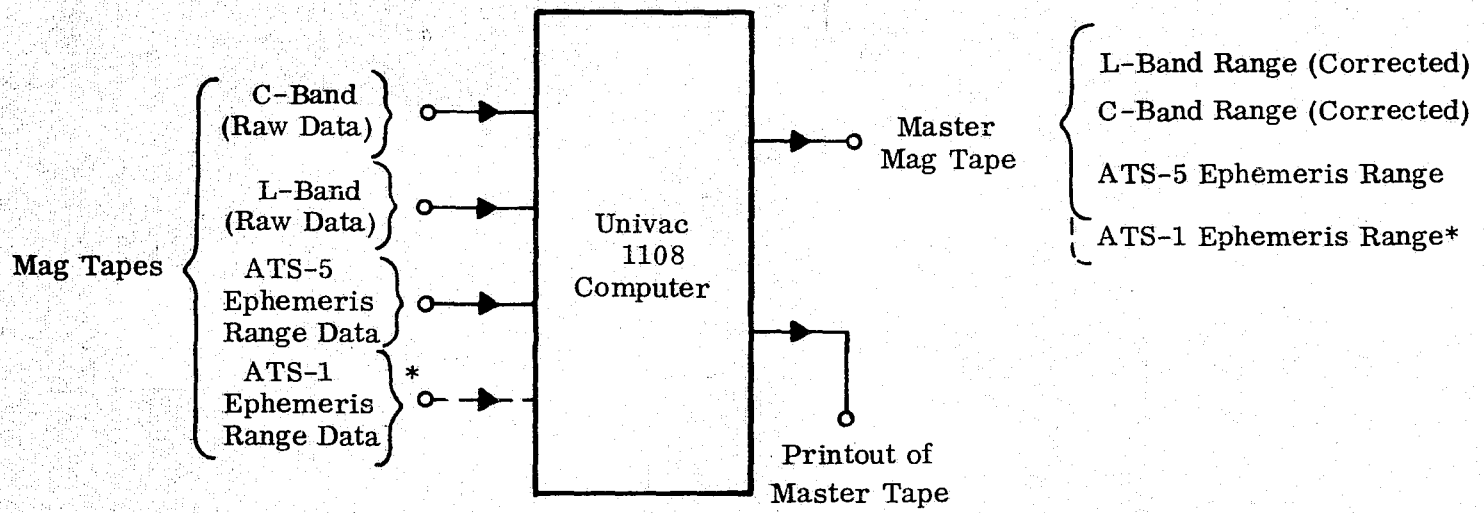

*Required only for Position Location Experiment

Figure 3.4 Data Processing Step II - Raw Data Magnetic Tape to Corrected Data Master Tape

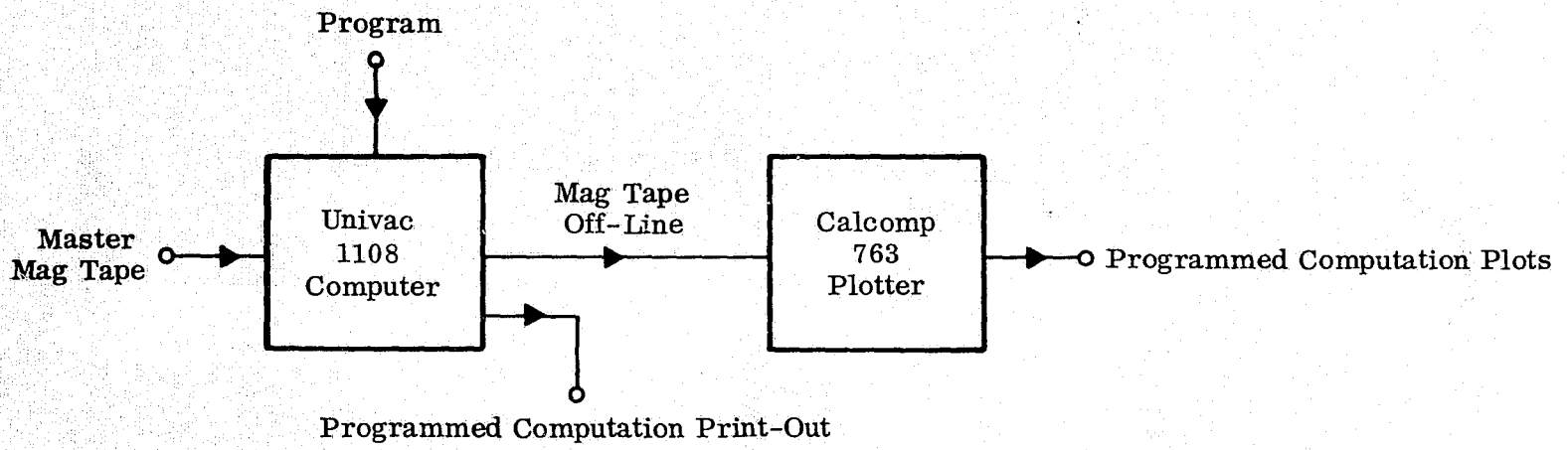

Programmed Computations:

A. Simultaneous Ranging Experiment
   1. Corrected Data Plot
   2. Smoothed Range Data Plot
   3. Autocorrelation
   4. Crosscorrelation
   5. Scatter Plot
   6. Probability Density Distribution
   7. Cumulative Distribution

B. Position Location Experiment
   1. Position Location Scatter Plot

Figure 3.5 Data Processing Step III - Master Magnetic Tape to Programmed Computation Outputs

1. Real time ranging data from ephemeris inputs, L-band ranging measurements, and C-band ranging measurements. The plots generated from these processing programs are:

a. Corrected Data Plot
   L-band range versus time
   C-band range versus time
   Ephemeris range versus time

b. Smoothed Range Data Plot
   L-band range versus time
   C-band range versus time
   Ephemeris range versus time

c. Position Location Plots
   L-band and C-band ranging
   Ephemeris data

2. Statistical analysis of the L-band and C-band data to determine error sources, equipment performance, range biases, and relative performance of the two ranging systems. The plots generated from these programs are:

a. Autocorrelation of Ranging Measurements Errors
   L-band
   C-band

b. Crosscorrelation of Ranging Measurement Errors
   C-band versus L-band

c. Scatter Plot of Range Measurements
   C-band versus L-band

d. Probability Density Distribution of Ranging Errors
   C-band % of time versus class number
   L-band % of time versus class number

e. Cumulative Distribution of Ranging Errors
   C-band measured error distribution on "normal" scale.
   L-band measured error distribution on "normal" scale.

3.2.3.1 Real Time Plots

The first programmed plot is a printout of the data on the master magnetic tape. This plot shows the corrected L-band and C-band range values and the ephemeris predictions over the measurement interval all plotted on a common time base. The data in the plots has been corrected for lane ambiguity.

A typical example of this plot is shown in figure 3. 6. The analyst can see how both the L-band range data and the C-band range data agrees with the ephemeris data during a particular experiment period. The plot shows the scatter of individual L-band range measurements compared to ephemeris range curve, which gives an indication of the peak to peak errors experienced during the measurement period.

The smoothed data plot is the second programmed output. The regression analysis program takes the ranging measurements, which are assumed equally spaced in time, and determines the coefficients of a second degree polynomial using the "method of least mean square fit" and determines the standard deviation of the measurements from this least square polynomial fit (i. e., the rms error). From these calculations the smoothed data plot of the measured data is obtained. A typical example of smoothed range is shown in figure 3. 7, which is the companion curve to figure 3. 6. From this plot the following calculated information is obtained for either the L-band or C-band smoothed range:

a. Range value in meters at the y - axis intercept (time = 0). (Example: C -band = 37, 263, 248 meters, from figure 3. 7).

b. Velocity coefficient, or average range rate of change in meters per second (Example: C-band = 3. 9921 M/S).

c. Acceleration coefficient or rate of curvature in meters per second squared (Example: C -band = -0. 0007 M/S^2).

d. Standard deviation or RMS error (in meters) between the polynomial fit and the actual measurement. (Example: C-band = 5. 8542 meters).

The third real time programmed output is a set of plots for the position location experiment. Figures 3. 8 through 3. 11 are typical plots from this program. In this experiment the L-band ranging was to the ATS-5 satellite and the C-band ranging was to the ATS-1 satellite. The position location scatter plot is this programmed output and is shown in figure 3. 8. In this plot the target in the center is the actual location of the Mojave ground station. The horizontal and vertical lines through this station point are marked off in 100-meter steps. This station point is also listed at the top of the graph. The range measurements to each satellite intersect in this graph in the southeast quadrant in a scatter as shown. The position of this scatter is listed at the top of the figure under "center of scatter." The distance from the station point to the center of the scatter is computed and printed in the data at the top of the chart. In this case this distance was 795 meters.

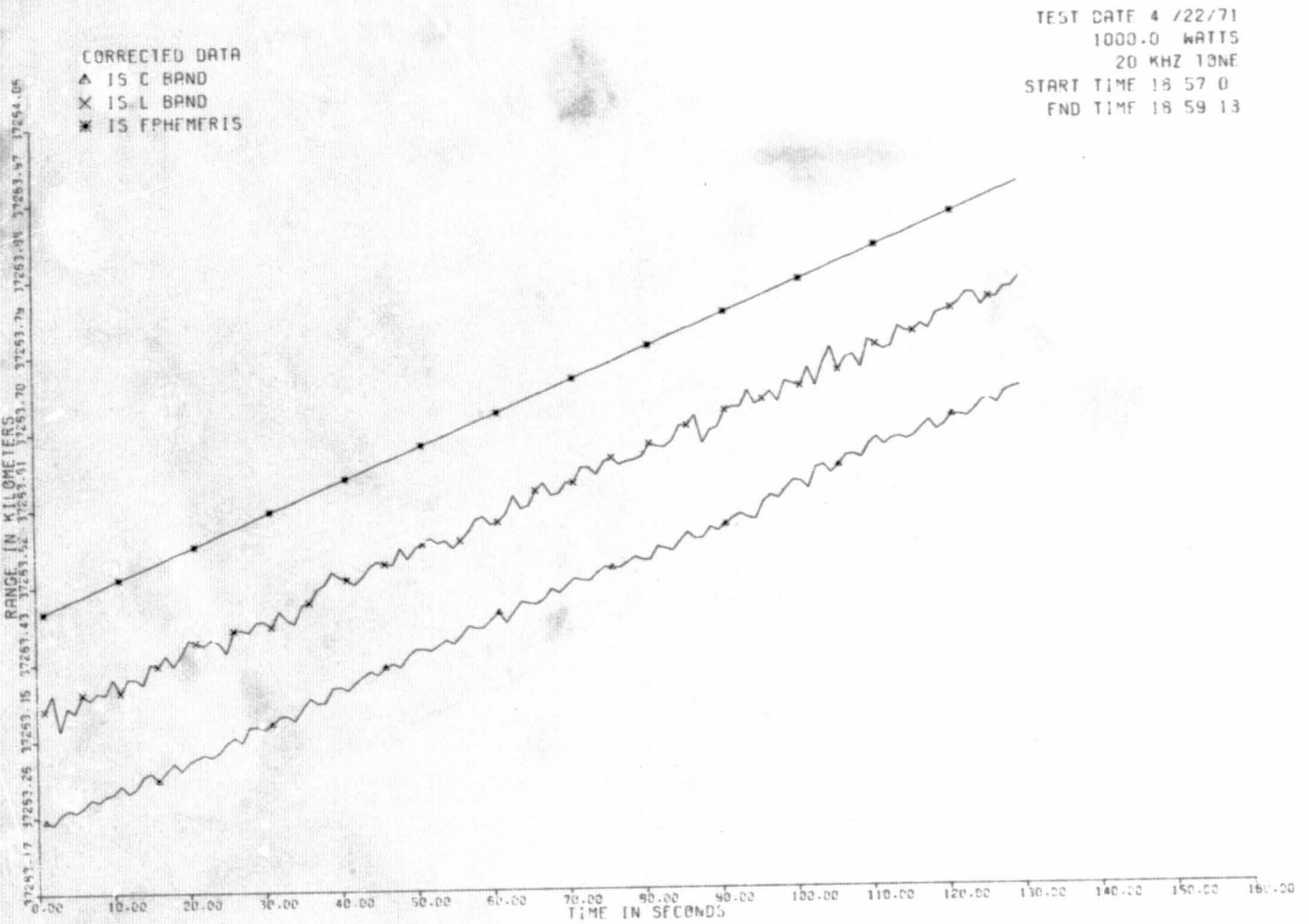

Figure 3.6 Typical Corrected Data Plot

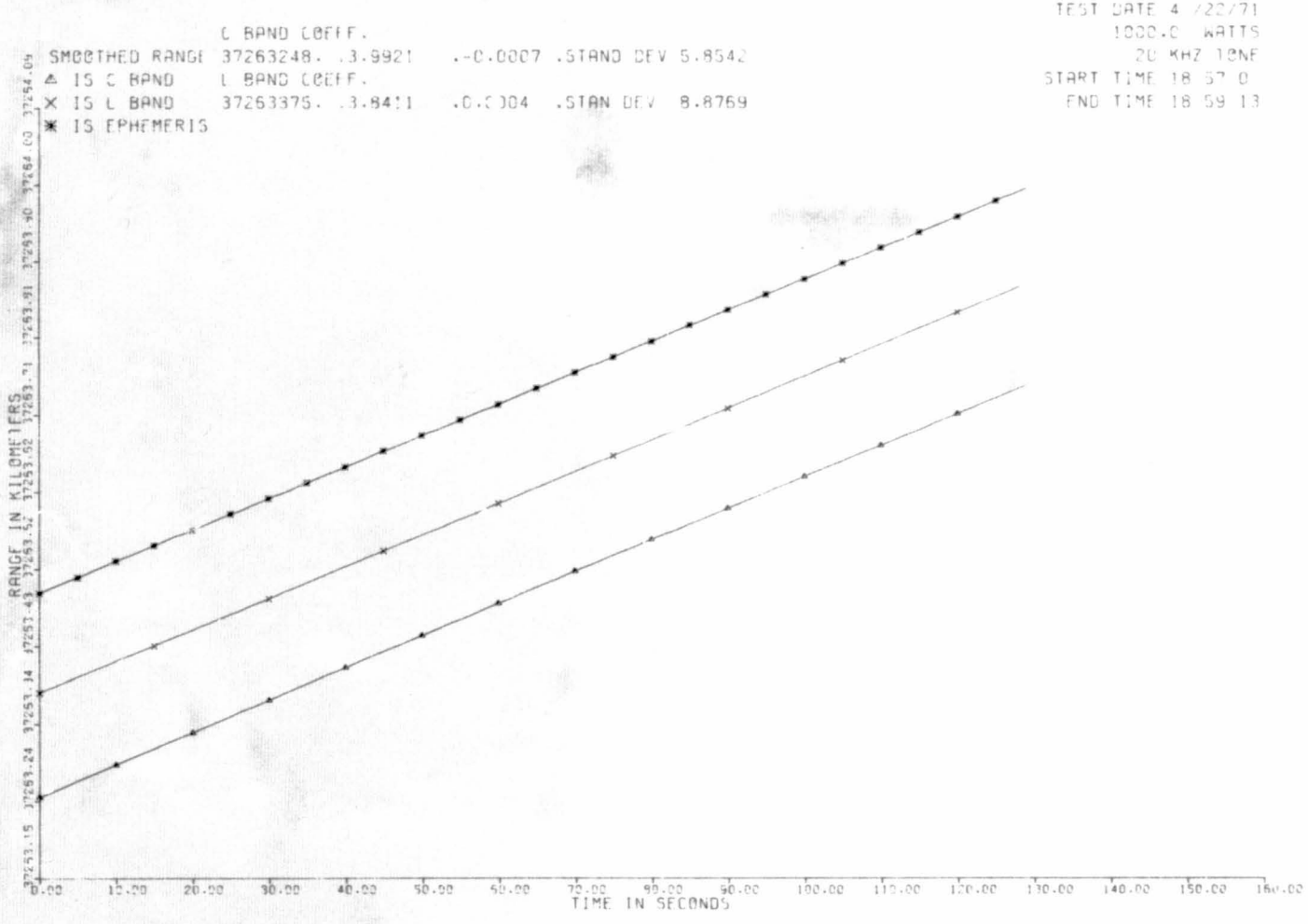

Figure 3.7 Typical Smoothed Range Plot

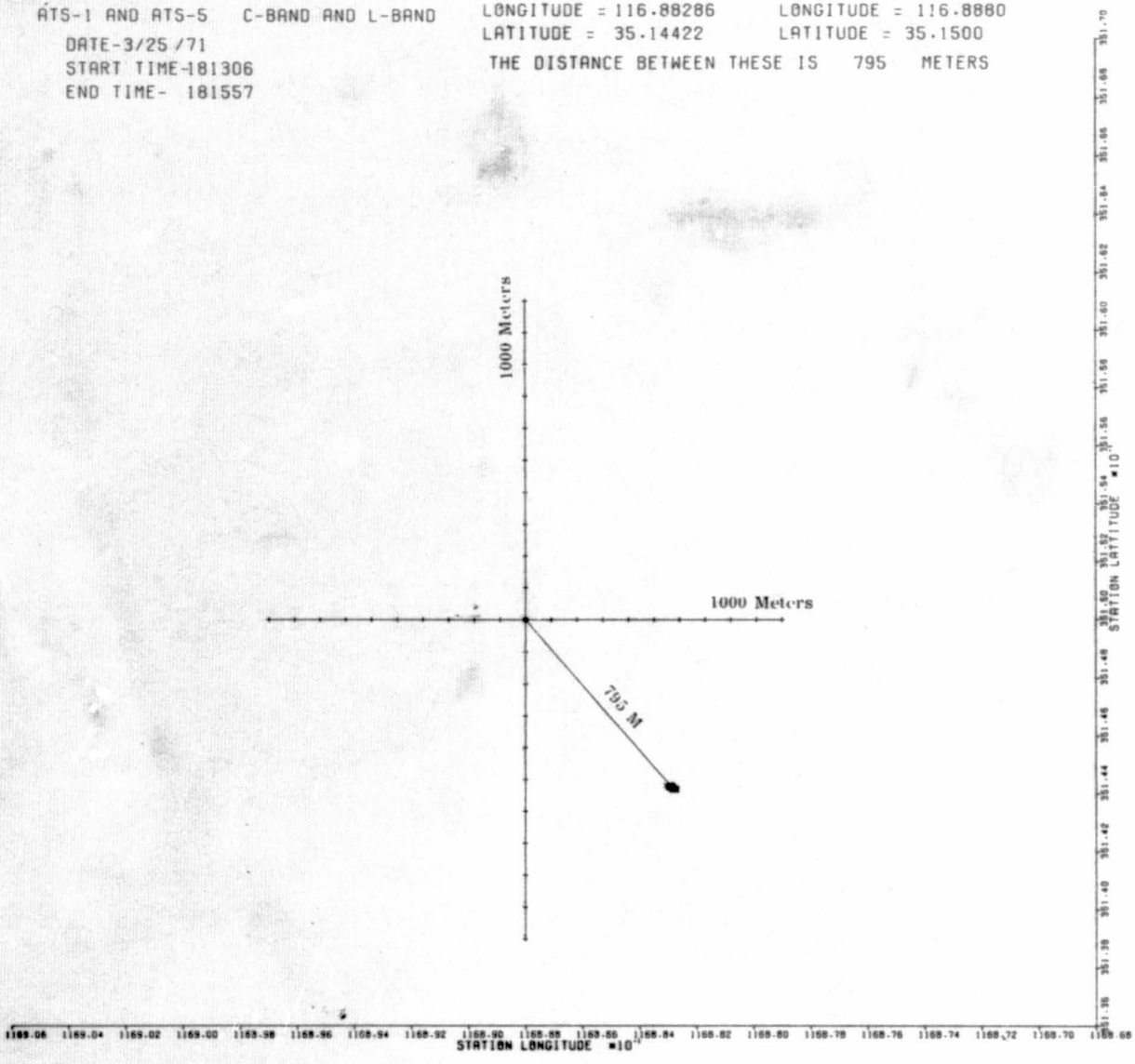

Figure 3.8 Typical Position Location Using Measured Range Data for ATS-1 and ATS-5

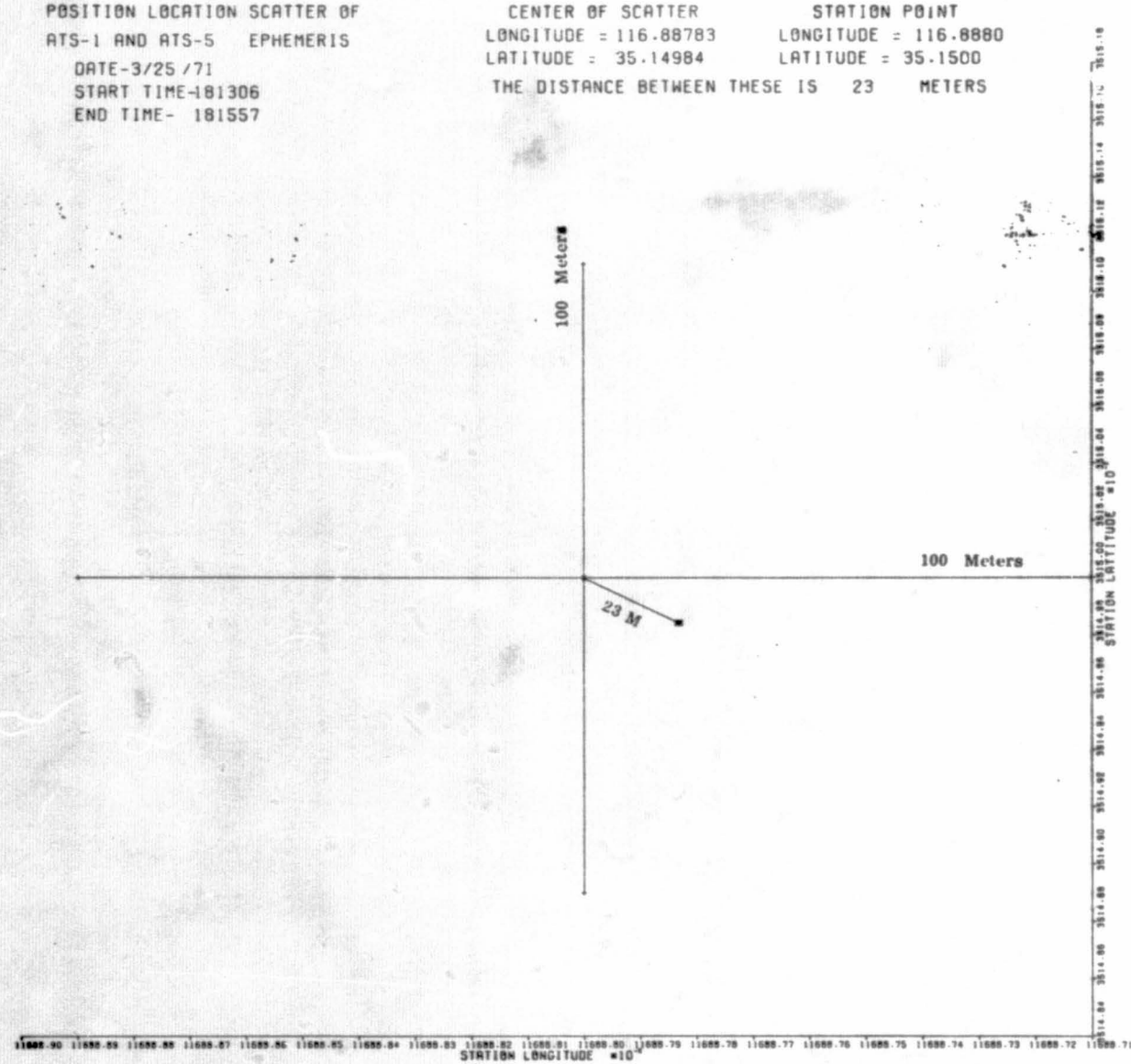

Figure 3.9 Position Location Using Ephemeris Range Data for ATS-1 and ATS-5

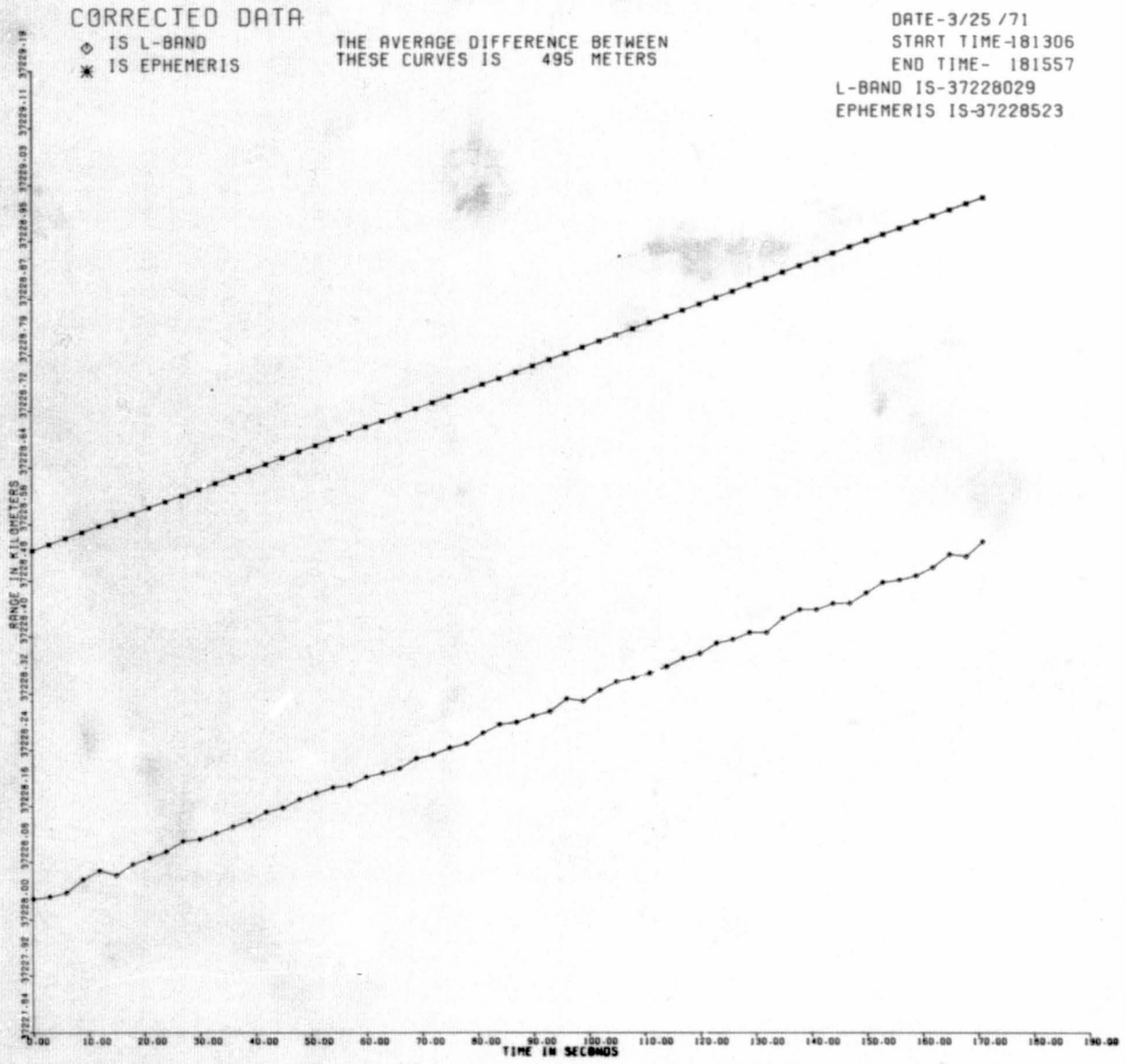

Figure 3.10 ATS-5 L-Band and Ephemeris Range Data

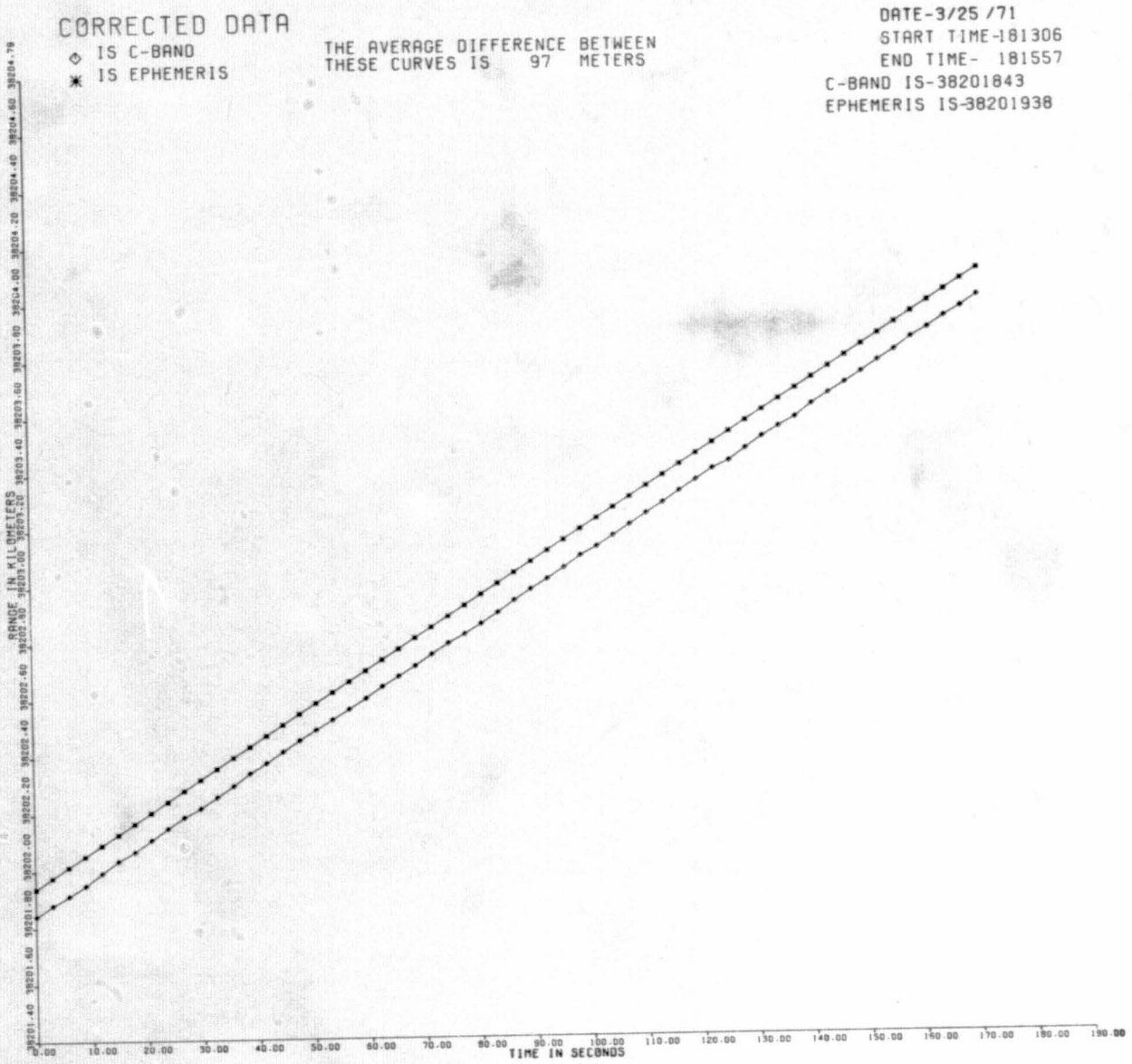

Figure 3.11 ATS-1 C-Band and Ephemeris Range Data

The other plots generated as part of this position location program are printed as an aid to the analyst in determining the source of errors in the position location. Figure 3.9 is a plot of the emphemeris data to determine if this data does come back to the station location. This is both a check on the program and on the ephemeris data. Several sets of this data were found in error and were detected by this plot. The plots of figures 3.10 and 3.11 are corrected data plots showing the measured data and its corresponding ephemeris data. The ATS-5 data is shown in figure 3.10 and ATS-1 data is shown in figure 3.11. The average distance between the two curves is printed at the top of each plot. These data plots show how the actual measurements compare with the ephemeris range, and how these measurements affect the position location, as shown in figure 3.8.

3.2.3.2 Statistical Presentations

Explanation and presentation of statistical data for C-band and L-band error autocorrelations, crosscorrelations, scatter plots, probability densities, and cumulative distributions are covered in greater detail in Section 5 with illustrated examples.

The first plots are the C-band and L-band error autocorrelation functions plotted on a single graph (example shown in figure 5.1). In general, the autocorrelation function has the following characteristics:

a. It is an even function (i.e., symetrical about $\tau = 0$).

b. $\phi_{11}(0)$ is the mean square value and also the maximum value

c. $\phi_{11}(\tau)$ is not unique

The purpose of the second plot (figure 5.2) which is the C-band and L-band error crosscorrelation is to determine if errors are caused by a common mechanism, such as inonospheric anomalies, or are caused by independent mechanisms. If errors are equally well correlated under all controlled signal conditions, these plots would indicate an independence of the error sources from the controlled variables. The crosscorrelation function basically describes how well the errors in two different measurements, or time varying functions, vary with respect to each other. If the measurements are correlated, there could be a causal relationship between errors.

The third plots (figure 5.3) are scatter plots which display the amount of agreement or disagreement for the corresponding sets of range measurements.

The probability density of the errors for the L-band and C-band range errors are plotted on a single graph (figure 5.4). The significance of these plots is the shape of the distribution and how closely it resembles a Gaussian distribution.

The cumulative distribution (figure 5.5) is the integrated probability density function and is plotted on a single graph for both C-band and L-band range errors.

SECTION 4

L-BAND RANGING EXPERIMENTS

4.1 SIMULTANEOUS C-BAND AND L-BAND RANGING EXPERIMENT

4.1.1 Objective

The primary objective of this experiment was to obtain L-band ranging measurements on the ATS-5 satellite using the GSFC L-band ranging receiver and to compare this data with the C-band ranging measurements simultaneously obtained to the same ATS-5 satellite using the standard ATSR ranging system. The C-band measurements were used as a basis for establishing the relative accuracy of the L-band measurements, since it is believed that this smoothed C-band range, versus elapsed time, represents the most accurate range measurement which would be available. The results of this experiment have indicated the relative accuracy to which these L-band ranging measurements can be performed.

4.1.2 Test Description

The test setup block diagram for this simultaneous C-band and L-band ranging experiment is shown in figure 4.1A and 4.1B for mode 5 and mode 1, respectively. The C-band ranging measurements were performed by the Mojave station ATSR ranging system. In addition, this same ATSR transmit signal was used (in mode 5) as the exciter signal for the L-band transmitter. The GSFC L-band ranging receiver then utilized that returned signal to perform the L-band ranging measurements. These readings were made concurrently over the specified test period.

The ATSR system has eight different ranging frequencies: 500 kHz, 100 kHz, 20 kHz, 4 kHz, 800 Hz, 160 Hz, 32 Hz, and 8 Hz. The highest frequency tone is used to determine the finest range increment, and the lower frequency tones to resolve range measurement ambiguities. This highest frequency tone used may be selected on a mode basis. In selecting mode 1, 500 kHz is the transmission frequency or major range tone. Operation in mode 5 makes 20 kHz the major range tone. Since the GSFC L-band ranging receiver was designed to perform with a 20 kHz ranging tone, mode 5 is selected in the ATSR system to accommodate the L-band ranging receiver. ATSR range readings in this mode exhibit approximately five meters

of range measurement jitter as compared to one meter of jitter for readings made in mode 1. The overall accuracy of the smoothed data is not affected. Most tests in this simultaneous experiment were performed with the ATSR system in mode 5. However, some tests were also performed with the ATSR system in mode 1. As seen in figure 4.1B, a separate source of 20-kHz modulation was required for this condition. This was provided by two Hewlett-Packard synthesizers. The HP-5102 synthesizer operated at 20 kHz and supplied the reference tone to the GSFC ranging receiver as well as modulating the 70 MHz output signal from the HP-5105 synthesizer. When operating in mode 1, these two ranging systems are completely independent of each other.

The first step of a ranging measurement is to "zero set" the ranging system to the known delays of the collimation tower. This setting removes delays caused by the equipment and the spacecraft. The calibration setting for the C-band ranging has been determined by the station system engineers to be 23,980 nanoseconds, two-way, or 11,990 nanoseconds, one-way. Since the L-band antenna was 80 meters (or 260 nanoseconds) closer to the collimation tower for this experiment, the calibration setting for the L-band ranging was assumed to be 11,730 nanoseconds. Since the completion of this testing, a descrepancy in the L-band "zero set" has been determined. When the equipment time delay for the spacecraft transponder was obtained from the manufacturer, a summation of the collimation tower and spacecraft delays revealed that an additional 390 nanoseconds delay should have been included in the "zero set" calibration. This yields a one-way calibration setting of 11,340 nanoseconds instead of 11,730 nanoseconds which had been used. This error causes the L-band range reading to be approximately 120 meters too long. Also, since the L-band antenna is located 90 feet south and 445 feet west of the C-band antenna, the geometry of these two antennas in respect to the ATS-5 satellite causes the L-band signal to travel 14 meters further than the C-band signal. This is discussed in more detail in Section 6. Therefore, summing these two errors showed that the L-band reading was approximately 134 meters longer than the C-band measurement.

For the measurements of this simultaneous C and L-band experiment, the C-band ranging readings were made in all tests with the transmitter power output ordinarily employed in the ATS program for orbit determination. However, to determine the effects of signal strength on the L-band ranging, several ranging tests were performed at the following various transmitter outputs: 1000, 500, 250, 64, 32,

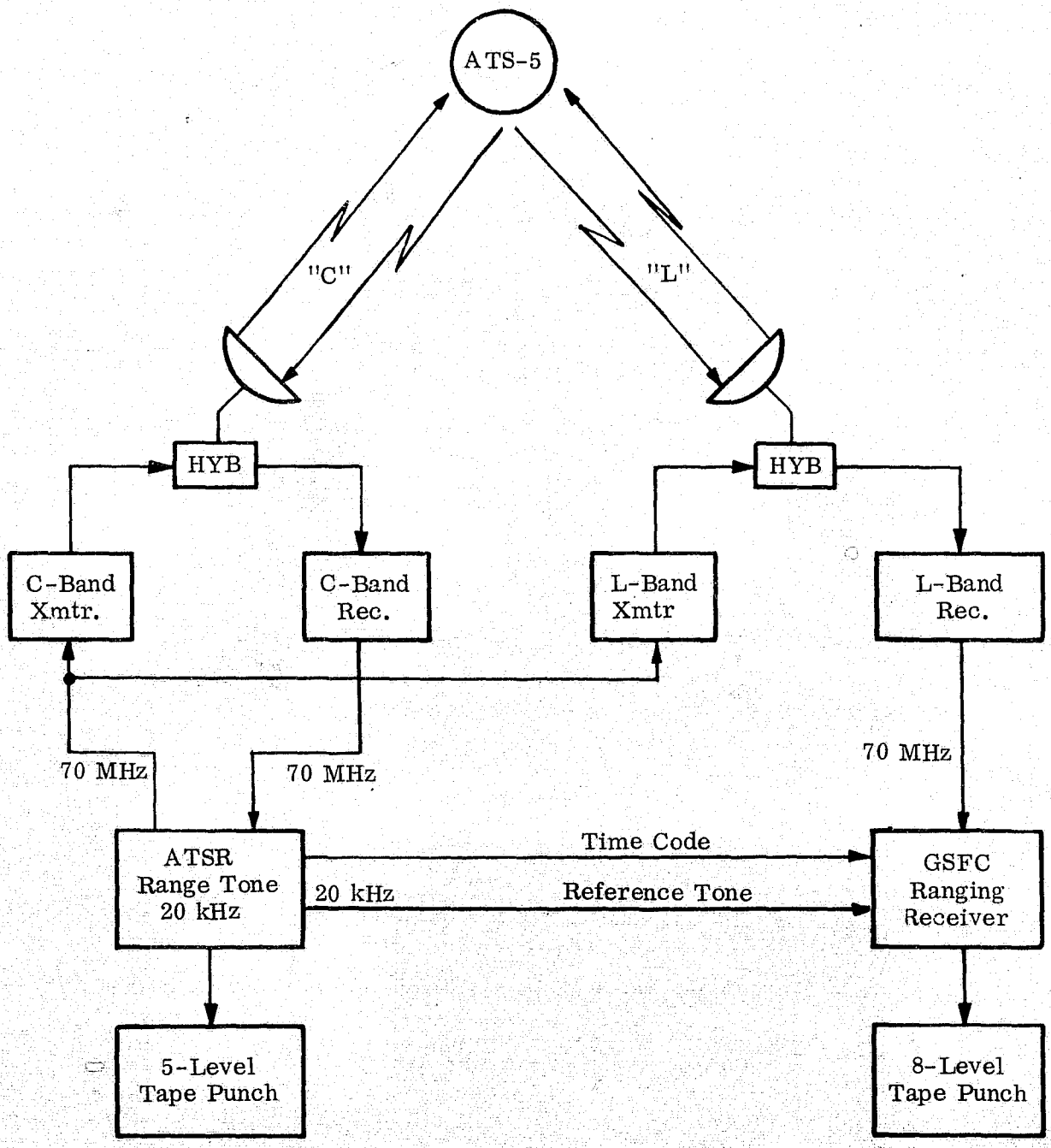

Figure 4.1A Simultaneous C- and L-Band Ranging Block Diagram (Mode 5)

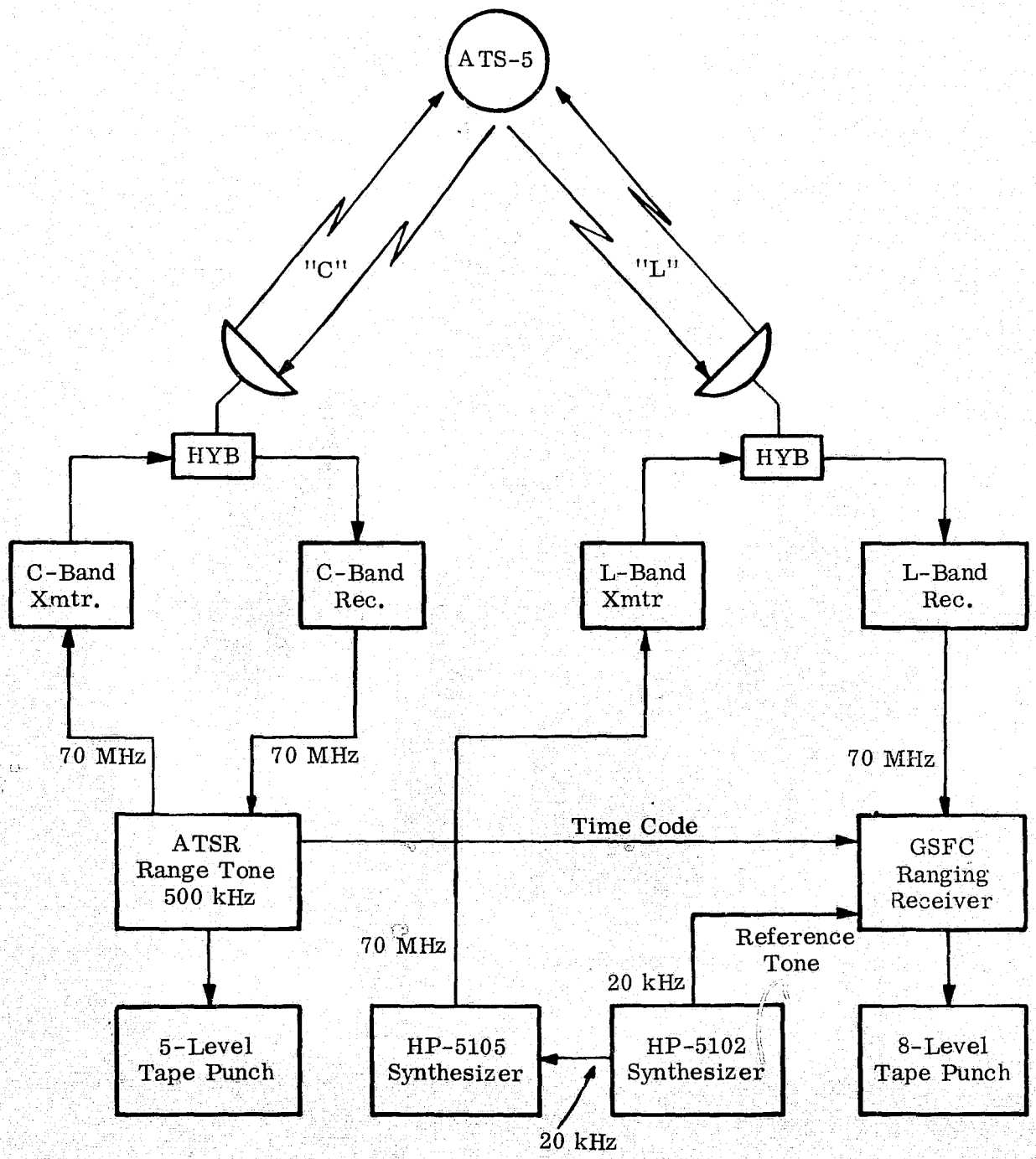

Figure 4.1B Simultaneous C- and L-Band Ranging Block Diagram (Mode 1)

16, 8, and 4 watts. Most of the tests, however, were performed at the 1000 watts transmitter output. Three minutes of ranging data were generally recorded for each test period.

4.1.3 Experimental Test Results

The results of the simultaneous C-band and L-band ranging tests performed at Mojave are presented in tables 4.1 and 4.2. The data presented in the first table is that obtained with the ATSR C-band ranging system operating in mode 5, thereby providing the L-band ranging system with its 20-kHz measuring tone. The data presented in the second table was obtained with the ATSR system in mode 1. For these measurements, the 20-kHz L-band ranging tone was externally inserted by the frequency synthesizers as shown in figure 4.1B. This measured data is divided into these two tables because of a descrepancy in the L-band measurements when operated in mode 1. This discrepancy will be fully discussed later in the data analysis paragraph 4.1.4.

The results shown in tables 4.1 and 4.2 are grouped into the days when each of the measurements were made. The first column shows this date and the time span from beginning to end of the test, such as: 1800 hours, 42 minutes (Zulu) to 1900 hours, 8 minutes (Zulu) on March 25, 1971. The second column denotes the transmitted power level of the L-band system. This output power was varied from a maximum of 1000 watts to the lowest power of 4 watts. The next three columns present the one-way range data; the first being the ephemeris range at each time of measurement, the second being the measured C-band range, and the third being the measured L-band range. Values given are the zero intercept points taken from the smoothed data plots for each measurement period. In the next three columns the difference in range values of the previous three columns are compared. The first is the difference between the ephemeris range and the C-band range. Next, the difference between ephemeris and the L-band range. The third column compares the difference in the L-band and C-band measured ranges. The fourth column is the "corrected L-C" column. For this data the 134 meter "zero set" error, explained in paragraph 4.1.2, has been removed from the differences of column three. The last two columns of the tables present the standard deviation (or sigmas) of the measured data, first for the C-band readings and then for the L-band readings.

In examining table 4.1 the data for March 25, 1971 appears to be the best example of a typical set of measurements; thus, a set of the data plots for this day are presented in figure 4.2 through 4.9. Since the 250 watts, 64 watts, and 32 watts data plots were essentially the same as the 1000 watts data plot, only the 1000 watts plot

TABLE 4.1 SIMULTANEOUS RANGING DATA ON ATS-5 (MODE 5 OPERATION)
(Coherent Ranging Tones)

Measurement Date	L-band Xmtr. Power	Range (Meters)			Difference in Range (Meters)				Sigma (Meters)	
		Ephemeris	C-band	L-band	E-C	E-L	L-C	Corrected L-C	C-band	L-Band
March 25, 1971 (1842Z - 1908Z)	1000W	37,233,730	37,233,405	37,233,530	[illegible]	+200	+125	-9	4.20	4.52
	250W	37,234,516	37,234,232	37,234,378	[illegible]4	+138	+146	+12	4.79	4.13
	64W	37,235,309	37,234,999	37,235,148	+310	+161	+149	+15	3.66	4.08
	32W	37,236,180	37,235,913	37,236,064	+267	+116	+151	+17	3.06	4.86
	16W	37,236,942	37,236,651	37,236,796	+291	+146	+145	+11	3.86	8.12
	8W	37,237,758	37,237,471	37,237,560	+287	+198	+89	-45	3.35	24.65
	4W	37,238,603	37,238,319	37,238,224	+284	+379	-95	-229	3.60	52.01
April 13, 1971 (1811Z - 1834Z)	1000W	37,243,342	37,243,079	37,243,204	+263	+138	+125	-9	16.16	11.07
	1000W	37,244,755	37,244,495	37,244,634	+260	+121	+139	+4	13.76	9.53
	1000W	37,247,449	37,247,20[illegible]	37,247,334	+247	+115	+132	-2	15.78	12.40
April 15, 1971 (1833Z - 1840Z)	1000W	37,250,354	37,250,063	37,250,206	+291	+148	+143	+9	3.97	8.72
	250W	37,251,196	37,250,917	37,251,061	+279	+135	+144	+10	3.55	8.43
April 20, 1971 (1833Z - 1904Z)	1000W	37,256,313	37,256,003	37,256,107	+310	+206	+104	-30	5.13	7.24
	1000W	37,257,213	37,256,913	37,257,023	+300	+190	+110	-24	5.28	12.69
	250W	37,258,115	37,257,823	37,257,942	+292	+173	+119	-15	4.34	7.30
	64W	37,259,019	37,258,736	37,258,855	+282	+164	+119	-15	6.24	7.84
	32W	37,259,924	37,259,645	37,259,766	+279	+158	+121	-13	4.66	7.83
	16W	37,260,831	37,260,565	37,260,686	+266	+145	+121	-13	7.28	9.75
	8W	37,261,754	37,261,493	37,261,621	+261	+133	+128	-6	5.47	8.74
	4W	37,262,874	37,262,627	37,262,732	+247	+142	+105	-29	5.36	14.65
April 22, 1971 (1857Z - 1923Z)	1000W	37,263,497	37,263,248	37,263,375	+249	+122	+127	-7	5.85	8.88
	250W	37,264,422	37,264,169	37,264,298	+253	+124	+129	-5	5.50	10.21
	64W	37,265,347	37,265,106	37,265,231	+241	+116	+125	-9	5.27	13.92
	32W	37,266,273	37,266,039	37,266,133	+234	+140	+94	-40	4.79	27.54
	16W	37,267,202	37,266,983	37,266,951	+219	+251	-32	-166	4.81	51.99
	8W	37,268,124	37,267,908	37,267,590	+216	+534	-318	-452	5.77	89.87
	4W	37,269,048	37,268,841	37,267,371	+207	+1677	-1470	-1604	5.37	246.42
April 27, 1971 (1900Z - 1922Z)	250W	37,268,501	37,268,335	37,268,458	+166	+43	+123	-11	4.41	11.70
	64W	37,269,362	37,269,209	37,269,306	+153	+56	+97	-37	5.38	24.76
	32W	37,270,232	37,270,093	37,270,074	+139	+158	-19	-153	5.57	45.87
	16W	37,271,094	37,270,960	37,270,828	+134	+266	-132	-266	5.46	64.83
	4W	37,272,833	37,272,727	37,275,717	+106	-2884	+2990	+2856	5.55	2217.32
April 28, 1971 (1908Z - 1935Z)	1000W	37,271,708	37,271,620	37,271,719	+88	-11	+99	-35	23.72	5.56
	250W	37,272,206	37,272,133	37,272,220	+73	-14	+87	-47	24.77	7.16
	64W	37,273,065	37,273,002	37,273,114	+63	-49	+112	-22	27.76	7.02
	32W	37,274,340	37,274,298	37,274,400	+42	-60	+102	-32	23.08	6.33
	16W	37,275,188	37,275,162	37,275,272	+26	-84	+110	-24	22.62	7.48
	8W	37,276,034	37,276,016	37,276,116	+16	-77	+93	-41	21.92	16.45
	4W	37,276,877	37,276,873	37,276,831	+4	-46	-42	-176	21.41	40.27
April 29, 1971 (1843Z - 1908Z)	1000W	37,267,523	37,267,332	37,267,472	+191	+51	+140	+6	11.61	5.83
	1000W	37,268,819	37,268,657	37,268,799	+162	+20	+142	+8	14.55	6.09
	1000W	37,269,684	37,269,555	37,269,676	+129	+8	+121	-13	22.52	6.30
	1000W	37,270,547	37,270,412	37,270,548	+135	-1	+136	+2	8.21	5.57
	1000W	37,271,712	37,271,590	37,271,730	+122	-18	+140	+6	11.17	6.05
	1000W	37,272,269	37,272,177	37,272,302	+92	-33	+125	-9	20.55	6.79

TABLE 4.2 SIMULTANEOUS RANGING DATA ON ATS-5 (MODE 1 OPERATION)

(Non-coherent ranging tones, 500 kHz - C-Band, 20 kHz - L-Band)

Measurement Date	L-band Xmtr. Power	Range (Meters)			Difference in Range (Meters)				Sigma (Meters)	
		Ephemeris	C-band	L-band	E-C	E-L	L-C	Corrected L-C	C-band	L-band
March 29, 1971	1000W	37,244,351	37,244,116	37,240,520	+235	+3831	-3596	+19	1.49	4.02
(1917Z - 1929Z)	1000W	37,245,661	37,245,438	37,241,851	+223	+3810	-3587	+27	1.46	3.95
	1000W	37,246,533	37,246,317	37,242,732	+216	+3801	-3585	+29	1.47	4.13
April 14, 1971	1000W	37,249,717	37,249,426	37,245,862	+291	+3855	-3564	+50	7.15	9.57
(1836Z - 1849Z)	500W	37,250,984	37,250,703	37,247,127	+281	+3857	-3576	+38	5.77	9.05
	250W	37,252,054	37,251,780	37,248,189	+274	+3856	-3582	+34	1.37	12.64
April 21, 1971	500W	37,261,792	37,261,494	37,257,903	+298	+3889	-3591	+23	1.70	10.60
(1853Z - 1904Z)	250W	37,262,940	37,262,655	37,259,055	+285	+3885	-3600	+14	1.64	14.92
	64W	37,263,864	37,263,580	37,259,922	+284	+3942	-3658	-44	1.74	26.79
April 26, 1971	1000W	37,262,213	37,261,922	37,258,374	+291	+3839	-3548	+66	0.79	5.07
(1837Z - 1852Z)	500W	37,263,088	37,262,811	37,259,264	+277	+3824	-3547	+67	0.79	4.74
	250W	37,264,187	37,263,927	37,260,374	+260	+3813	-3553	+61	0.83	4.53
	64W	37,265,076	37,264,824	37,261,278	+252	+3798	-3546	+68	0.84	4.49
April 29, 1971	*1000W	37,259,904	37,259,576	37,255,953	+328	+3951	-3623	-9	10.08	4.86
(1808Z - 1836Z)	*1000W	37,261,861	37,261,592	37,257,956	+269	+3905	-3636	-22	15.93	5.76
	1000W	37,263,607	37,263,316	37,259,741	+291	+3866	-3575	+39	1.41	4.72
	1000W	37,264,474	37,264,199	37,260,616	+275	+3858	-3583	+31	1.44	4.62
	1000W	37,265,344	37,265,085	37,261,503	+259	+3841	-3582	+32	1.02	4.52

*Special Test (ATSR in Mode 5)

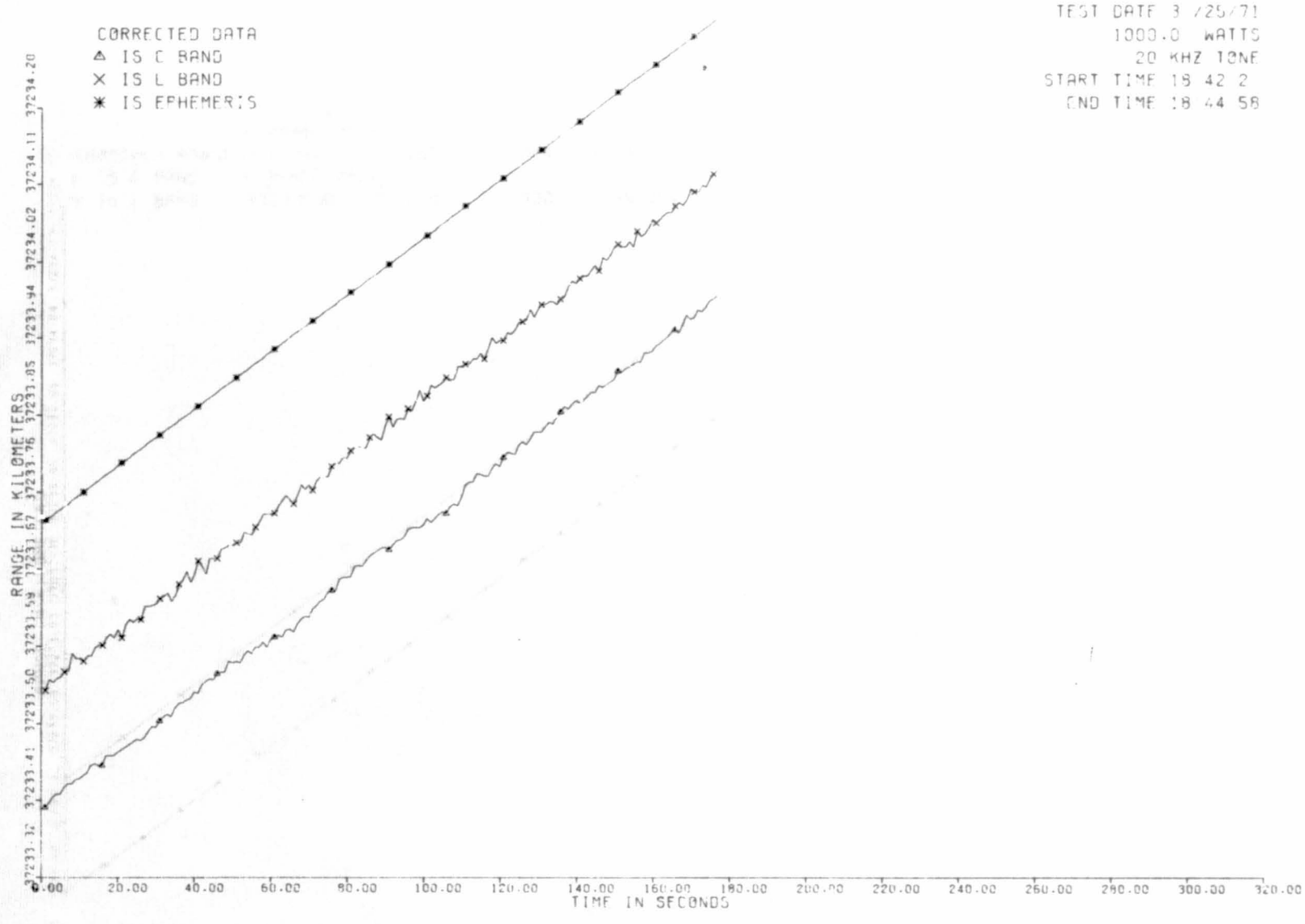

Figure 4. 2 Corrected Data Plot: 1, 000 Watts

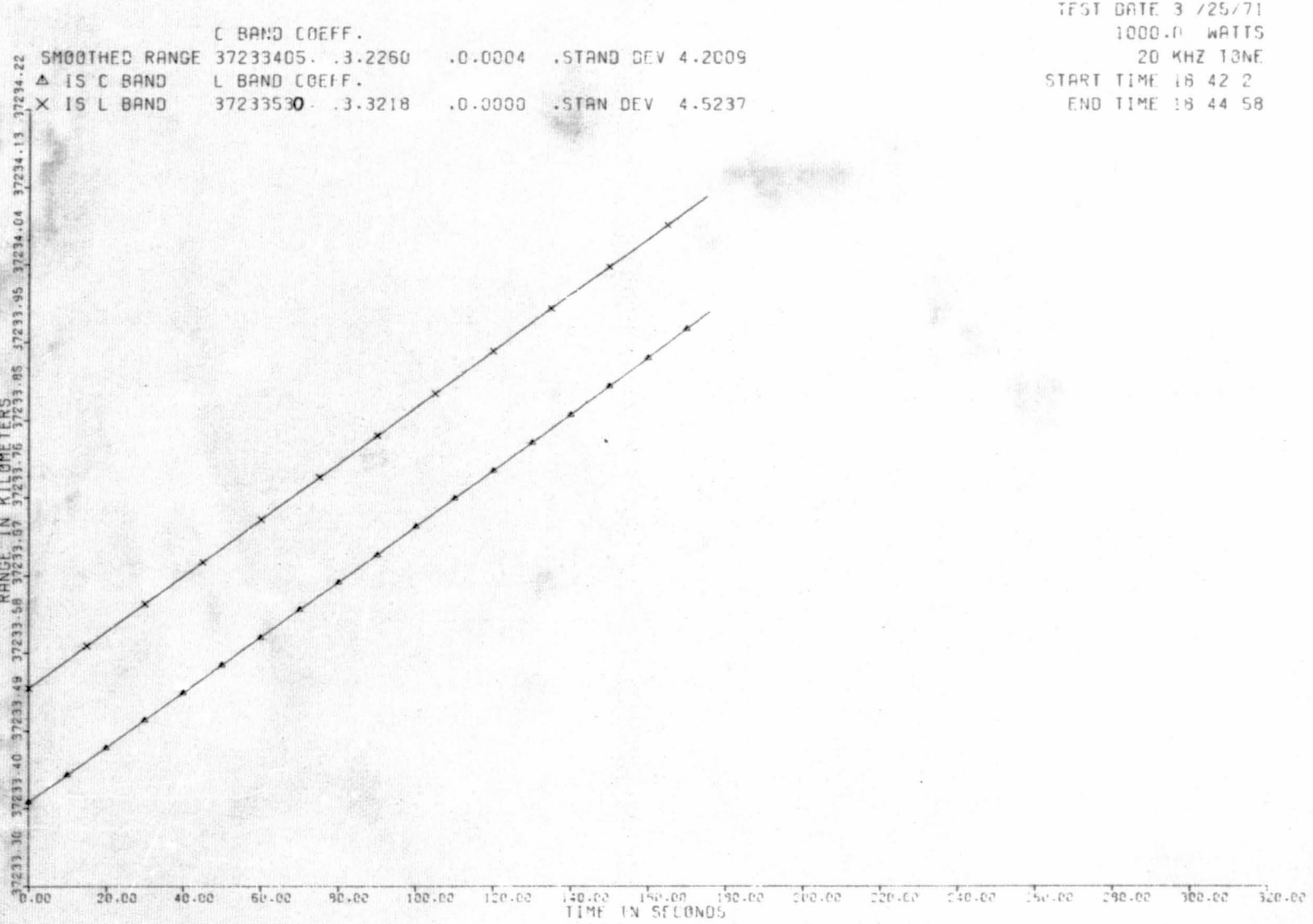

Figure 4.3 Smoothed Range Plot: 1,000 Watts

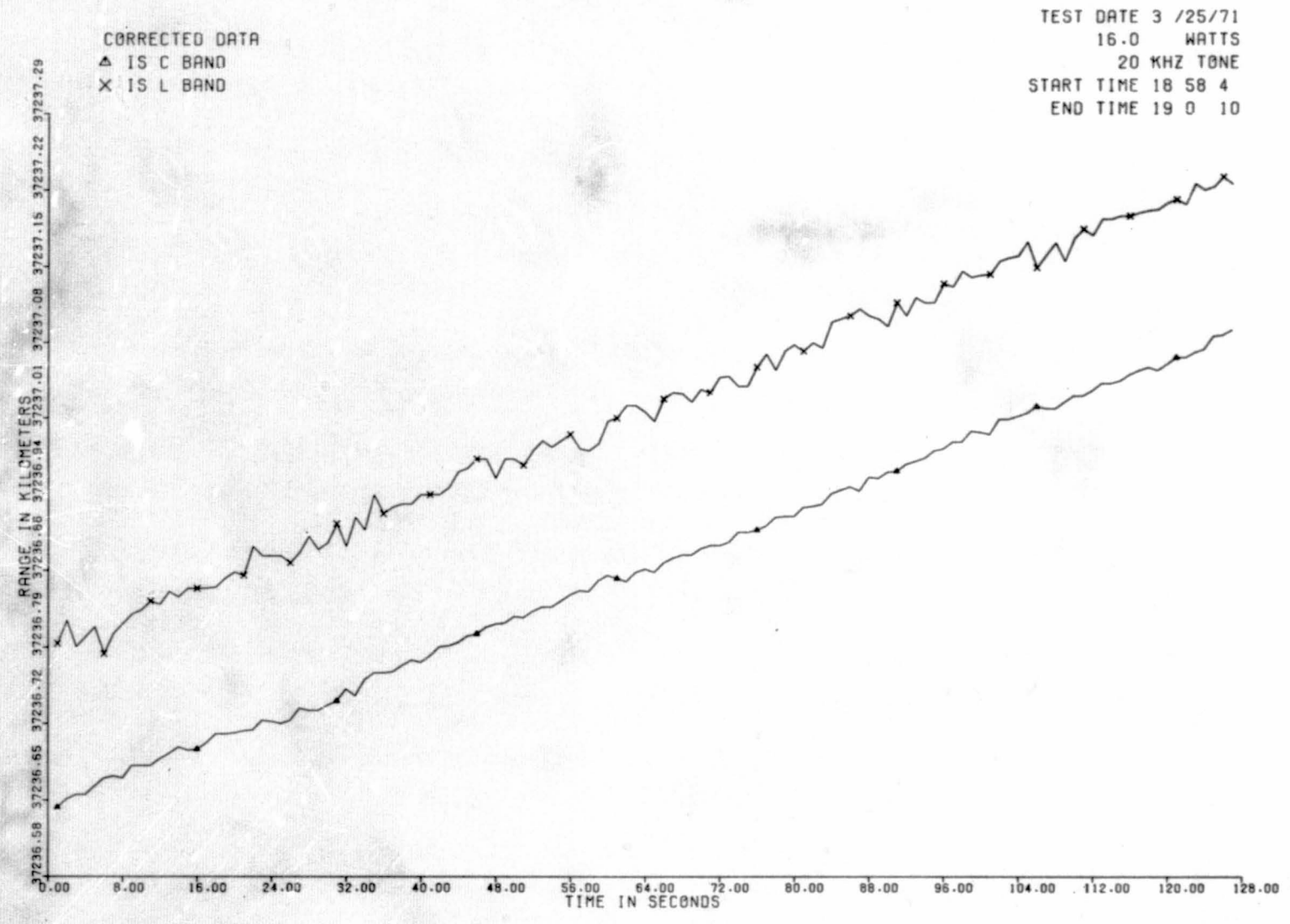

Figure 4.4 Corrected Data Plot: 16 Watts

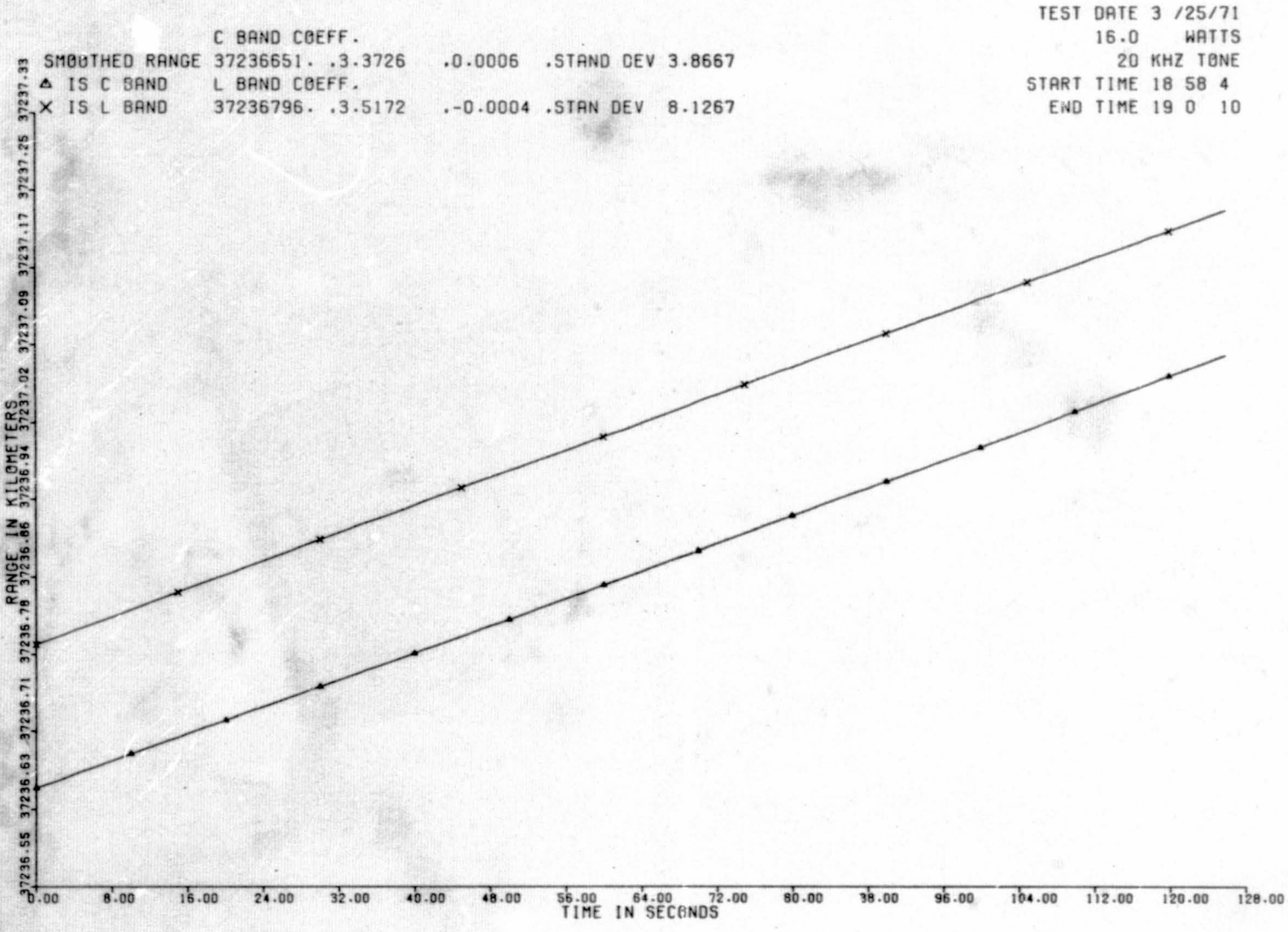

Figure 4.5 Smoothed Range Plot: 16 Watts

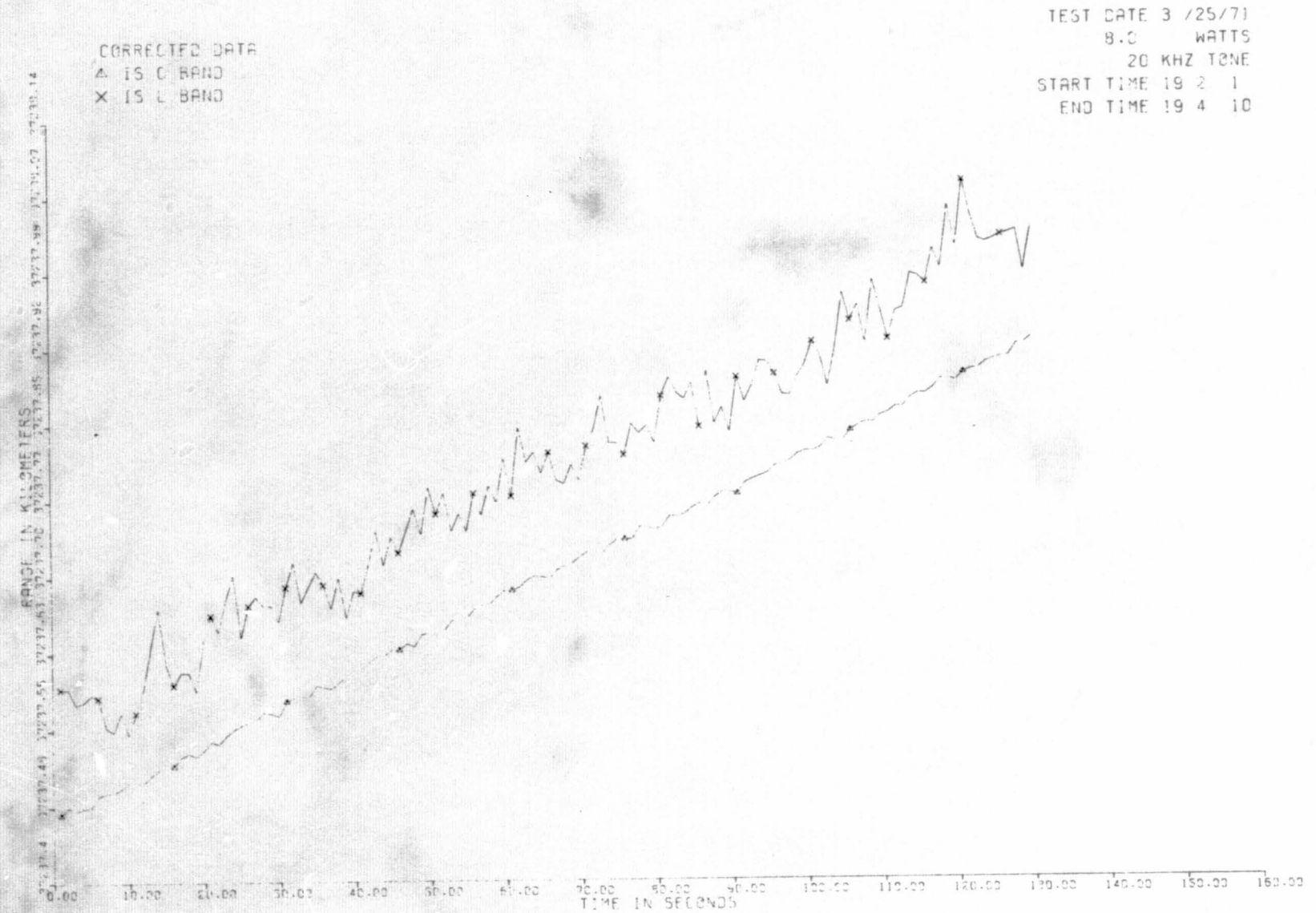

Figure 4.6 Corrected Data Plot: 8 Watts

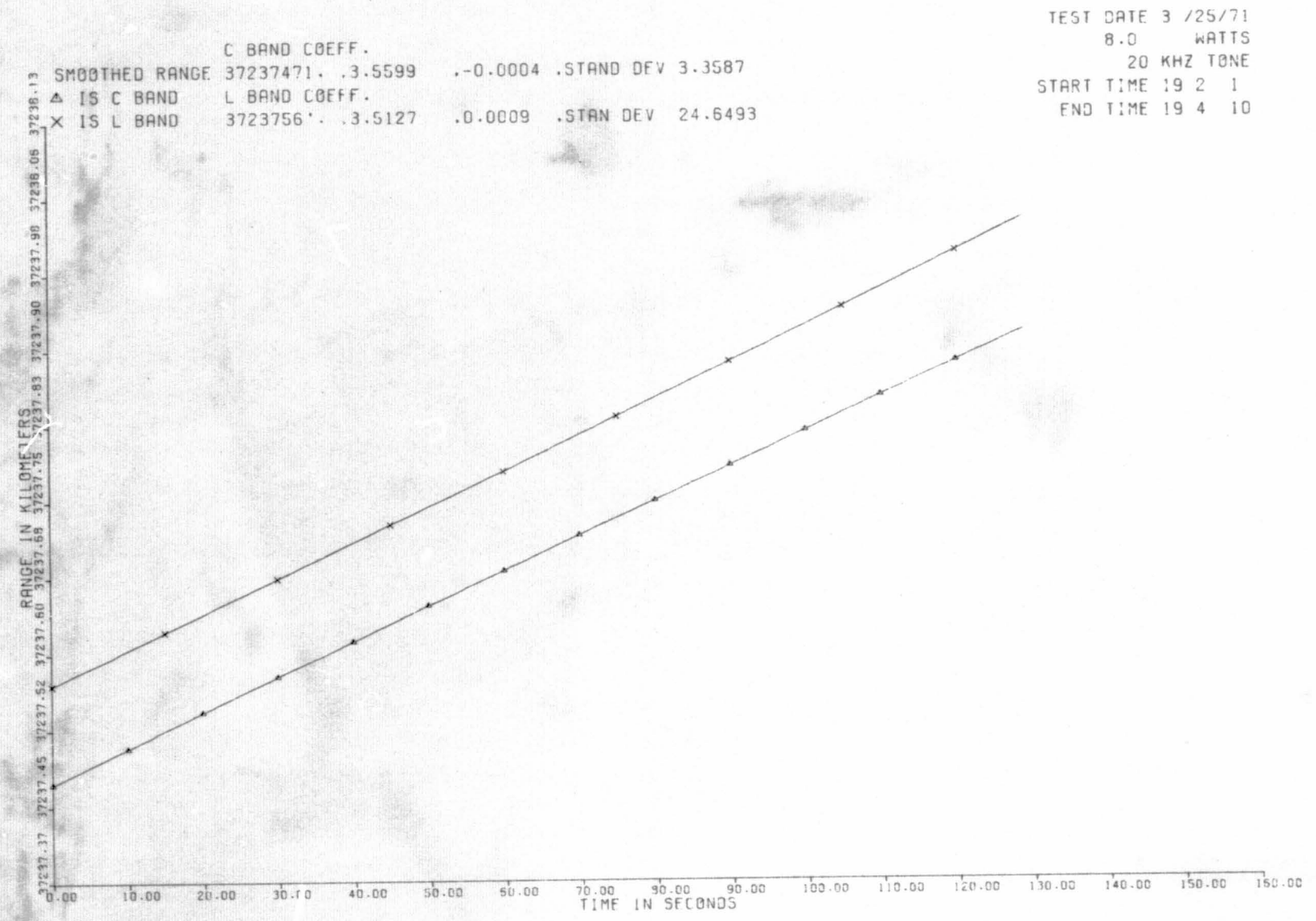

Figure 4.7 Smoothed Range Plot: 8 Watts

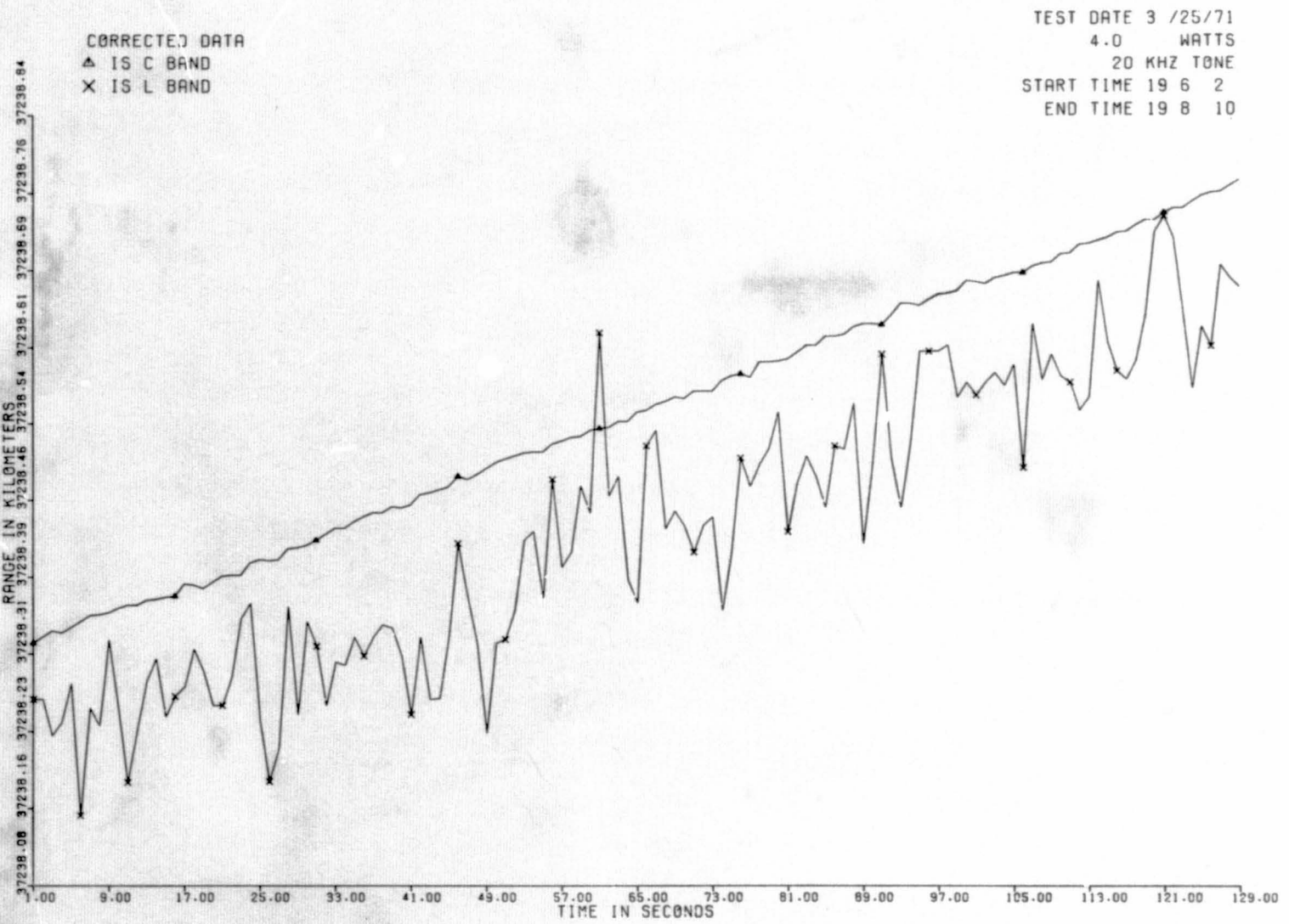

Figure 4.8 Corrected Data Plot: 4 Watts

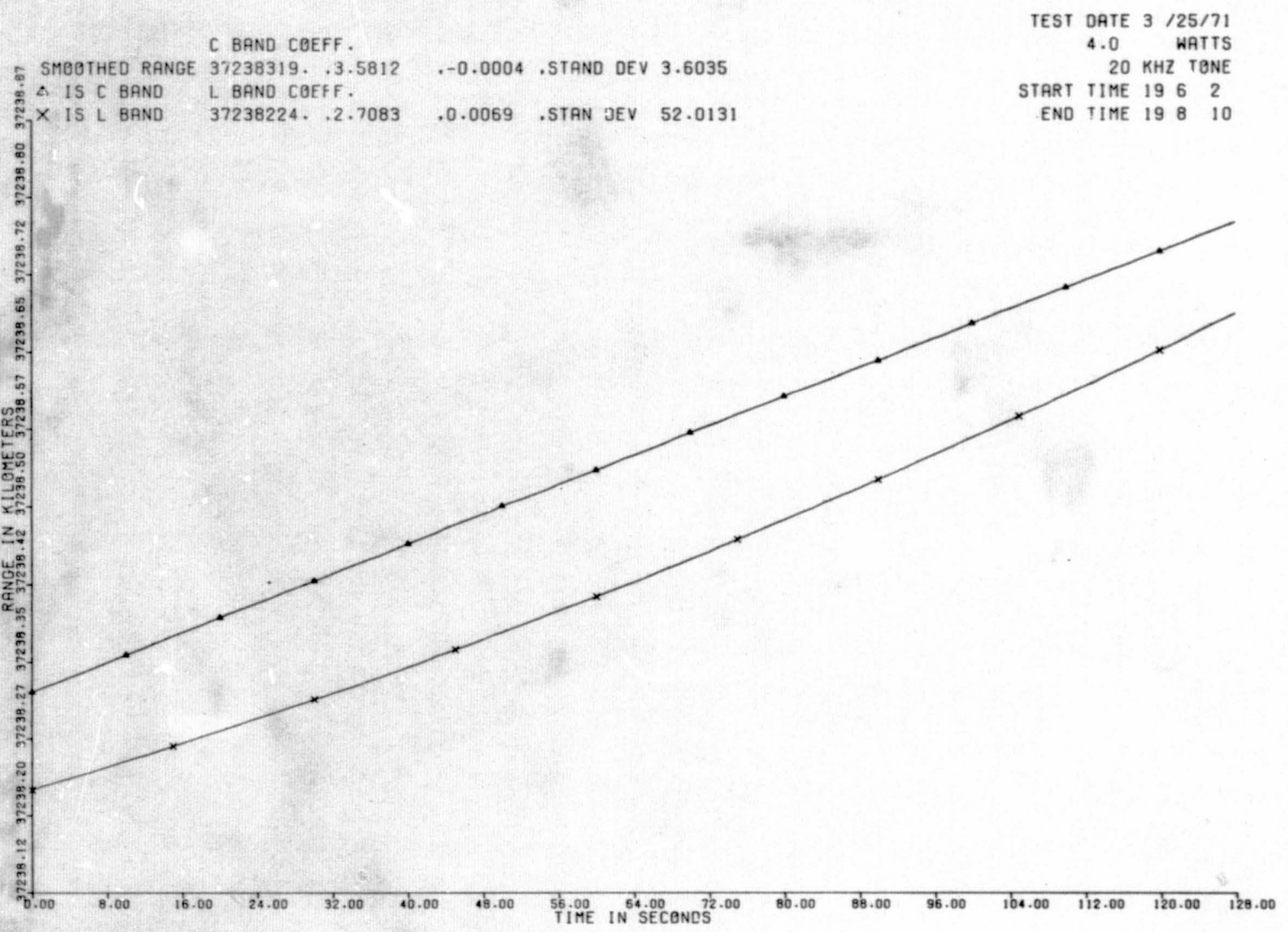

Figure 4.9 Smoothed Range Plot: 4 Watts

was included. The other plots included are 16 watts, 8 watts, and 4 watts. In each case the corrected data plot and the smoothed range plots are given for each test. The ephemeris data appears only on the first plot (figure 4. 2). All other plots were made before the ephemeris data had been obtained. The slope of the graphs is caused by the movement of the satellite during the test period. The upward slope indicates that the satellite was moving away from the measuring station. The plots of figures 4. 2, 4. 4, 4. 6, and 4. 8 show the raw experimental data with the L-band and C-band points "corrected" for lane ambiguity. The "smoothed range" curves of figures 4. 3, 4. 5, 4. 7, and 4. 9 were obtained by fitting the raw data as shown on the previous curves to a second degree polynomial using the method of "least mean squared fit." The program for the smoothed range curves also computes for each range curve the standard deviation (sigma), the zero time intercept, and the velocity and acceleration coefficients.

The data obtained during this series of simultaneous ranging tests was also computer processed as described in paragraph 3. 2. 3 to provide all the statistical data output plots, such as: autocorrelation, crosscorrelation, scatter plots, probability density distribution, and cumulative distribution. A detailed analysis of these statistical plots, giving typical examples, is presented in Section 5.

4. 1. 4 Analysis

The data plots of figures 4. 2 through 4. 9 are typical examples of the measurements obtained for this simultaneous C-band vs L-band ranging experiment. These plots include variations in L-band transmitted power from the highest level of 1000 watts to the lowest of 4 watts. The "smoothed range" plots list at the upper left corner the coefficients of the second degree curve which has been fitted to the range data. The first number (approximately 37, 238, 000) is the range in meters to the spacecraft at the start of the data run (time 0. 00). This value has been tabulated in tables 4. 1 and 4. 2.

In examining each of the plots of the "corrected data" (figures 4. 2, 4. 4, 4. 6, and 4. 8), the effects of degrading the S/N ratio can be seen. As the L-band transmitted power was decreased, the L-band range measurements progressively had more jitter, or fluctuation, in the readings. The standard deviation varied from 4. 52 meters at the 1000 watt power level to 52. 01 meters at the 4 watt power level. This lower power has a detrimental effect on the accuracy of the individual ranging measurements. Since the C-band ranging was performed at its full power level, those simultaneous C-band readings can be considered as a standard with which to compare the

L-band measurements. This comparison is tabulated in table 4.1 as the Difference in Range (L-C) column. For March 25, 1971, as the transmitted power was decreased, another degradation can be seen which was caused by the lower signal levels. The L-C differential decreased and even reversed sign indicating that these lower signal levels created a shift in the L-band range readings. This phenomenon is also present in the tabulated readings of table 4.1 for other days. This shift was caused by a noise bias effect in the range tone filter in the front end of the demodulation drawer. This filter has since been redesigned to correct this biasing condition.

In examining the three Difference in Range columns, it is seen that the L-band range is longer than the C-band range (except at low transmitted power levels). As was previously explained in paragraph 4.1.3, this discrepancy was due to an error in the initial "zero set" when ranging to the collimation tower and to a difference in path lengths. This made all L-band range readings approximately 134 meters too long. By making this correction, the E-L column will increase by 134 meters while the L-C column will decrease by 134 meters. This would now make the L-band and the C-band ranging measurements essentially equal. However, both of these readings are still 200 to 300 meters away from the ephemeris range which was calculated from the Goddard orbit determination program. The reason for this difference was not revealed until the results of the 24-hour simultaneous experiment were processed. When this ephemeris data was observed over a day, a cyclic variation was discovered in the (E-C) or (E-L) differences which showed that this ephemeris data actually varied from +450 meters longer than the C-band reading to -100 meters shorter than the reading. This is discussed in greater detail in paragraph 4.3.4.

In examining the test results presented in tables 4.1 and 4.2, it is seen that a large difference between the L-band range readings and either ephemeris or C-band range exists when operating in mode 1 (table 4.2) as compared to the difference in the same columns for mode 5 (table 4.1) operation. This is caused by the L-band readings obtained in mode 1 being much shorter than they should be. The L-band ranging system was dismantled and moved from Mojave before this data was processed and this discrepancy discovered; therefore, the true cause of this problem could not be investigated. However, the following is theorized. The mode 1 configuration used the frequency synthesizers to provide the 20-kHz range measuring tone for the L-band ranging system. If, in connecting these synthesizers, a phase reversal of the ranging tone occurred for either the reference or modulation in respect to the phase of the

ATSR system, then the measurements could be off 180° or 1/2 of a lane. For the 20-kHz ranging tone, the one-way lane width is 7496 meters or 3748 meters for 1/2 of a lane. Since the L-band data is short, then this 1/2 lane value is added to the L-band reading. If the 134-meter "zero set" error is removed, this correction value becomes 3614 meters. This is the constant used for the "corrected L-C" column in the table 4.2. It is seen that this 1/2 lane correction does cause the L-band ranging reading to now be approximately the proper magnitude; thereby, giving credibility to this theory for the cause of the discrepancy in the L-band readings.

In table 4.2 on April 29, 1971 the two test runs with the asterisk were special in that the synthesizers were used for the L-band range measurement, but the ATSR system was switched to its 20 kHz ranging tone. The effect of this caused the standard deviation of the C-band measurements to be much higher than corresponding readings for the same day when operating in mode 1 (500 kHz tone). However, the L-C difference remained essentially the same as the other readings. This test demonstrated that the resultant bias error is not a function of the ATSR tone frequency, but is due to the phase difference between the ATSR tone and the tone provided by the L-band synthesizer.

With a 20 kHz range tone used for the L-band measurements, a large number of ambiguity lanes (approximately 5000 lanes) exist and a small error in the precision of this measuring frequency can cause a large error in the range reading due to the cumulative effect. Calculations show that if the 20-kHz measuring tone is only 0.1 hertz off frequency, the measurement error will be 187 meters. In the "corrected L-C" column of table 4.2 the L-band reading appears to be roughly an average of 40 meters longer than the C-band readings. If the synthesizer frequency set was only 0.02 hertz high in frequency (20.00002 kHz), the error would be 38 meters. Thus, the use of this L-band ranging system at locations where there is no ATSR ranging system will require a highly accurate source for the 20-kHz measuring tone. Also, before the use of an external tone source (synthesizer), an investigation should be conducted to insure that this source does not cause the phase reversal and resultant 1/2 lane error in the L-band reading.

4.1.5 Conclusions

From the data obtained in the simultaneous C-band and L-band experiment, the L-band ranging system compared very well with the ATSR C-band ranging system. If the data is examined which exhibits a low standard deviation and thus good signal conditions, it is found that the average L-band range agrees with the C-band range to

within plus or minus 15 meters.

It was found that when the ranging tone was derived from an external source and not the ATSR equipment, the possibility of error was introduced. With the awareness of these problems and care in configuring the ranging system, errors can be eliminated.

It was also shown that the L-band ranging data tended to become "noisy" when the power level dropped below 64 watts. With the 15-foot antenna at Mojave, this was an effective radiated power of +53 dBw. Thus, when future applications of this ranging system are comtemplated, these conditions should be considered with respect to the accuracy of the ranging data.

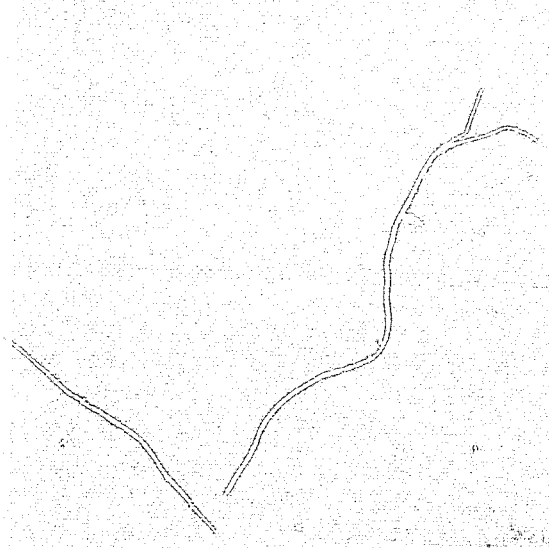

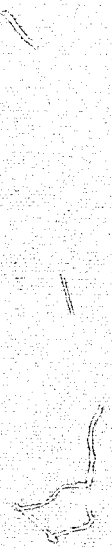

4.2 SIMULTANEOUS C-BAND AND VHF RANGING EXPERIMENT

4.2.1 Objective

The primary objective of the simultaneous C-band and VHF ranging experiment was to obtain a comparison of range measurements to a given satellite using C-band with the GSFC ranging receiver, and VHF with the ATSR ranging system at the same time. Simultaneous ranging runs were made to both ATS-1 and ATS-3 for this experiment. The C-band measurements, as in the simultaneous C-band and L-band experiment, were used as the measuring base for establishing the relative VHF ranging accuracy, since the C-band data was the best available information.

4.2.2 Test Description

The test setup for performing the simultaneous C-band and VHF ranging experiment is shown in figure 4.10. In this experiment the station ATSR ranging system was used in conjunction with the VHF equipment to establish an unambiguous spacecraft range. The GSFC ranging receiver was used in conjunction with the C-band equipment to provide an ambiguous range reading which was then corrected for lane ambiguity against the ATSR range reading.

All simultaneous C-band and VHF tests were performed with the ATSR equipment in mode 5. Mode 5 provides a maximum ranging tone frequency of 20 kHz. No higher frequency ranging modes can be used with the VHF transponders on ATS-1 and ATS-3 because the transponder bandwidth is only 100 kHz. The higher frequency ATSR range tones fall outside the transponder passband.

The two ranging systems were completely separate in this experiment, except that the ATSR ranging tone was used for both systems. The ATSR ranging tone was used to phase modulate an HP 5105 frequency synthesizer which produced a carrier frequency (74.61 MHz) of one half the final VHF transmission frequency of 149.22 MHz. The frequency synthesizer output was amplified sufficiently to drive the VHF transmitter, where the carrier frequency was doubled and the level amplified to approximately one kilowatt.

The 20-kHz modulated 70-MHz output from the ATSR equipment was used to drive the C-band transmitter where the signal was up-converted and amplified to a level of approximately five kilowatts. The 70-MHz output from the C-band receiver was fed to the GSFC ranging receiver, rather than to the ATSR, as it is in the normal ranging mode. The GSFC ranging receiver was designed to operate on a pulsed signal which was received from ATS-5. Consequently, it was necessary to obtain a one

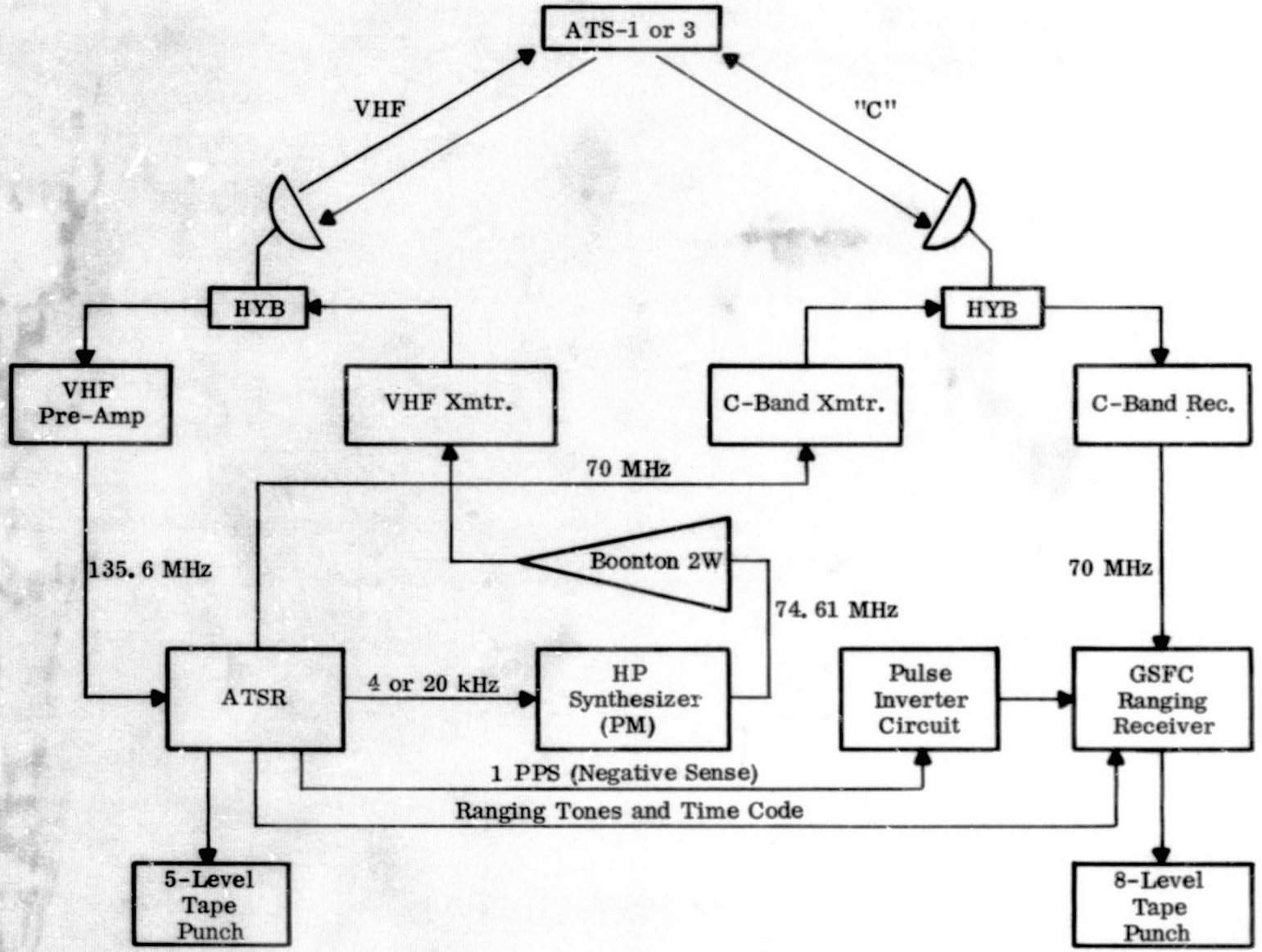

Figure 4.10 Simultaneous C-Band and VHF Ranging Block Diagram

pulse per second signal from the ATSR equipment to gate the ranging receiver. A range reading was punched out on eight level paper tape on a one reading per second basis. The reference tone from the ATSR equipment was delivered to the GSFC ranging receiver to use in making the phase determination.

Calibration or zero setting of the two ranging systems performed similarly to the zero setting for the simultaneous C-band and L-band ranging experiment. The primary difference in the C-band calibration is that the GSFC ranging receiver reads out in one-way range delay time. Thus, the readout is set to 11.99 microseconds, which is the one-way C-band range to the collimation tower rather than 23.98 microseconds or two-way range as is used when the ATSR is used on the C-band link. Calibration of the VHF system using the ATSR equipment was accomplished in the same manner as when the C-band link is used. The calibration for the VHF system requires setting the ATSR readout to -4.7 microseconds. Since the ATSR cannot be set to negative numbers it was necessary to set the readout to 124995.30 microseconds which is 4.7 microseconds less than the reset or zero range reading. It should be noted that the ATSR equipment maximum reading is 124999.99 microseconds which is equivalent to an 8-Hz wavelength.

Antenna physical location at Mojave played a part in the range measurements for the C-band and VHF experiment. No correction was made in the calibration of the ranging systems to account for the difference in physical position of the VHF and C-band antennas. The correction must be taken into consideration when the processed data is analyzed. When ranging to ATS-1, the C-band range is 80 meters longer than the VHF range due to antenna location. When ranging to ATS-3, the VHF range is 107 meters longer than the C-band range for the same reason. The antenna geometry included in Section 6 shows the various antenna locations and spacecraft directions with respect to the Mojave station. This section should be consulted for additional information on the physical layout of the Mojave station and the antenna location.

A limited number of test days were obtained for simultaneous C-band and VHF ranging measurements. Consequently, all test conditions in terms of power and modulation index were made at nominal station conditions. For the VHF transmitter the nominal power level was at least 500 watts when ranging to either spacecraft. Due to the difference in spacecraft receiver front ends, the C-band power level was at least 500 watts for ATS-3 ranging and 5000 watts for ATS-1 ranging. All data runs were approximately three minutes in length.

4.2.3 Experimental Test Results

The results of the simultaneous C-band and VHF ranging measurements performed at the Mojave station to ATS-3 are summarized in table 4.3. Table 4.4 is a data summary of the same results to ATS-1. All listed data was taken in mode 5 using the 20-kHz range tone.

For both tables column 1 lists the date and start time for the individual three minute data runs. Column 2 lists the one-way range to the spacecraft as obtained from the ephemeris magnetic tape. Column 3 lists the C-band range as measured on the GSFC ranging receiver after it has been corrected for lane ambiguity. Column 4 provides the VHF range as measured on the ATSR equipment after it has been corrected for lane ambiguity and divided by two, making it one-way range. Columns 2, 3, and 4 are obtained from the smoothed range plots and correspond to the respective ranges at the beginning of the individual data runs. Columns 5, 6, and 7 show the differences between the ephemeris and C-band ranges, ephemeris and VHF ranges, the VHF and C-band ranges, respectively. Columns 8 and 9 are the standard deviation (or sigmas) of the C-band and VHF data, respectively. Columns 10 and 11 present the same data as columns 6 and 7 except that the VHF data has been corrected to account for the antenna separation. The VHF range measurements have been corrected to place the VHF antenna location at the same point as the C-band antenna. Thus, column 11 does provide a measure of the propagation path length difference between the two range measurements for the two frequency bands.

Figure 4.11 is a plot of range difference measurements between the simultaneous VHF and C-band range data. As noted on the plot the data covers 6/19/71 and 6/25/71, which are the only two days on which a number of data runs were obtained which covered a significant time span. Each day data was taken over approximately 5 hours. Figure 4.12 depicts plots of ephemeris minus VHF range and ephemeris minus C-band range for the same days and times as given on figure 4.11.

Figure 4.13 is a plot of a typical three minute data run depicting the corrected raw data for C-band and VHF and the ephemeris data as extracted from the GSFC supplied magnetic tape. This particular run was made on 6/19/71, at 0310 Zulu as noted on the figure. The vertical axis is one way range in kilometers while the horizontal axis is time in seconds. Figure 4.14 is a plot of the same information after a second degree polynomial curve was fitted to the raw data. At the top left of the figure is a listing of the coefficients of the curves to which the data was fitted. For

TABLE 4.3 SIMULTANEOUS C-BAND AND VHF RANGING TO ATS-3

Measurement Date/Time (Zulu)	Range (Meters)			Difference in Range (Meters)			Sigma (Meters)		VHF Corrected For Ant. Sepearation		Remarks
	Ephemeris	C-Band	VHF	E-C	E-VHF	VHF-C	C-Band	VHF	E-VHF	VHF-C	
6/10/71											
181000	38,214,045	38,214,055	38,215,313	-10	-1268	1258	6.25	15.84	-1161	1151	
181500	38,212,193	38,212,203	38,213,450	-10	-1257	1247	7.47	3.22	-1150	1140	
182000	38,210,406	38,210,416	38,211,681	-10	-1275	1265	7.38	11.73	-1168	1158	
182556	38,208,368	38,208,379	38,209,655	-10	-1287	1277	7.11	63.45	-1180	1170	
183000	38,207,026	38,207,029	38,208,312	-3	-1286	1283	6.19	14.01	-1179	1176	
183500	38,205,436	38,205,445	38,206,733	-9	-1297	1288	7.13	5.71	-1184	1181	
184000	38,203,913	38,203,918	38,205,199	-5	-1286	1281	6.97	6.36	-1179	1174	
6/19/71											
031003	38,507,771	38,507,397	38,507,928	374	-157	531	5.96	6.62	-50	424	
033003	38,520,039	38,519,661	38,520,163	378	-124	562	6.15	6.22	-17	455	
040002	38,537,575	38,537,166	38,537,578	409	-2	412	6.97	9.99	105	305	
043014	38,553,946	38,553,519	38,553,891	427	55	372	7.50	149.6	162	265	Many bad points on VHF
050002	38,568,569	38,568,124	38,568,396	445	173	272	7.06	6.52	280	165	
053002	38,581,514	38,581,053	38,581,294	461	220	241	6.66	6.62	327	134	
060003	38,592,469	38,591,970	38,592,194	499	275	224	970.3	7.71	382	117	Many bad points on C-Band
063001	38,601,229	38,600,719	38,600,922	510	307	203	6.07	46.80	414	96	Large spike on VHF
070003	38,607,673	38,607,143	38,607,340	530	333	197	8.38	16.13	440	90	
073003	38,611,658	38,611,105	38,611,342	553	316	237	7.98	6.71	423	130	
080002	38,613,114	38,612,533	38,612,789	581	325	256	7.52	5.63	432	149	
6/25/71											
073802	38,699,789	38,698,954	38,699,286	835	503	332	9.34	4.57	610	225	
080020	38,698,961	38,698,120	38,698,409	841	552	281	10.50	5.14	659	174	
083002	38,695,706	38,694,824	38,695,107	882	599	283	11.15	6.32	706	176	
090003	38,689,954	38,689,026	38,689,324	928	630	298	9.20	6.20	737	191	
093203	38,681,178	38,680,206	38,680,556	972	622	350	4.12	6.22	729	243	
100002	38,671,378	38,670,409	38,670,722	969	656	313	4.80	7.13	763	206	
103002	38,658,818	38,657,834	38,658,147	984	671	313	4.40	10.46	778	206	
105502	38,646,868	38,645,896	38,646,175	972	693	279	5.03	5.63	800	172	
122002	38,598,149	38,597,209	38,597,517	940	632	308	4.41	22.92	739	201	VHF one Bad Spike
125003	38,578,838	38,577,932	38,578,277	905	561	345	5.34	5.46	668	238	

TABLE 4.4 SIMULTANEOUS C-BAND AND VHF RANGING TO ATS-1

Measurement Date/Time (Zulu)	Range (Meters)			Difference In Range (Meters)			Sigma (Meters)		VHF Corrected For Ant. Seperation		Remarks
	Ephemeris	C-Band	VHF	E-C	E-VHF	VHF-C	C-Band	VHF	E-VHF	VHF-C	
6/9/71											
185002	38,235,416	38,235,330	38,236,393	286	-977	1063	85.77	3.89	-1057	1343	
185600	38,230,986	38,230,527	38,231,940	459	-954	1413	99.11	4.62	-1034	1493	
6/14/71											
180002	38,253,742	38,254,165	38,254,772	-423	-1030	607	194.5	4.77	-1130	687	4 Bad Spikes on C-Band
180507	38,251,241	38,251,665	38,252,279	-424	-1038	614	5.18	5.17	-1118	694	
181006	38,248,099	38,248,529	38,249,167	-430	-1068	638	4.79	20.20	-1148	718	3 Small Spikes on VHF
6/17/71											
181502		38,234,554	38,234,968			414	5.06	4.92		494	
182002		38,230,986	38,231,404			418	5.22	5.01		498	
182502		38,227,305	38,227,720			415	5.44	5.46		495	
183002		38,223,602	38,224,026			424	5.61	4.53		504	
183502		38,219,795	38,220,204			409	5.14	4.12		489	
184002		38,215,389	38,216,318			429	5.79	7.67		509	

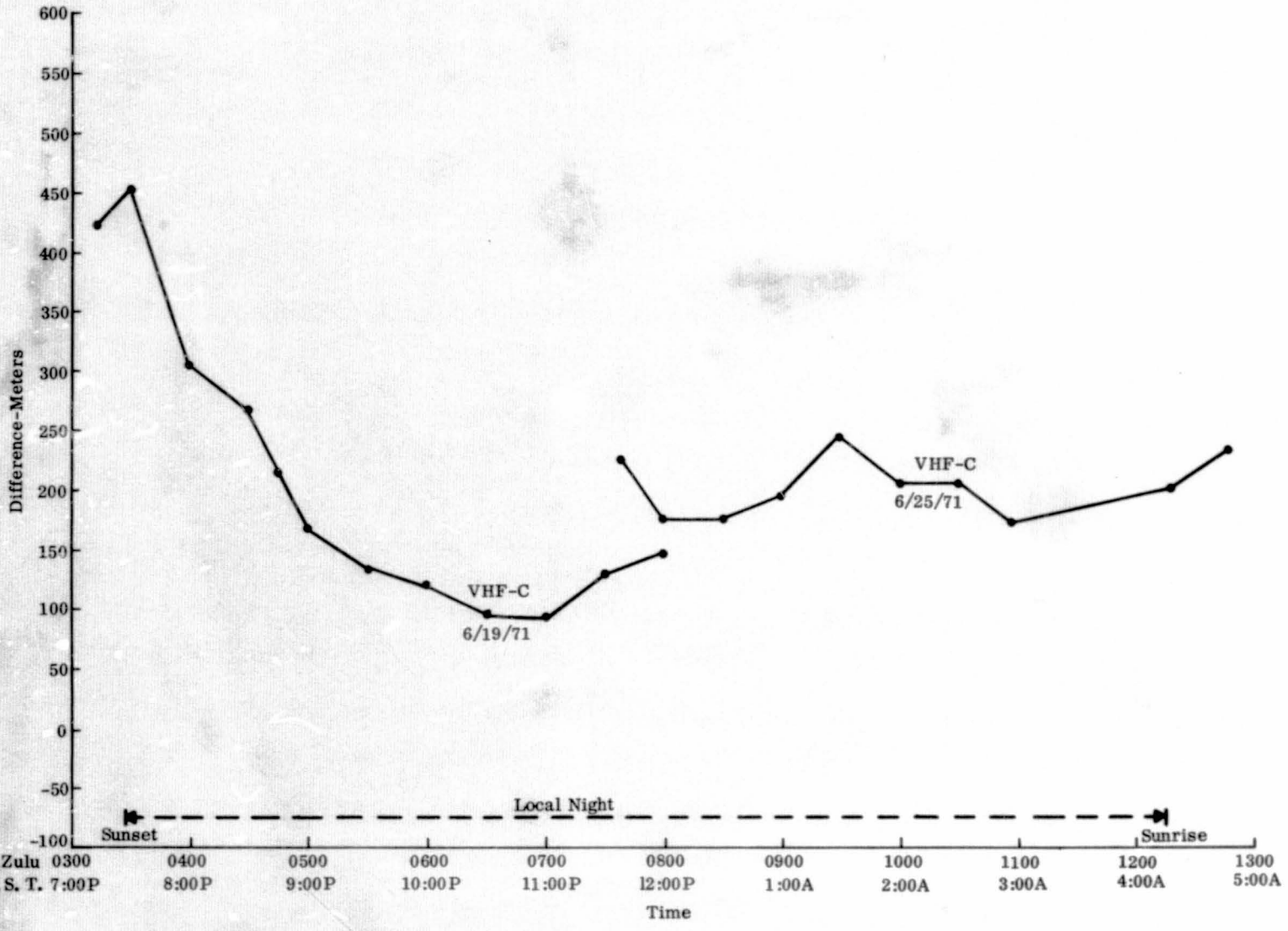

Figure 4.11 Diurnal Variation of the VHF Ranging Data as Compared to the C-Band Ranging Data

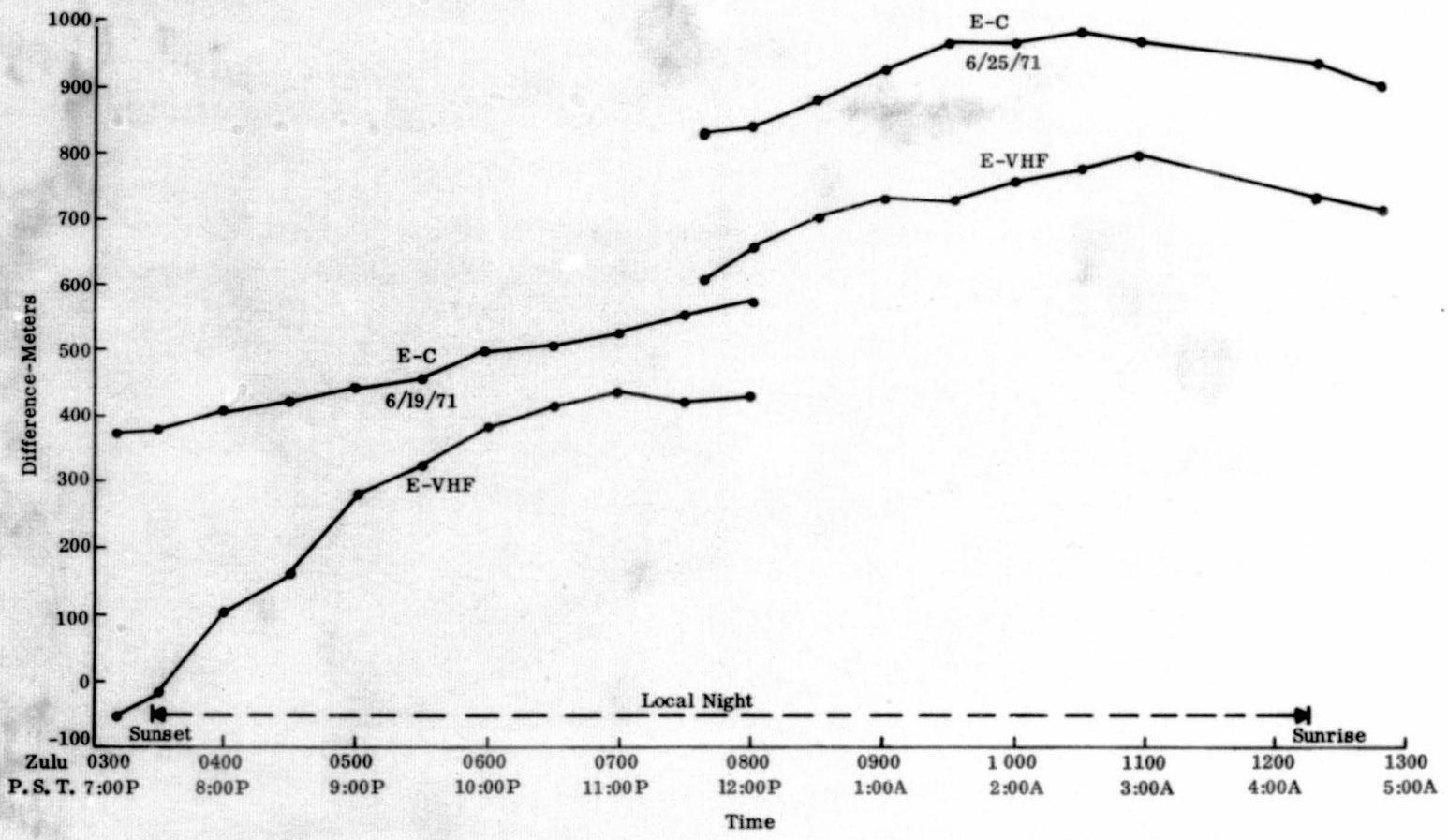

Figure 4.12 Comparison of C-Band and VHF Ranging Data to Ephemeris Ranging Data

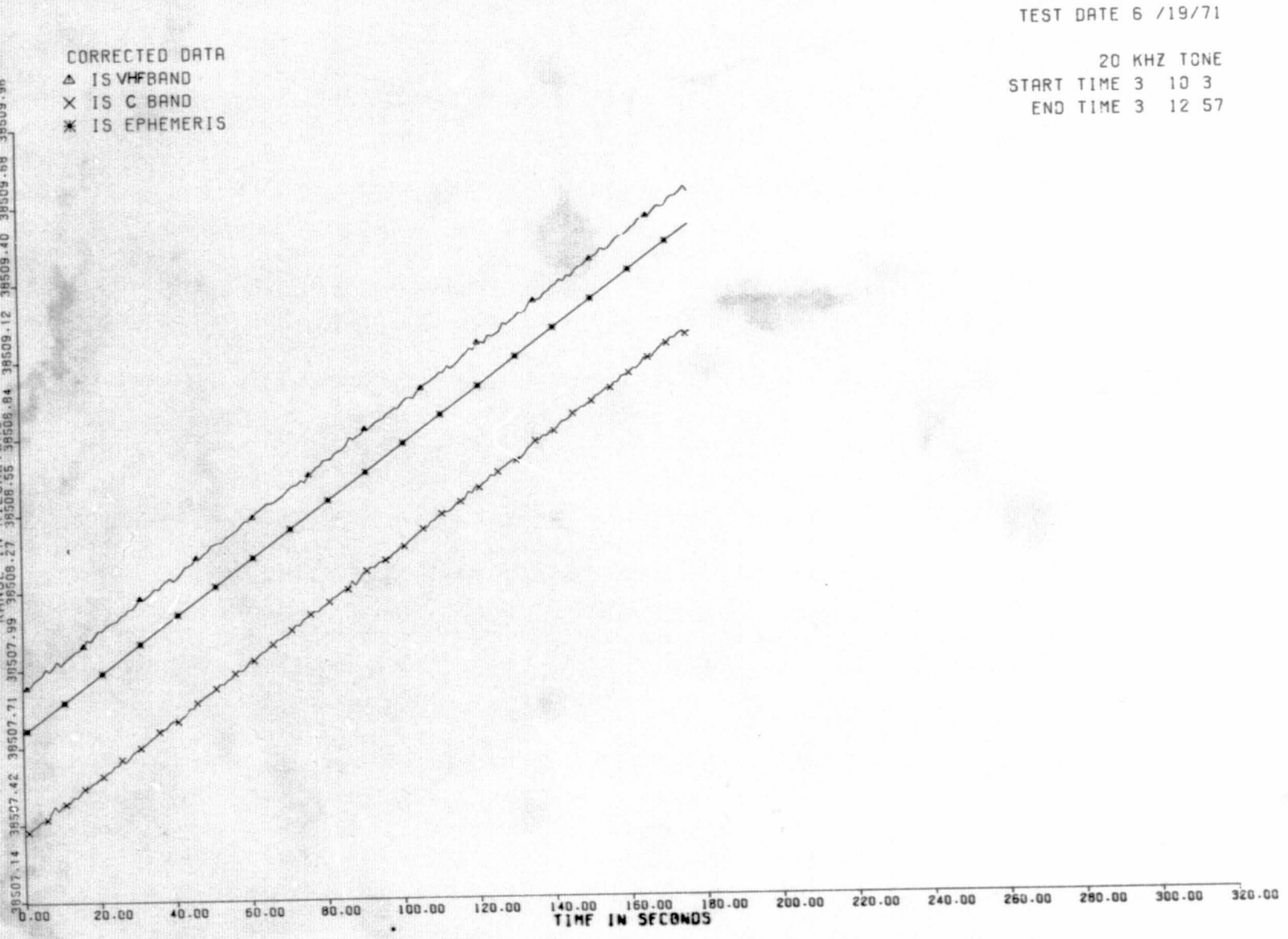

Figure 4.13 Corrected Data Plot: Simultaneous C-Band and VHF Ranging

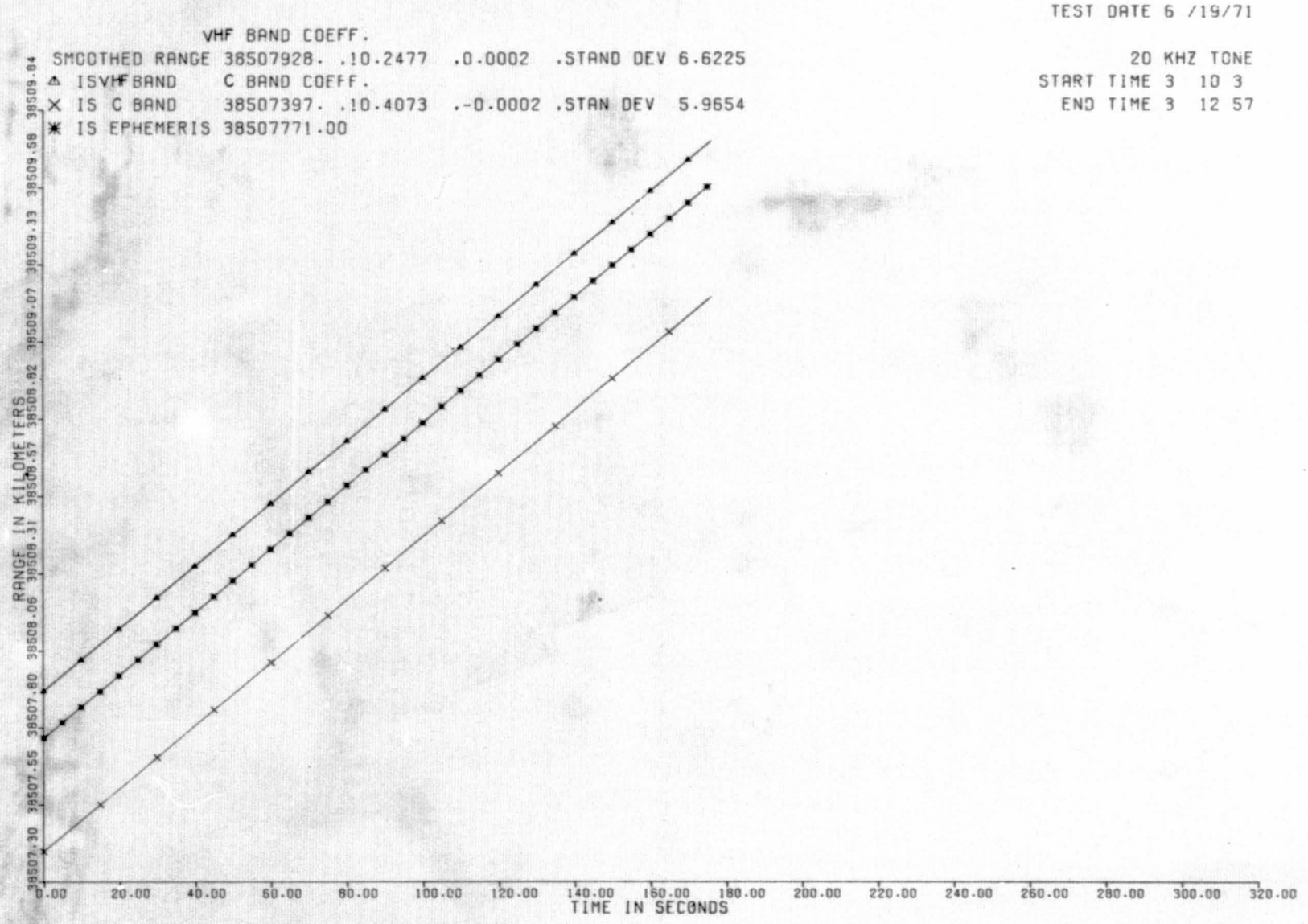

Figure 4.14 Smoothed Range Plot: Simultaneous C-Band and VHF Ranging

the VHF curve the range at the start of the run, on the vertical axis intercept; is given as 38,507,928 meters, with the velocity coefficient being 10.2477 meters per second and the acceleration coefficient being 0.0002 meters per second squared. The standard deviation is the deviation of the raw data about the smoothed curve and for the VHF is 6.6225 meters. The format of the C-band data is the same, while only the starting range is given for the ephemeris data.

All of the data was taken at the nominal transmit power levels for both VHF and C-band for the satellite being used in the test. All range measurements during these runs were made using the 20-kHz range tone.

4.2.4 Analysis

Several points were noted before the data presented in the previous paragraphs were analyzed. First, there was very limited data over a limited time period on which to base this analysis. Consequently, analysis of the simultaneous C-band and VHF range measurements was tempered by these constraints. Second, the results of an individual run, 6/25/71 12207, were distorted somewhat by one bad data point. This one bad point on the VHF range measurement caused the standard deviation to be 22.92 meters, although the data for the run was no more noisy than for the other data runs that day. The one bad point may have been a punch error, although it is not known for sure that this was the case. Where this situation occurred, a note was added to the remarks column of tables 4.3 and 4.4.

In the simultaneous C-band and VHF tests, as in the C-band/L-band tests, the C-band data was taken as the reference since it was the best available data for comparison. In comparing the ephemeris range to the C-band range the difference varied between -10 meters to +984 meters for ATS-3 and from -430 meters to +459 meters for ATS-1. This difference resulted from the prediction error in the orbit determination program. As noted in paragraph 4.3.2, this error was cyclic, varying substantially in magnitude over the period of a day. Discussion with GSFC personnel indicated that prediction accuracy was considered to be approximately one kilometer. This was substantiated by measurements made during this phase of the test program.

One of the most useful comparisons made with the data was that between C-band and VHF. As expected, the VHF range measurement in all cases was longer than the C-band measurement for the same moment of time. The value of (VHF-C) varied between +90 meters to +1181 meters for ATS-3 and from +489 to +1493 meters for ATS-1. These values were taken from columns 10 and 11 of tables 4.3 and 4.4 and

were corrected for the difference in antenna location. The values of the range difference for 6/19/71 and 6/25/71 were plotted on figure 4.11. Referring to this figure reveals the large difference that existed on 6/19/71 just prior to local sunset and the relatively large reduction in the difference immediately following sunset. After decreasing to a difference of 100 to 200 meters this value was relatively constant throughout the local night. There was some offset between the data of 6/19/71 and 6/25/71; however, the diurnal trend was as expected.

During the daylight hours the electron content of the ionosphere is high, reaching a peak near local noon. The electron content decreased rapidly after sunset and remained relatively constant during the dark hours. The high electron content during the day results in a group velocity less than the speed of light and less than the group velocity during the night time hours. The result was that the measured range during daylight hours was in general longer than the range measured during night time hours for a given spacecraft distance.

Tables 4.3, 4.4, and figure 4.11 indicate that the range difference between VHF and C-band does, in fact, appear to be much greater during the day than at night. Since the ionospheric group velocity varies on a $1/f^2$ basis, the VHF range data should contain a propagation delay error of approximately 1000 times the C-band propagation delay error. A report* gives the nominal noon time peak integrated electron content of 2.4×10^{17} electrons/meter^2 and a typical maximum value on the order of 10^{18} electrons/meter^2. Using these values for ATS-3 one obtains a VHF range bias during daytime hours between 735 meters and 3500 meters and a C-band range bias between 0.735 meters and 3.5 meters. For ATS-1 these values were somewhat lower because of the higher look angle to the spacecraft, being 586 meters and 2300 meters, respectively. Variations between daytime highs and nighttime lows in integrated electron content are wide, with a ratio of seven being a reasonable number. If this ratio is assumed, then we find that a nighttime range bias at VHF between 105 meters and 500 meters for ATS-3 is quite reasonable. The range difference measurements between VHF and C-band for both spacecraft fell within these values for both daytime and nighttime ranging periods.

Information on the actual electron content was requested from Dr. A. V. daRosa at Stanford University but the data was not currently available. Variations in

*Wernlein, C. E. "Summary Report 1540 to 1600 MHz Propagation Between Geostationary Satellites and Aircraft", NASA Document X-409-71-72, 1970.

electron content of the ionosphere are quite wide and vary with time of day, time of year, and sunspot activity. Consequently, without actual values available for the integrated electron content it was only possible to speculate whether or not the range bias was reasonable.

4.2.5 Conclusions

In analyzing the simultaneous C-band and VHF data, a significant point was the difference between the C-band and VHF range measurements and magnitude of the change between them from day to night. The range bias during mid-day for ATS-3 was approximately 1181 meters with VHF being longer. This is a reasonable value to expect as a result of the group velocity being less than the speed of light through the ionosphere. Plots of the range difference between VHF and C-band versus time of day followed the expected pattern for the limited amount of data that was obtained. That is, the VHF range exceeded the C-band range by approximately 1181 meters during the daytime peaks in electron content and 100 to 150 meters during the night time low in electron content.

The standard deviation of the data for both VHF and C-band was in the order of 5 to 6 meters for most of the data runs. On several runs spikes of unknown origin caused one or the other of the sets of data to exhibit a high sigma value. On those runs where spikes were noted, the data was, in general, quite good with the exception of the spikes. Keeping this in mind, it was found that very little difference in range jitter could be noted between the VHF and the C-band data.

With the conditions outlined in the preceding paragraphs in mind, the following conclusions were summarized.

1. Raw VHF range measurements included sufficient bias to render them unsatisfactory for accurate ranging or position location determination.
2. The daytime and nighttime range bias at VHF frequencies varied between 1181 and 100 meters, respectively, and these values were quite reasonable, based upon expected ionospheric electron content.
3. The variation in range bias followed the theoretical trend, being greater during daylight hours when the ionospheric electron content was high and lower during nighttime hours when the electron content was low.
4. Little difference was noted between the quality of the VHF ranging data and the C-band ranging data except for the VHF range bias.

4.3 SIMULTANEOUS 24-HOUR RANGING

4.3.1 Objective

The objective of this experiment was to perform simultaneous intervals of L-band and C-band ranging measurements on the ATS-5 satellite over a 24-hour period. Again the C-band measurements were used as a basis for establishing a reference against which the L-band measurements were compared. The results of this experiment provided a "one-shot" examination of the diurnal effects on this ranging data.

4.3.2 Test Description

The test setup for this 24-hour simultaneous C-band and L-band experiment was the same as that shown in figure 4.1A. This experiment was performed with the equipment operating in mode 5, such that the 20-kHz ranging tones were obtained from the station ATSR system. At the end of the simultaneous test runs, the experiment was reconfigured for sequential testing. This was a special test in which ranging measurements for both C-band and L-band were alternately made through the GSFC Ranging receiver. From these tests, any differences between readings obtained by the GSFC receiver and the ATSR receiver may be compared.

Though this experiment was called a 24-hour test, the period of time over which these measurements were performed was only 17 hours (0300Z to 2000Z). Each measurement interval of this experiment was three minutes. The first measurement interval started at Mojave's sunset time (0256 Zulu or 6:56 PM, PST). The next measurement time started seven minutes later (0303Z). After this, there was a test interval at the beginning of each hour until 1130Z which was an hour before sunrise. For an hour before and after sunrise the measurements were performed every 30 minutes. At 1400Z the hourly schedule was resumed until 2000Z, which was the last simultaneous test interval performed. It was unfortunate that the allotted time for this experiment did not allow a 24-hour cycle to be completed, since the results, which are presented later, were beginning to show a trend which should have been more fully investigated.

The purpose of the sequential test was to determine if there were any unknown built-in constants in the GSFC L-band ranging system. The preferred method

3341 5/5

to perform this test would have been to sequentially range at L-band with the GSFC ranging system and then the ATSR ranging system. However, the ATSR system cannot use the L-band system on ATS-5 for ranging due to the satellite spin. Thus, the sequential test was performed by alternately using the GSFC ranging receiver to measure the L-band range and then the C-band range, which this system can do. The sequential tests were performed such that, first a test interval of L-band ranging measurements was made through the GSFC ranging receiver; then the C-band receiver was connected to the GSFC ranging receiver and a period of C-band ranging measurements was made. This alternating of L-band and C-band was continued for seven 3-minute test periods in sequence. Instructions were to have the elapsed time between the test periods as short as possible. The elapsed time was from 2 to 3 minutes between all the test runs except between the first and second which was 14 minutes. Thus, the second through the seventh test runs were the ones which could best be compared for any differences in measurement constants.

4.3.3 Experimental Test Results

The results of the 24-hour simultaneous C-band and L-band ranging tests are presented in A. of table 4.5 with the results of the sequential tests presented under B. In this table the test interval start times are presented in both Greenwhich (Zulu) time and the local Pacific Standard Time (PST). Other column heads are the same as for the previous tables for simultaneous ranging except there is an extra column labeled "corrected L-C." For this, the L-band data was corrected by deducting the 120-meter "zero set" error and the 14 meter difference in path lengths due to antenna positions. With this correction, the ranges measured at L-band and C-band should have approximately the same readings. Any variations in these readings should now be due to propagation anomalies.

The curves presented in figures 4.15 and 4.16 are graphical representations of the data in table 4.5. The curves of figure 4.15 show the differences between the ephemeris range data and the C-band range measurements, and also the ephemeris and the L-band range measurements (uncorrected) as they varied over the day. The curve in figure 4.16 is a plot of the "corrected" difference between the L-band ranging measurements and the C-band ranging measurements (corrected L-C) over the day. The zero line represents the point where these two rangings are equal. A positive reading indicates that the L-band ranging reading is longer than the C-band ranging reading, and a negative reading indicates that the C-band ranging is longer.

TABLE 4.5 24-HOUR SIMULTANEOUS AND SEQUENTIAL RANGING DATA FOR ATS-5

Measurement Time		Range (Meters)			Difference In Range (Meters)				Sigma (Meters)	
Zulu	Local PST	Ephemeris	C-Band	L-Band	E-C	E-L	L-C	Corrected L-C	C-Band	L-Band
A. Simultaneous										
0256Z (Sunset)	6:56P	37,295,243	37,295,273	37,295,394	-30	-151	+121	-13	4.78	5.89
0303Z	7:03P	37,294,151	37,294,184	37,294,286	-33	-135	+102	-32	4.51	5.34
0403Z	8:03P	37,283,093	37,283,097	37,283,189	-4	-96	+92	-42	5.94	5.61
0430Z	8:30P	37,277,569	37,277,501	37,277,639	+68	-70	+138	+4	5.50	NA
0503Z	9:03P	37,270,392	37,270,298	37,270,419	+94	-27	+121	-13	3.83	5.74
0601Z	10:01P	37,257,749	37,257,589	37,257,720	+160	+29	+131	-3	4.68	5.50
0700Z	11:00P	37,245,112	37,244,895	37,245,032	+224	+87	+137	+3	3.58	5.45
0800Z	12:00P	37,233,617	37,233,328	37,233,454	+289	+163	+126	-8	3.66	5.49
0903Z	1:03A	37,223,964	37,223,617	37,223,753	+347	+211	+136	+2	3.66	4.81
1000Z	2:00A	37,218,021	37,217,627	37,217,759	+394	+262	+132	-2	3.10	6.22
1102Z	3:02A	37,215,011	37,214,584	37,214,714	+427	+297	+130	-4	3.31	6.25
1130Z	3:30A	37,214,881	37,214,439	37,214,578	+442	+303	+139	+5	3.79	5.36
1200Z	4:00A	37,215,582	37,215,134	37,215,271	+448	+311	+137	+3	3.09	5.59
1230Z (Sunrise)	4:30A	37,217,125	37,216,678	37,216,809	+447	+316	+131	-3	3.72	4.77
1300Z	5:00A	37,219,466	37,219,016	37,219,144	+450	+322	+128	-6	3.65	NA
1330Z	5:30A	37,222,554	37,222,112	37,222,251	+442	+303	+139	+5	3.72	5.91
1400Z	6:00A	37,226,318	37,225,888	37,226,015	+430	+303	+127	-7	4.58	4.84
1500Z	7:00A	37,235,560	37,235,169	37,235,303	+391	+257	+134	0	3.53	5.45
1600Z	8:00	37,246,507	37,246,158	37,246,297	+349	+210	+139	+5	3.70	5.28
1700Z	9:00A	37,258,414	37,258,138	37,258,267	+276	+147	+129	-5	2.89	6.04
1800Z	10:00A	37,270,530	37,270,322	37,270,439	+208	+91	+117	-17	3.50	6.22
1900Z	11:00A	37,282,122	37,281,993	37,282,112	+129	+10	+119	-15	2.87	5.33
2000Z	12:00A	37,292,547	37,292,496	37,292,606	+51	-59	+110	-24	3.62	5.11
B. Sequential										
2026Z	12:26P	37,296,469	-	37,296,555	-	-86	-	-	-	10.82
2043Z	12:43P	37,298,853	37,298,853	-	0	-	-	-	11.57	-
2049Z	12:49P	37,299,652	-	37,299,759	-	-107	+105	-29	-	10.03
2053Z	12:53P	37,300,303	37,300,306	-	-3	-	-	-	10.82	-
2059Z	12:59P	37,300,993	-	37,301,103	-	-110	+104	-30	-	11.97
2103Z	1:03P	37,301,488	37,301,497	-	-9	-	-	-	9.86	-
2109Z	1:09P	37,302,207	-	37,302,324	-	-117	+105	-29	-	10.79

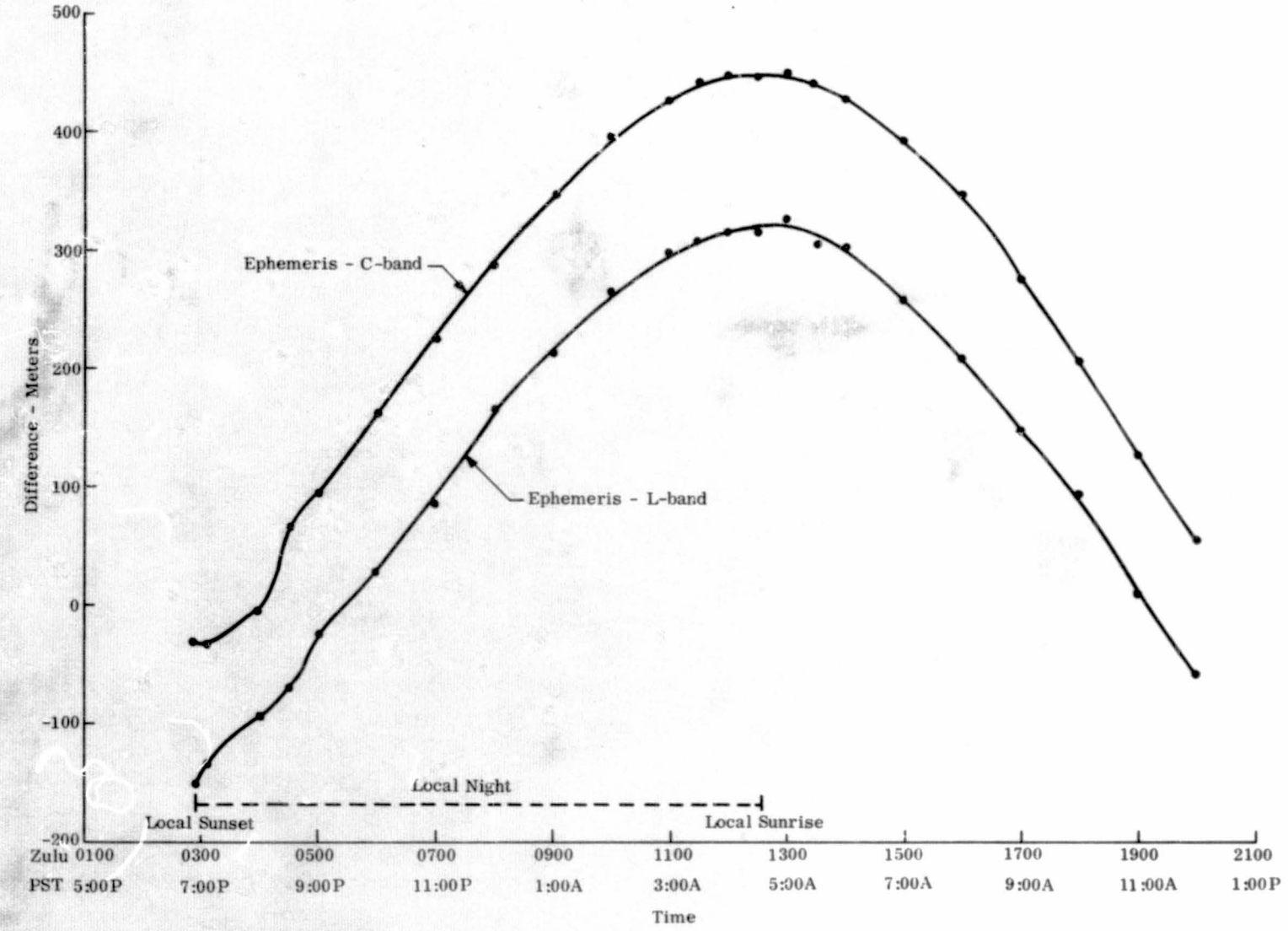

Figure 4.15 Comparison of L-Band and C-Band Ranging Data to Ephemeris Ranging Data

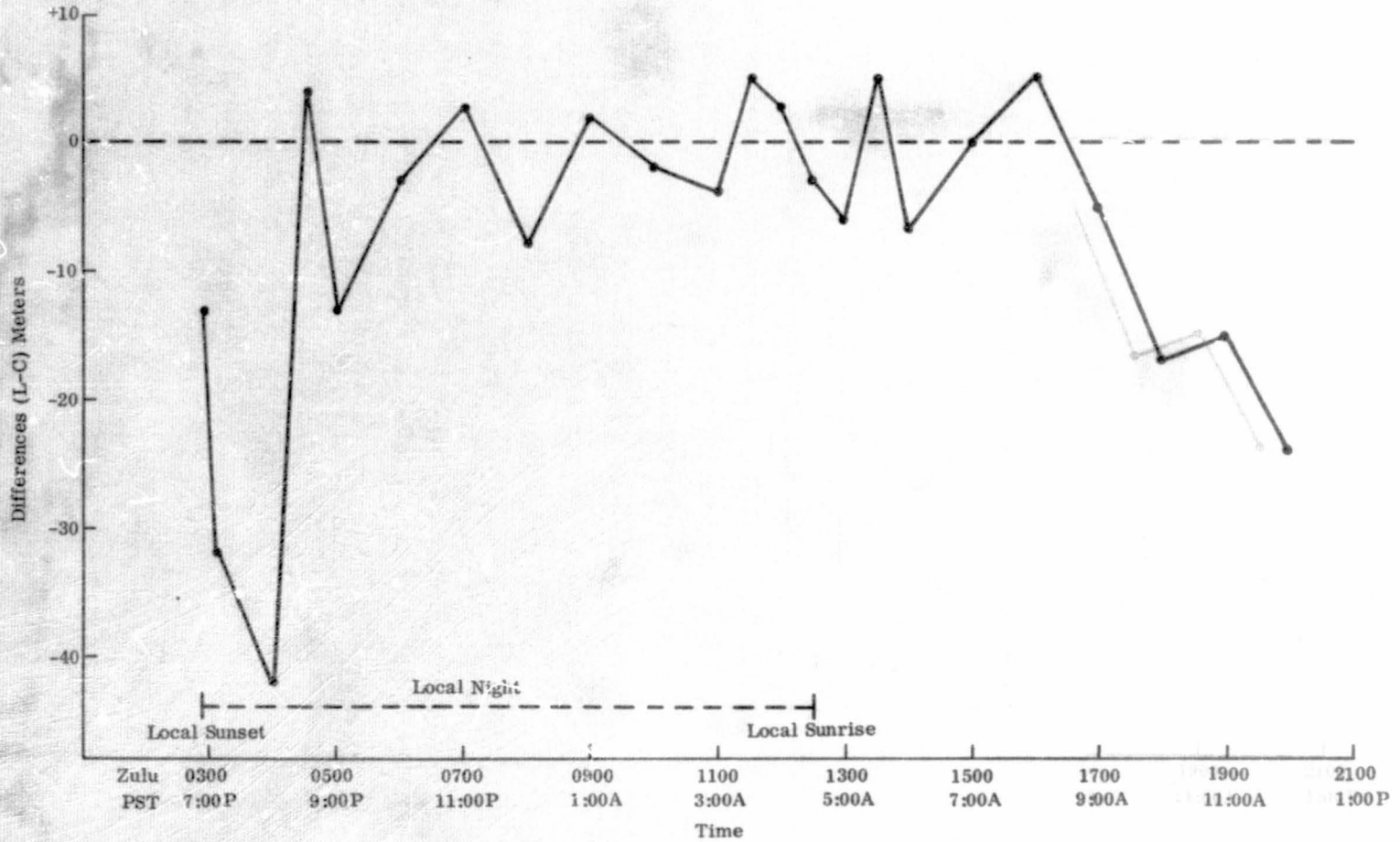

Figure 4.16 Diurnal Variation of the L-Band Ranging Data as Compared to the C-Band Ranging Data

The sequential test results are shown in the B portion of table 4.5. As previously stated, the elapsed time between the end of first test run (2026Z) and the beginning of the second test run (2043Z) was 14 minutes, making it difficult to extrapolate this data. Thus, the first test is shown here but not used in these comparisons. Between the 2043Z test and 2053Z test, which were C-band rangings, the E-C difference changed from 0 to -3 meters. Thus at 2049Z (L-band test) the C-band E-C reading could be interpolated to be -2 meters which, when compared to the -107 meters for the E-L difference, gives an L-C difference of +105 meters. Likewise, the other L-C differences were similarly calculated for this table.

4.3.4 Analysis

In examining the 24-hour simultaneous ranging data, it can be seen in figure 4.15 that the calculated emphemeris range data obtained from the Goddard orbit determination program, when compared to the actual measured C-band range data, has a cyclic nature. This E-C difference varied from +450 meters to approximately -100 meters in a 12-hour period. After investigation it was found that this is a characteristic of the orbit determination program and that past measured results from other experiments have also indicated a similar cyclic discrepancy. In this same figure, when the ephemeris was compared to the measured L-band range data, this same cyclic characteristic was present, indicating that it was truly the ephemeris which was causing the cyclic effect.

This above fact provides an answer to the question which arose in paragraph 4.1, table 4.1, as to why the ephemeris range data was always approximately 200 to 300 meters longer than the actual C-band measurements (E-C). All those readings were made between 1800Z and 1930Z, thus causing the ephemeris data to come from the same time portion of the cyclic curve and thereby, all being essentially the same positive discrepancy. As the measurements were made from March 25, 1971 to April 29, 1971, these E-C differences decreased showing that there was also a slow drift to this cyclic difference causing a small daily shift to the curve. This cyclic effect of the ephemeris data will also cause some errors in the location of a position from two sets of ranging measurements as described in paragraph 4.4.

Much work has been done in the theory of ionospheric propagation in the F-Region. In summary, as previously stated in paragraph 4.2.4, it is expected that the propagation effects will generally change as the "integrated electron content" of the ionosphere varies. That is, during the night when the electron content is the lowest there will be the least effect; while during the day, the effect will be the greatest. Just at and after sunset and sunrise when the electronic content is rapidly changing it is expected that abnormal effects will occur. These propagation variations will be a function of $1/f^2$, the higher the frequency the less the effect. Therefore, it would be expected that the L-band ranging data will show more diurnal variation than the C-band ranging data. Figure 4.16 is a representation of the diurnal variation of the L-band ranging measurement compared to the C-band (corrected L-C). This experiment started at local sunset at the Mojave ground station. For the first hour after sunset the L-C difference decreased sharply. By referring back to figure 4.15 it is seen that the C-band ranging was more severely affected than the L-band ranging during this hour. From this, it was obvious that both the C-band and the L-band range readings were longer than normal, but the C-band range had increased more than the L-band. This was opposite to what would be expected.

In figure 4.16 the portion of the curve during the night and early morning (9:00 PM to 9:00 AM) varied in a random nature. There seemed to be no significant abnormalities around the sunrise time. However, from 9:00 AM until noon the curve showed that the L-C difference was decreasing. This means that the C-band range reading was becoming longer than the L-band ranging as the electronic content was increasing during the day. Again, this was an opposite effect to what the theory said should be expected to happen. Unfortunately, this test was terminated at noon so that a complete picture of what would have happened for the remainder of the day was not available.

In the sequential test, by measuring the C-band range on the GSFC ranging receiver instead of measuring it on the ATSR system, a comparison was made of the results obtained from these two systems. The results of this test in B. of table 4.5 showed that the E-C, E-L, and L-C differences were continuing in the same trends as established in the simultaneous results shown in A. of table 4.5. The conclusion can be made that the C-band readings obtained by both systems are essentially the same; and, therefore, the GSFC ranging system was providing accurate readings and there were no apparent unknown biases or constaints within this new system.

4.3.5 Conclusions

The results of the 24-hour simultaneous C-band and L-band experiment have shown that for this one day of testing the C-band ranging, during the daylight hours, has increased in length more than the L-band ranging. Also, during the hours after sunset the C-band ranging was again longer. These phenomena are unexplained since they react in an opposite manner to any theory of propagation delays through the ionosphere. The L-band range reading, being measured at the lower frequency, should have been the one to become longer by as much as 35 meters during these times. If the propagation delays were caused by the troposphere, they should have been the same at both frequencies for the period of the measurement. Since this is only one day of data, no definitive conclusion can be drawn from these results. However, they definitely dictate that additional study of this subject should be made.

In addition it was shown that cyclic variation occurred for both the C-band and L-band ranging data when compared with the ephemeris. This again demonstrated that the ephemeris data is inaccurate, and that the magnitude of the inaccuracy varies over a 24 hour period.

Since the ephemeris was so inaccurate and varied with time, the dirunal ionospheric effect on the L-band and C-band range measurements could not be measured.

4.4 POSITION LOCATION BY RANGING TO TWO SATELLITES

4.4.1 Objective

With L-band range measurements to ATS-5 and simultaneous C-band measurements to ATS-1 from the same station, it was possible to demonstrate a capability for determining the position of the station on the earth's surface by means of the "line of position" method to be described. Satellite ephemeris corresponding to the time interval over which ranging measurements were performed must also be available. It is the purpose of this experiment to show that station position can be located reasonably accurately by ranging to two satellites. In addition, position location using simultaneous VHF and C-band range measurements to ATS-1 and ATS-3 was investigated.

4.4.2 Test Description

The test setup for position location is shown in figure 4.17 for L-and C-band measurements and figure 4.18 for C-band and VHF measurements. Satellite pairings were as follows:

L-band to ATS-5 and C-band to ATS-1

C-band to ATS-3 and VHF to ATS-1

VHF to ATS-3 and C-band to ATS-1

These simultaneous rangings together with satellite ephemeris were used to determine the position of the Mojave station.

4.4.2.1 General Discussion of Position Location

Location of a point in space requires the specification of three independent quantities relative to a known reference point in space. These quantities can be a distance and two independent angles. If the point is on or near the earth's surface, a natural reference point is the center of the earth. Therefore, one of the three quantities specifying the location of the point can be chosen to be its distance from the center of the earth. This determines a sphere upon which are the possible positions of point. Mathematically, the position on this surface can be unambiguously located by specifying two angular coordinates, such as latitude and longitude. Rather than measuring the two angles directly, it is often more convenient to calculate them from measurements made relative to other known reference points in space. Unfortunately, the introduction of other reference points leads to ambiguity in position location unless redundant measurements are made. In other words, more than two measurements are necessary to locate a point on the earth if ambiguities are to be resolved. How-

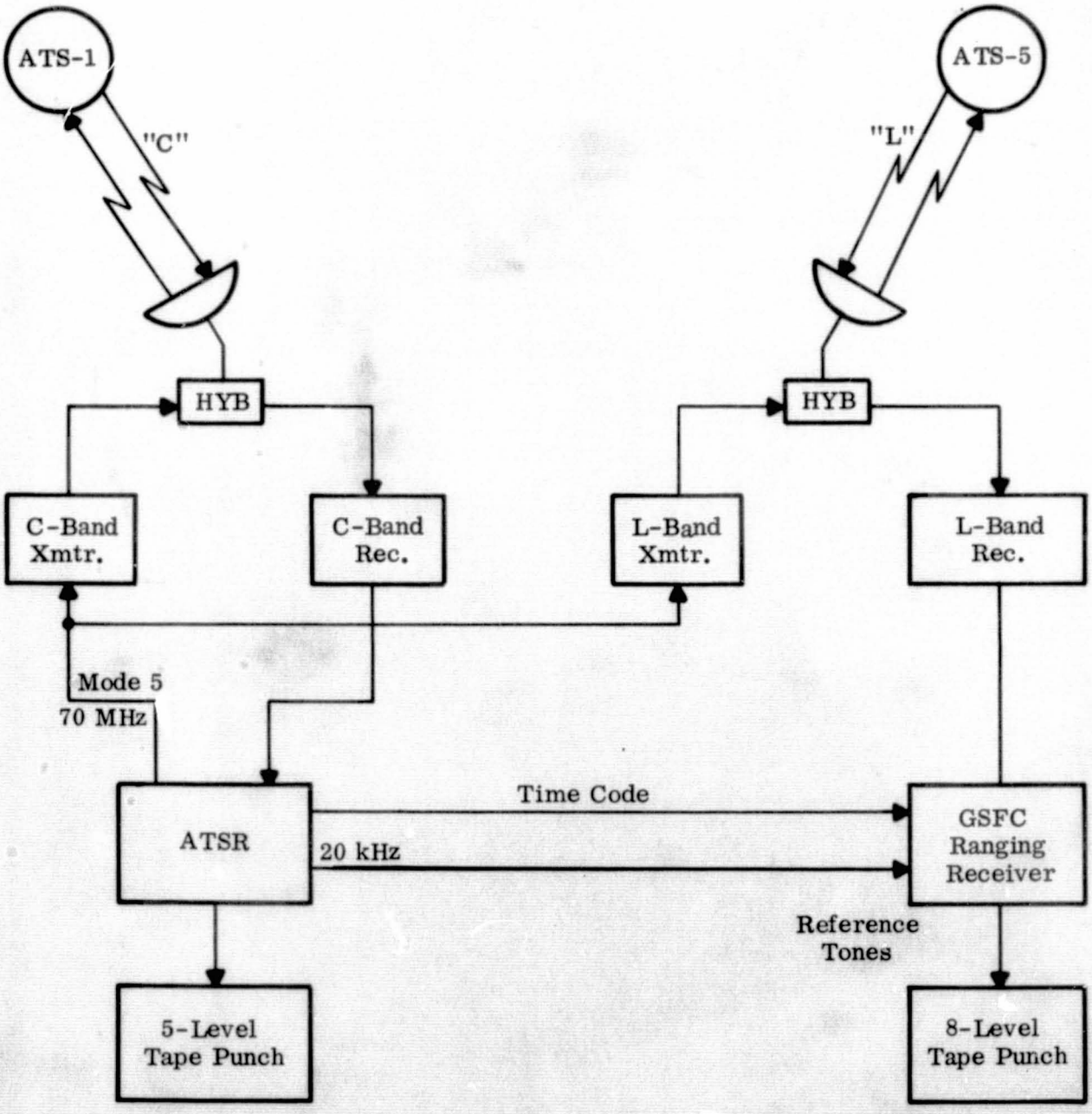

Figure 4.17 Position Location L and C-Band Block Diagram

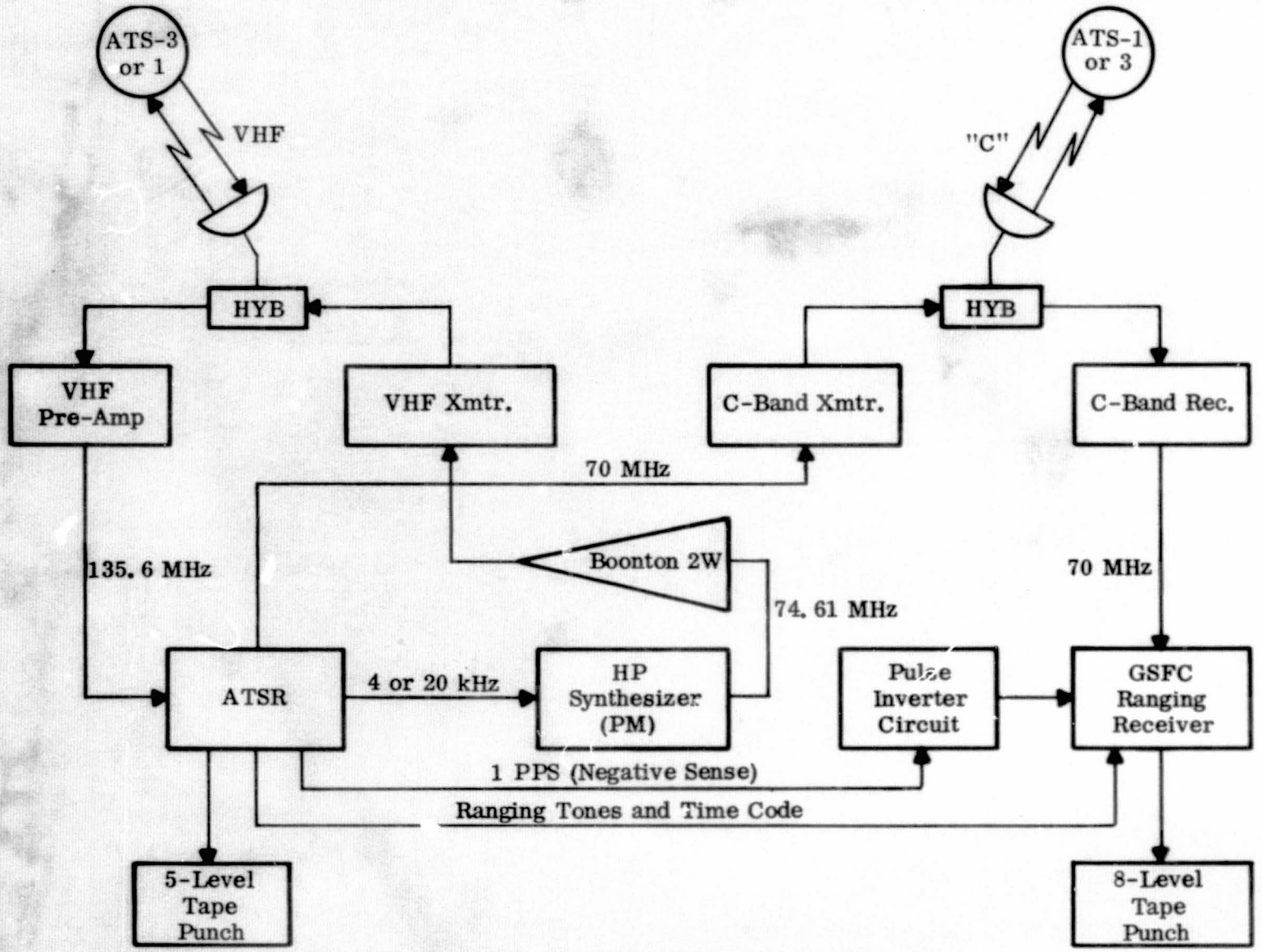

Figure 4.18 Position Location C-Band and VHF Block Diagram

ever, ambiguities are of little concern in this experiment, so we assume here that the two required quantities can be chosen to be the distances of the point from two known reference points.

These two reference points are two of the ATS satellites, and the distances needed for position location are obtained by range measurements from the point whose position is to be determined, to the two spacecraft. Of course, accurate satellite ephemeris is necessary to specify the positions in space of the two reference points themselves. These range values determine two spheres centered at the spacecraft upon which are the possible positions of the point. The intersection of these two spheres is a circle. This circle, in turn, intersects the third sphere centered at the center of the earth. This defines two points, one on each side of the equator. These two points of intersection specify possible positions of the unknown point. This is an example of the ambiguities involved when more than one reference point is used for position location.

4.4.2.2 Data Required for Position Location

Inputs needed to locate a station on the earth's surface (or an aircraft flying at a known altitude) are simultaneous rangings from the target station to two satellites, and the space coordinates of the two satellites relative to a known point on earth. This point does not have to be the station from which range measurements are made. In this experiment, however, the station was used because it allowed us to compare the calculated station position with its known position without introducing possible errors due to the use of a second station.

Satellite positions were obtained from the Goddard orbit determination program. The program yielded predicted satellite coordinates in terms of the range of the satellite from Mojave, and also its longitude, geocentric latitude, and distance from the center of the earth. These four quantities were computed at three second intervals during the time period over which range measurements were made.

Because the earth is not a perfect sphere, its radius is a function of latitude. The Mercury Geoid* is used as an earth model. According to this model the earth radius at geocentric latitude ψ is:

$$R_o = A\,(0.998317 + 0.001683 \cos 2\psi)$$

where A is the equatorial radius (assumed to be longitude independent). A rough estimate of station latitude was needed beforehand because the earth radius is required in this method of position location.

* See Glossary

4.4.2.3 Description of the Method

Suppose ψ_1, and λ_1, are the geocentric latitude and longitude respectively of one of the satellites, say ATS-5. These quantities are given to us from the Goddard orbit determination program. If ψ_o and λ_o are the geocentric latitude and longitude of the station, which we wish to calculate, and if γ_1 is the angle defined in figure 4.19, then:

$$\cos\gamma_1 = \sin\psi_o \sin\psi_1 + \cos\psi_o \cos\psi_1 \cos(\lambda_o - \lambda_1)$$

Solving for λ_o, the unknown station longitude, we get

$$\lambda_o = \lambda_1 \pm \cos^{-1}\left[\frac{\cos\gamma_1 - \sin\psi_o \sin\psi_1}{\cos\psi_o \cos\psi_1}\right].$$

The ambiguity implied by this result means simply that the station can be either east or west of the subsatellite point. This ambiguity, of course, must be resolved by prior information, but it is usually clear which sign should be used in the equation.

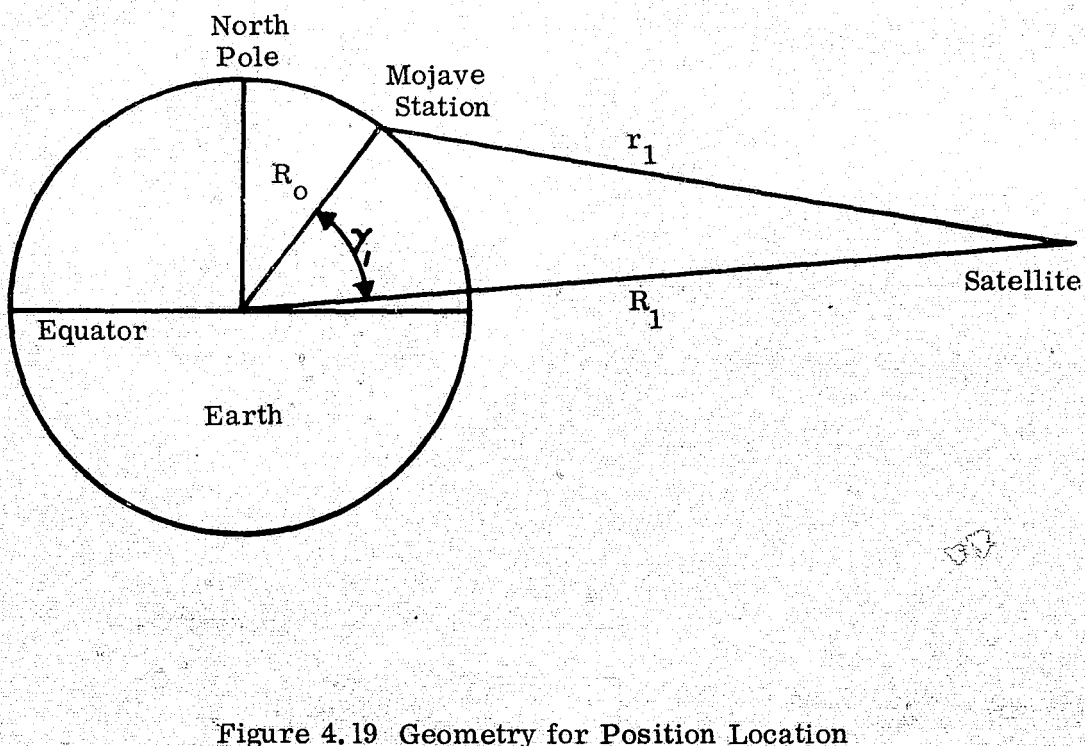

Figure 4.19 Geometry for Position Location

Thus, when $\cos \gamma_1$ is determined, λ_o is expressed as a function of the unknown station latitude ψ_o, with the known quantities γ_1, ψ_1, and λ_1 as parameters. A graph of λ_o versus ψ_o is called a "line of position" (LOP). The value to use for $\cos \gamma_1$ is determined from figure 4.19.

$$\cos \gamma_1 = \frac{R_1^2 + R_o^2 - r_1^2}{2R_1R_o}$$

where r_1 is the measured range of the satellite from the station whose position is being determined and R_1 is the distance of the satellite from the center of the earth. R_1 is obtained from the Goddard orbit determination program. When $\cos \gamma_1$ is substituted into the equation for λ_o, the station LOP is determined.

To locate the station on this line of position we carry out this same procedure using a second satellite, say ATS-1. A second independent LOP is thereby determined:

$$\lambda_o = \lambda_2 \pm \cos^{-1} \left[\frac{\cos \gamma_2 \quad -\sin \psi_o \quad \sin \psi_2}{\cos \psi_o \quad \cos \psi_2} \right]$$

$$\cos \gamma_2 = \frac{R_2^2 + R_o^2 - r_2^2}{2R_2R_o}$$

where ψ_2, λ_2, r_2 and R_2 are the latitude, longitude, measured range, and distance from the center of the earth, respectively, of the second satellite. The times at which these four quantities are obtained must be the same as the times at which the corresponding quantities for the first satellite are obtained. The position on the earth's surface where these two lines of position intersect is the location of the station. This point is compared with the known coordinates of the Mojave station to evaluate this technique for position location.

A computer program has been developed to calculate the coordinates of the intersection of the lines of position and to plot them as a point on a graph of station latitude versus station longitude. Each graph consists of such points computed from range measurements and satellite ephemeris obtained every three seconds of the run. This cluster of points can then be visually compared with the actual station location, which is also plotted. In the program an ambiguity arises in the computation of station latitude; the station can be either north or south of the equator. This ambiguity is readily resolved in this experiment.

4.4.3 Experimental Test Results

Table 4.6 summarizes the results of the position location experiment. Times listed in this table are close to the start times of the range measurements. Each set of range measurements corresponding to the start time consists of about 60 range values spaced by three seconds. These values, together with the corresponding computed range values extracted from the satellite ephemeris, were inserted in the program described in paragraph 4.4.2.2, yielding 60 possible locations of the Mojave station.

Two typical position location plots (obtained from a subroutine of the position location program) using C-band and VHF ranging data are shown in Figures 4.20 and 4.21. An example of position location with L and C-band range measurements and with ephemeris range values is shown in figures 3.8 and 3.9 of paragraph 3.2.3.1.

Table 4.6 lists, for each set of range measurements, the distance in meters between the actual station position and the average position computed from the range measurements. This average position corresponded roughly to the center of the cluster of about 60 possible station locations. The scatter of possible station positions about the average position was also tabulated. This scatter is defined as the root-mean-square deviation from the average position.

To determine the causes of position location error, we need an estimate of the difference between the range measurements and the corresponding ranges obtained from satellite ephemeris for each run. An average difference for the 60 points used in each run was computed, and table 4.6 lists these values for all runs.

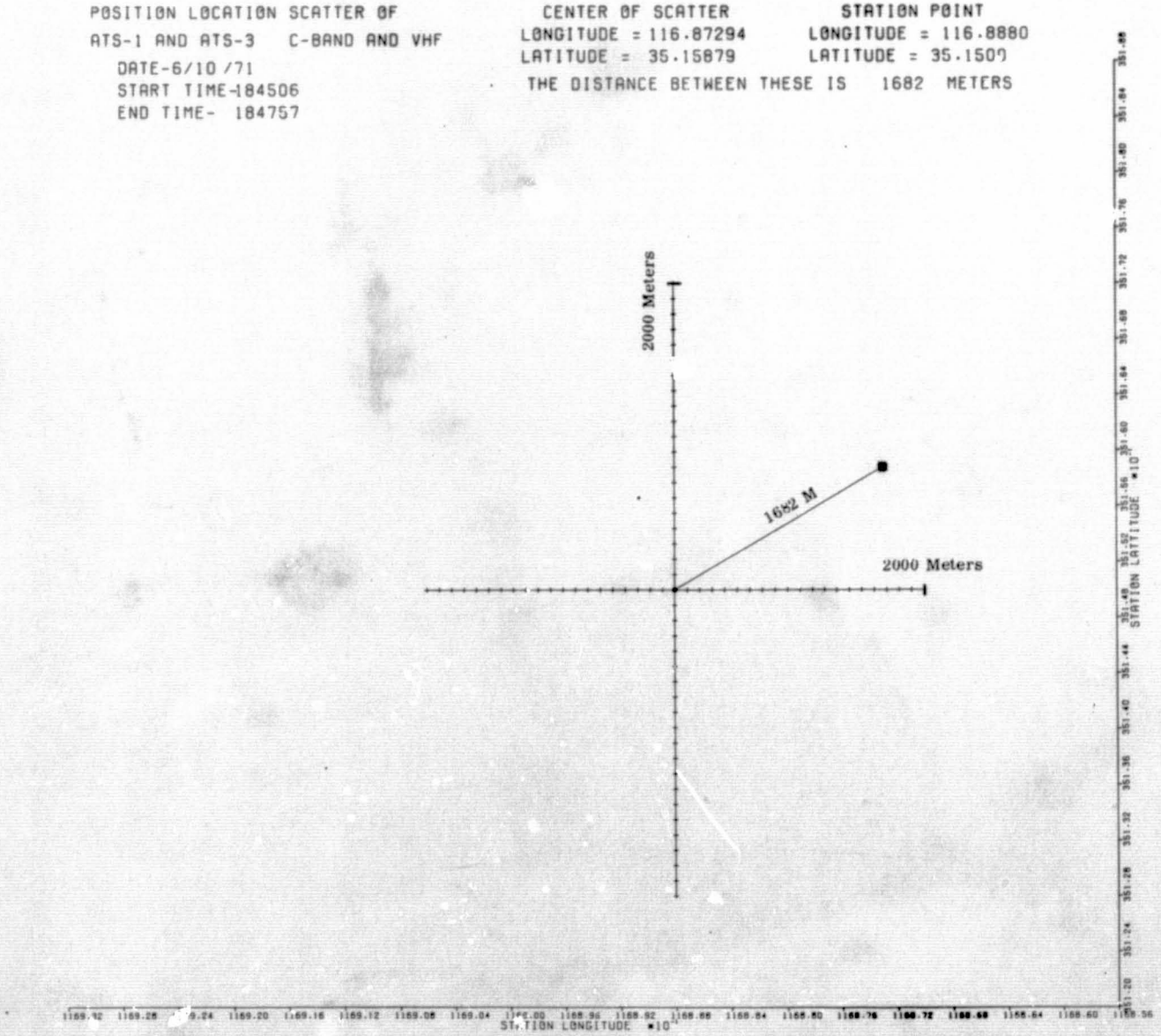

Figure 4.20 Position Location Using Measured Range Data for ATS-1 (VHF) and ATS-3 (C-Band)

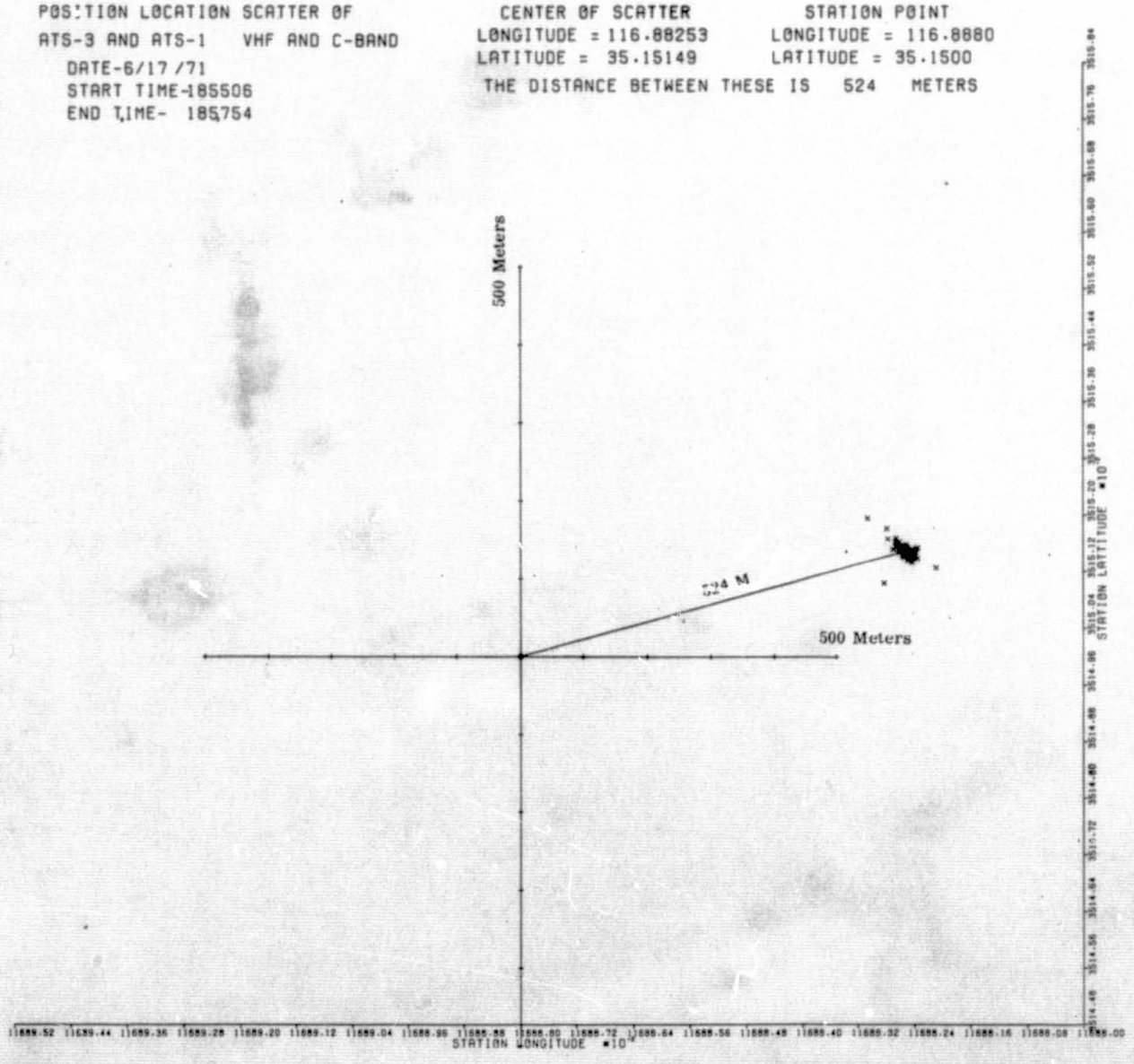

Figure 4.21 Position Location Using Measured Range Data for ATS-1 (C-Band) and ATS-3 (VHF)

TABLE 4.6 SUMMARY OF POSITION LOCATION RESULTS

Ranging Systems Used For Position Location	Date	Time	Distance Between Actual and Computed Station Position Using Range Measurements (Meters)	Scatter of Computed Position About Its Mean (Meters)	Distance Between Actual and Computed Station Position Using Satellite Ephemeris (Meters)	Scatter of Ephemeris Position About Its Mean (Meters)	Difference Between Measured and Ephemeris Range for ATS-5 (Meters)	Difference Between Measured and Ephemeris Range for ATS-1 (Meters)	Difference Between Measured and Ephemeris Range for ATS-3 (Meters)
L-Band to ATS-5 C-Band to ATS-1	March 24 1971	180630	1411 Northwest	8.86	23 Southeast	0.13	846	-77	
		181502	1442 "	9.54	"	0.14	868	-68	
		182200	1458 "	7.65	"	0.14	879	-62	
		182700	1468 "	7.18	"	0.15	887	-56	
	March 25 1971	181302	795 Southeast	7.87	"	0.12	-495	-97	
		182202	774 "	8.83	"	0.14	-480	-89	
		182713	754 "	7.99	"	0.15	-468	-86	
	April 14 1971	181102	1311 "	19.14	"	0.12	-430	628	
		181702	1294 "	19.19	"	0.11	-413	630	
		182301	1289 "	22.27	"	0.16	-410	633	
	April 15 1971	180602	1386 "	11.32	24 Southeast	0.12	-455	664	
		181202	1373 "	14.65	"	0.15	-442	668	
		181802	1362 "	12.49	"	0.14	-437	670	
		182502	1370 "	16.09	"	0.16	-433	675	
	April 20 1971	181002	1753 "	16.76	27 Southeast	0.20	-518	903	
		182201	1738 "	12.28	"	0.18	-482	928	
	April 21 1971	181803	1635 "	18.01	28 Southeast	0.18	-499	821	
		182202	1627 "	17.64	"	0.17	-492	822	
		182601	1633 "	17.85	"	0.18	-492	827	
	April 22 1971	180402	3969 Northeast	16.88	29 Southeast	0.15	-539	2643	
		181102	4045 "	18.64	"	0.17	-517	2718	
		182001	4144 "	19.80	"	0.17	-499	2807	
		182602	4098 "	18.30	"	0.18	-355	2872	
	April 26 1971	180802	11910 "	16.56	32 Southeast	0.18	-477	8705	
		181511	12012 "	16.58	"	0.20	-445	8799	
		182002	12088 "	17.83	"	0.18	-425	8867	
		182502	12171 "	18.03	"	0.19	-408	8939	
	April 28 1971	183201	16403 "	17.63	34 Southeast	0.17	-394	12125	
		184002	16525 "	25.37	"	0.14	-352	12238	
		184718	16673 "	19.54	"	0.14	-326	12361	
		185412	16808 "	20.36	"	0.16	-299	12475	
C-Band to ATS-3 VHF to ATS-1	June 10 1971	184500	1682 "	13.89	24 Southeast	0.06		1370	-426
		185000	1680 "	13.74	23 Southeast	0.05		1366	-435
		185500	1674 "	13.86	"	0.04		1361	-428
VHF to ATS-3 C-Band to ATS-1	June 17 1971	184600	524 "	11.30	28 Southeast	0.04		373	-265
		185000	528 "	13.61	"	0.08		378	-245
		185500	524 "	18.62	"	0.09		385	-246
		190000	531 "	29.00	"	0.08		399	-232

Finally, the station locations calculated by inserting into the program the ranges obtained from satellite ephemeris are tabulated. This information is used mainly as a check on the validity of the position location procedure. It does not reflect the accuracy of range measurements or the accuracy of the satellite ephemeris. This will be discussed in more detail in paragraph 4.4.4. Also listed in table 4.6 is the scatter of possible station locations about their mean.

Figure 3.8 shows that the station position obtained from typical L and C-band range measurements is roughly 800 meters from the actual position. With good satellite ephemeris, this error varies from 800 meters to about 1300 meters. When old satellite ephemeris is used, results can be much worse, as discussed in paragraph 4.4.4. Scatter about the computed location, for the example shown in figure 3.8, is about 8 meters, so position location precision is quite good. The scatter for most runs is less than 20 meters.

Figures 4.20 and 4.21 and table 4.6 show that position location accuracy using VHF and C-band range measurements varies from about 500 meters to about 1700 meters.

4.4.4 Analysis

Examination of the position location plots revealed that there is very little scatter of possible station locations about the average position. This indicated that thermal noise and short term jitter in the equipment had little effect on our capability for position location. The RMS scatter for most runs was less than 20 meters.

Accuracy of position location, measured by the difference in meters between the calculated and actual station positions, was determined more by the satellite ephemeris accuracy than the ranging accuracy. Range measurements were affected by propagation effects, station zero set errors, and station antenna placement. With the exception of the VHF measurements, propagation effects are believed to be small (on the order of 10 meters) compared to other error sources. Zero set inaccuracy has already been discussed in paragraph 4.1.2. The 120 meter range error due to zero set inaccuracy in the L-band equipment was compensated for prior to data processing. Therefore, this error does not contribute to position location inaccuracy revealed in the plots and in table 4.6.

Section 6 of this report discusses effects of antenna placement at Mojave on range measurements and position location. It is noted that the following position location distance errors occurred as a result of the antenna separations:

C-band to ATS-1, L-band to ATS-5: 100 meters

C-band to ATS-1, VHF to ATS-3: 60 meters

VHF to ATS-1, C-band to ATS-3: 151 meters

Table 4.7 presents the corrections in latitude and longitude which must be applied to the calculated coordinates for precise position location. Comparison of these values with the position errors listed in table 4.6 reveals that the antenna separation was a relatively insignificant source of position location error. In fact, these corrections tended to slightly increase the position error in some cases.

TABLE 4.7 POSITION LOCATION CORRECTIONS DUE TO ANTENNA SEPARATIONS

Ranging Systems	Latitude Correction	Longitude Correction
C-Band to ATS-1 L-Band to ATS-5	25 meters north	98.5 meters west
C-Band to ATS-1 VHF to ATS-3	56 meters south	22.5 meters west
VHF to ATS-1 C-Band to ATS-3	139 meters north	62.5 meters west

Satellite ephemeris inaccuracy was the major source of position location error in this experiment. Sample range-versus-time curves are shown in paragraph 3.2.3.1, Figures 3.10 and 3.11. These figures compare C and L-band range measurements with the corresponding ranges obtained from satellite ephemeris. Table 4.6 summarizes these results for all runs. L and C-band range measurements differ from ephemeris range by a few hundred meters typically, and this explains to a large extent the position location inaccuracy. Consider, for example, the ranging data obtained March 25, 1971 (see table 4.6). The difference between L-band range to ATS-5 and the corresponding ephemeris range was about 480 meters. This error alone would yield a position location error of roughly

$$\frac{480}{\text{cosine (elevation angle)}} \text{ meters} = \frac{480}{\cos.\ (47.5^{\circ})} \text{ meters} = 710 \text{ meters}$$

This is nearly equal to the computed position location error of 774 meters on that day. The remaining 60 meters error is due to the small difference between C-band and ephemeris range to ATS-1 and to the other error sources mentioned above. Similar results are obtained for the other tests listed in table 4.6. The difference between measured and ephemeris range oscillated with a period of about one day. Therefore, the differences are a function of the time of day, and one would expect position location errors to behave in a similar manner. That this

behavior was not observed was a consequence of the fact that all measurements were made at about the same time of day.

The poor position location accuracy obtained with range measurements in the latter part of April was due to the fact that the satellite ephemeris was almost one month old at that time. Table 4.8 lists the dates for range measurements and the corresponding epochs for the satellite ephemeris. If the epochs given in this table are compared with the station position errors listed in table 4.6, it becomes evident that there was a correlation between the position location errors and the time interval

TABLE 4.8 MEASUREMENT DATES AND EPHEMERIS EPOCHS

Range Measurement Date	Satellite Ephemeris Epoch
March 24 March 25	March 10
April 14 April 15 April 20 April 21 April 22 April 26 April 28	March 31
June 10 June 17	June 10

between range measurements and satellite ephemeris epoch. It was very difficult, therefore, to compare the accuracy of L and C-band position location with the accuracy of VHF and C-band position location, unless the range measurements were performed on the same day and, ideally, the same hour.

Figure 4.22 is a typical position location plot corresponding to ATS-1 and ATS-3 range values obtained from satellite ephemeris. These plots were made to verify that the position location procedure is compatible with the Goddard orbit determination program. Ideally, when ephemeris ranges are inserted in the position location program, the calculated station coordinates should be identical to the actual station coordinates regardless of the accuracy of the ephemeris. The fact that the two sets of station coordinates differ by 20 to 30 meters indicated that either there are small round-off errors involved in computing station coordinates, or there are small

Figure 4.22 Position Location Using Ephemeris Range Data for ATS-1 and ATS-3

differences in physical constants (such as the earth's radius or the speed of light) used in the orbit determination and position location programs. This position difference can be considered as a lower bound on possible attainable position location errors.

Finally, the precision with which station position can be determined is influenced by the geometrical arrangement of the station and the two satellites. Table 4.6 shows that the ultimate precision (discussed in the last paragraph) was higher when ATS-1 and ATS-3 were used for ranging, rather than ATS-1 and ATS-5. This was because ATS-1 and ATS-3 were widely separated in longitude, which means that the two lines of position intersected at an angle close to 90 degrees. On the other hand, the lines of position obtained from measurements to ATS-1 and ATS-5, intersected at a small angle. Noise added to the range measurements or round-off errors in the computer programs would, therefore, increase the scatter of possible station positions in this case.

4.4.5 Conclusions

This experiment demonstrated a capability for determining the position of a station on the earth's surface by ranging simultaneously to two synchronous satellites from the station. Accuracy was limited mainly by the accuracy and age of the satellite ephemeris. With recent updated ephemeris from the present Goddard orbit determination program, it is possible to locate the station to within one or two kilometers with C-band and either L-band or VHF range measurements. With accurate ephemeris data it would be possible to perform position location to within 100 meters using this position determination program. The scatter of possible station positions due to thermal noise or equipment jitter was generally less than 20 meters, which implies excellent position location precision. Other sources of error, such as propagation effects are small compared with ephemeris inaccuracies, so their effects on position location were not analyzed in great detail. Improved satellite ephemeris would permit a more careful analysis of these other error sources.

Ultimate position location precision is affected by the geometry of the situation. When ephemeris range values were used in the position location program, station scatter was less than 0.10 meters rms when ATS-1 and ATS-3 were used, and 0.10 and 0.20 meters when ATS-1 and ATS-5 were used for position location.

SECTION 5

STATISTICAL ANALYSIS OF RANGING ERRORS

5.1 STATISTICAL INFORMATION OBTAINED FROM RANGING MEASUREMENTS

In addition to the information concerning range measurements described in Sections 3 and 4, certain statistical information concerning various range errors was desired. Unless otherwise stated, the range error is defined as the difference between a second order polynomial least squares fit to the range measurements during an approximate three-minute time interval and the actual range measurements (which is also a 40 msec average) at a given time during the same three-minute time interval. The coefficients of the polynomials are obtained using the "method of least squares" from approximately 180 measurements during a three-minute time interval, (the L-band measurements are actually made approximately every 790 msec) for both simultaneous L-band and C-band, or C-band and VHF range measurements.[1] Simultaneous measurements, as used in the previous sentence means measurements obtained within one second of each other. A pair of polynomial coefficients is therefore available defining curves for range versus time for both L-band and C-band range measurements or C-band and VHF range measurements for each three-minute test interval. The difference between the least squares polynomial curve and the actual measurement for corresponding times is defined as the range error and it is statistical information concerning these errors which is sought. Specifically it is desired to determine:

1) The mean squared error of the range measurements.
2) If range error is caused by propagation anomalies common to C-band, L-band, or VHF carrier frequencies.
3) The magnitude of the noise power reduction achieved by using a second degree least squares polynomial curve approximation to the raw data.

---

[1] Fitzhugh, H. S. II, "ATS-5 L-Band Ranging and Position Location Experiment Plan" July 1970, Westinghouse Electric Corporation, pp. 26-29

4) The mean range bias for L-band and VHF range measurements as compared with C-band range measurements.

5) If the L-band range errors contain periodic components at multiples of the spin period of the satellite (790 msec) or periodic components at some other frequency.

6) If the actual range jitter follows the theoretical jitter as a function of the link signal to noise ratio.

7) If the range error is gaussian and if not how the range errors are distributed.

5.2 METHODS OF OBTAINING THE DESIRED STATISTICAL INFORMATION FROM THE RANGING ERRORS

The statistical information on the ranging errors is obtained by computing and graphically displaying the following functions:

1) The autocorrelation functions,

$$\phi_{11}(\tau) = \lim_{T \to \infty} \frac{1}{2T} \int_{-T}^{T} f_1(t)\, f_1(t \pm \tau)\, dt$$

of the ranging errors $f_1(t)$ as a function of time displacement τ for each three minute test interval.

The autocorrelation function of the range errors $\phi_{11}(\tau)$ is computed and graphically displayed so that the variance of the range error can be estimated and periodic components in the error detected. The autocorrelation function of the error will always be symetrical about $\tau = 0$ and the magnitude $|\phi_{11}(\tau)|$ of the autocorrelation function at $\tau = 0$ is proportional to the square of the range error $(\text{meters})^2$ and also proportional to the power in the range error. If the error contains periodic components, these components will cause $\phi_{11}(\tau)$ to have periodic components. If the error does not contain periodic components, $\phi_{11}(\tau)$ tends to the mean value as the argument of the range error τ, tends to infinity. For errors with zero mean, $|\phi_{11}(\tau)|_{T \to \infty} = 0$.

Addition general characteristics of continuous autocorrelation functions are given in Lee.[1]

2) The crosscorrelation of the L-band and C-band or VHF and C-band ranging errors as a function of time displacement for each three-minute test interval.

The crosscorrelation function,

$$\phi_{12}(\tau) = \lim_{T \to \infty} \frac{1}{2T} \int_{-T}^{T} f_1(t)\, f_2(t \pm \tau)\, dt$$

[1] Lee, Y. W. "Statistical Theory of Communication" John Wiley & Sons, 1960, pp. 73-74

of the ranging errors is also computed and graphically displayed so that the ranging errors obtained at one carrier frequency and with one set of equipment can be compared with ranging errors simultaneously obtained at a different carrier frequency and another set of ranging equipment. The crosscorrelation function is a measure of the coherence between the two random or correlated range error functions $f_1(t)$ and $f_2(t)$. For two random range error functions which are independently generated, crosscorrelation yields a constant which is the product of the individual mean value of the two random error functions. Under this condition the error functions are uncorrelated. In case either $f_1(t)$ and $f_2(t)$ has zero mean value, the crosscorrelation function is zero for all τ. If two random functions are uncorrelated, $\phi_{12}(\tau)=0$, they will not, in general, be statistically independent unless, for example, they are gaussian and real. If the error functions $f_1(t)$ and $f_2(t)$ have periodic components of the same fundamental frequency, crosscorrelation yields the same fundamental frequency and the same harmonics which are present in both $f_1(t)$ and $f_2(t)$, together with their phase differences. The crosscorrelation function does not imply that if the measurements are highly correlated there is a causal relationship between the measurements. However, some common propagation phenomena could be affecting both sets of measurements simultaneously, causing common frequency perturbations in the measurements. When the responses or measurements are highly correlated, it is possible to predict one from the other.

3) Scatterplots of L-band versus C-band range measurements or C-band versus VHF range measurements to a common satellite.

The scatter plots of the L-band range versus C-band range provide a sample by sample comparison of simultaneously obtained range measurements. Because the L-band range measurements are obtained approximately every 790 msec, when two measurements fall within the same one-second time interval, the two measurements are averaged and a single value tabulated for that one-second interval. A best fit line through the points should show a slope of one meter/meter, or 45° when the ordinate and abscissa are drawn to the same scale. From these plots one can determine:

- If the C-band and L-band measurements are tracking over the test interval. If not, the best fit line will be at a different slope, or the differences in individual range measurements will show a wide scatter about the "best fit" straight line.

- The intercept of the best fit line with either the ordinate or abscissa gives a pair of numbers; range as measured at L-band and range as measured at C-band. The difference between these two numbers is the "best-fit" zero-offset between the two ranging systems.
- Curvature of the best fit line indicates that comparative ranging performances for the two systems is changing with time, probably because of frequency drifts in the two systems.
- A large scatter about the best fit line is indicative of a large noise (error) component in one or both range data, and peak deviations from the best fit straight line measure the peak differential range error.
- Clustering of points is indicative of "preferred" range errors, which could be caused by the data processing program or the ranging equipments.

4) Probability density distributions of range measurement error.

To determine the nature of the range errors the probability density distribution of the range measurement error is computed and graphically displayed. From this type of display, mixtures of both normal and non-normal error sources may be detected. If there is a single, non-normally distributed error source, which would be caused by a system error source, then the density curve will show a single skewed peak, with minor sidelobes. If there is more than one normally distributed source of error, each having a different mean, then the density curves will show more than one peak. This could be an indication that errors are being caused by both normally distributed ionospheric range jitter and random errors in the ranging equipment or by data reduction. If the sidelobes are not normally distributed, then errors that occur on the tails of the cumulative distribution can be attributed to equipments or the limited sample sizes. Loss of lock, or a similar equipment problem, will cause spiked distribution near each range limit point ($\pm 180^{o}$ from phase lock).

The density curves also shown the relative magnitudes of each source of error, assuming that each sidelobe is caused by an independent source of errors. The relative standard deviations of the distribution, as seen on this presentation, are the relative magnitudes of the error sources. The standard deviation of the central distribution is a measure of the range precision in the presence of thermal noise

only in the range error.

The salient features of the probability density presentations can be summarized as follows:

- Thermal noise, alone, causes the distribution to have a single peak. Any offset of the peak from 0 indicates that the ranging equipment contains a systematic (constant) error.
- Loss of lock in the ranging equipment causes the density function to contain peaks other than the one at class zero.[1] These peaks will be at the most commonly encountered range errors, which can be related to the range that would be obtained for locking the ranging tones in phase quadrature or 180^{o} out of phase.
- Variations in the range bias from test interval to test interval are exhibited as variations in the zero offset from run to run.
- Numerous small sidelobes, or hash on the distribution, which is not at the error ranges, indicate that the errors are being generated by a mixture of mechanisms such as slipping out of lock, as differentiated from false locks which generate the patterns mentioned previously.

5) Cumulative probability distributions of range measurement errors.

If the errors in the range measurements are normally distributed, the graphical displays of the cumulative probability distributions will be a straight line. This is so because the cumulative probability distributions are plotted against the integrated gaussian density function, (error function erf) so as to magnify the difference between the actual cumulative probability distributions and a cumulative gaussian distribution. This method of presentation offers a simple check on whether range errors are normally distributed. If the error distribution is caused by thermal noise alone, then this distribution should be a straight line. If the distribution has more than one slope, particularly when one compares the slope near 50% with the slope near 90%, then the errors are being caused by more than one error source. However, the "tails" on the distribution that may exist below 10% or above 90%

---

[1] There are 16 "classes", spanning 100% of the range errors associated with a test interval. The magnitude of the range error associated with a given "class" is related to the "class number" by the following expression:

$$\text{Range Error for Class N} = [\text{BIN SIZE X N}] \quad \text{meters}$$

cumulative distribution may or may not be representative of the actual error distribution, in that the distribution is obtained from a limited set of data points. If the distributions are not linear, the non-linearity can be attributed to one or more of the following effects:

- Errors caused by a single error source, that are not normally distributed.
- A combination of two or more normally distributed error sources, one contributing the maximum excursions from the mean error, and one that defines the shape of the central portion of the total error distribution.

5.3 ANALYSIS OF SAMPLES OF ACTUAL RANGING DATA

For the purposes of this analysis, three computer generated statistical presentations of ranging and ranging error data have been selected. Example 1 is typical of the majority of the results obtained during the test program. Example 2 illustrates a case where the C/N in the ranging receiver is low. Example 3 is a case where the L-band and C-band ranging tones are not coherently related, since the L-band tone was not derived from the ATSR tone generators. (Mode 1 operation).

5.3.1 Example 1: Typical Results - Run of 4/15/71 at 1000 Watts on L-Band.

The data shown in figures 5.1 through 5.5 are representative of data acquired during runs when all equipment was operating properly, and where system performance was not significantly reduced by thermal noise. These presentations are typical of those obtained when the rms errors on both systems were small, as was the case in 40 of the 65 test periods.

Referring to figure 5.1, the L-band autocorrelation peak at $\tau = 0$ is approximately 38, while the C-band peak at $\tau = 0$ is approximately 7.8. These numbers can be related to the standard deviations by the expression

$$\sigma_{\Delta R} = \sqrt{2\,\phi\,(0)} \qquad \text{meters}$$

In table 4.1, paragraph 4.1.3, the standard deviations, as calculated from the autocorrelation functions, are:

$$\sigma_C = 3.95 \qquad \text{meters}$$

and

$$\sigma_L = 8.7 \qquad \text{meters}$$

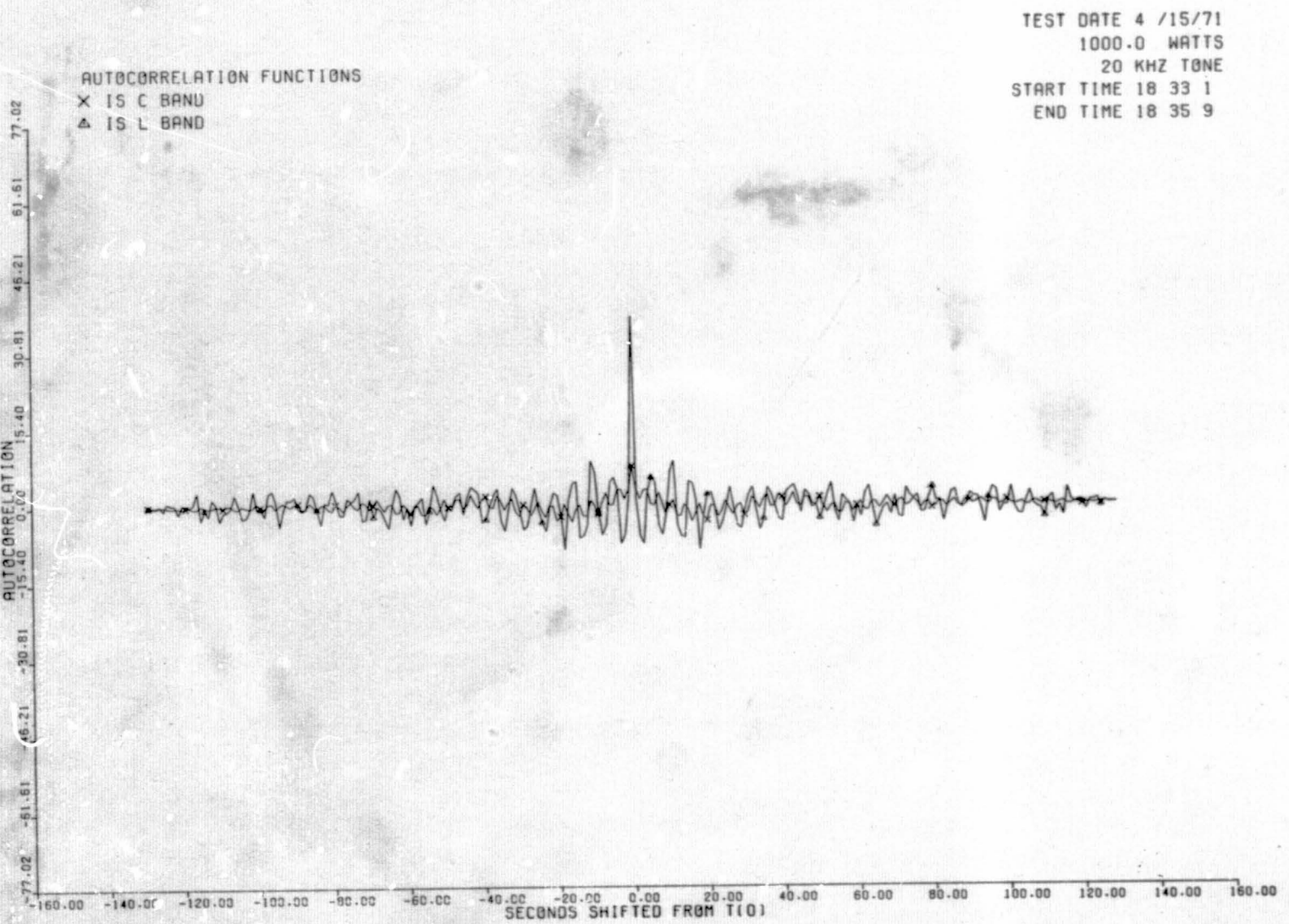

Figure 5.1 Autocorrelation Functions of C-Band and L-Band Ranging Errors (Example 1)

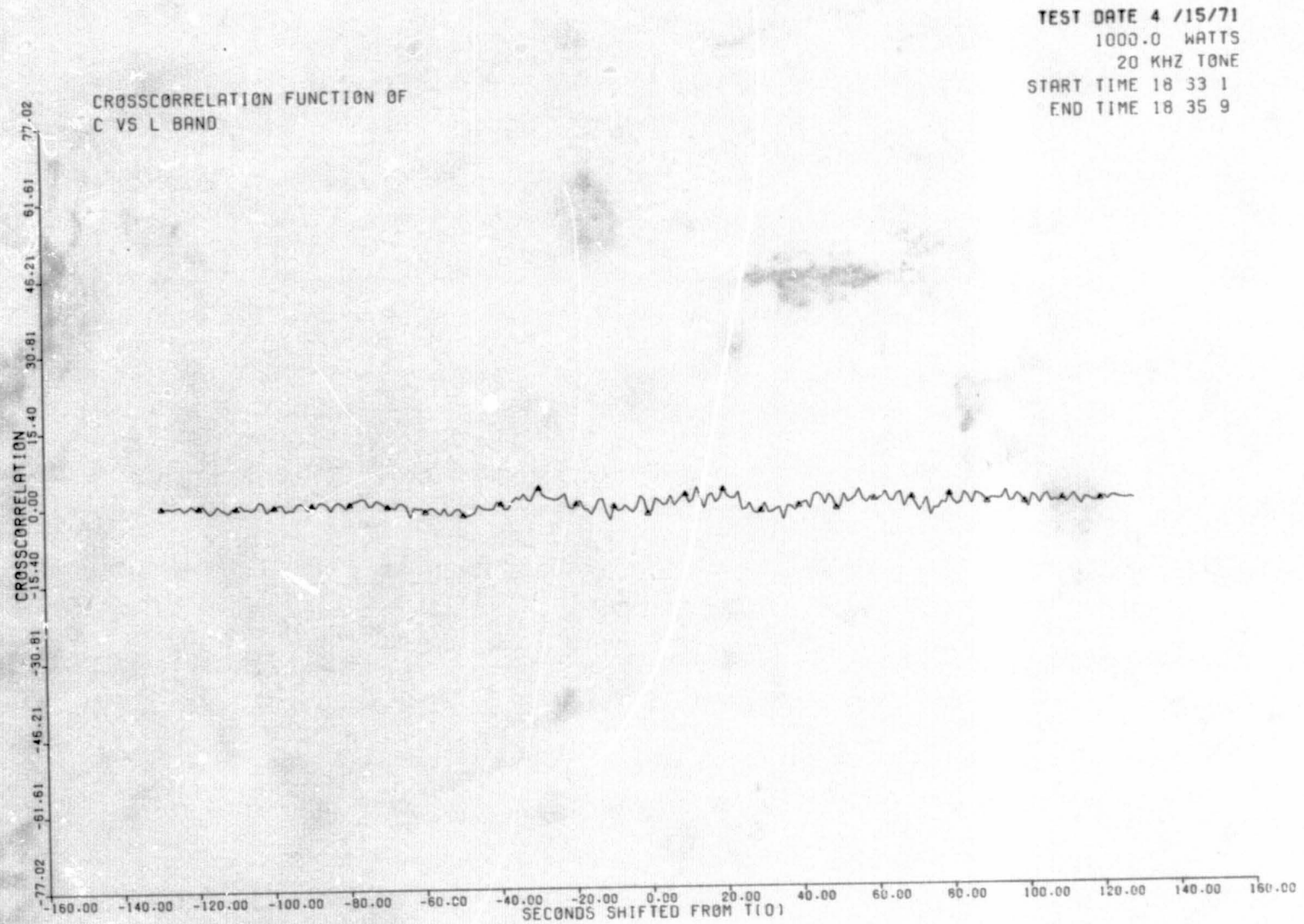

Figure 5.2 Crosscorrelation Function of C-Band and L-Band Ranging Errors (Example 1)

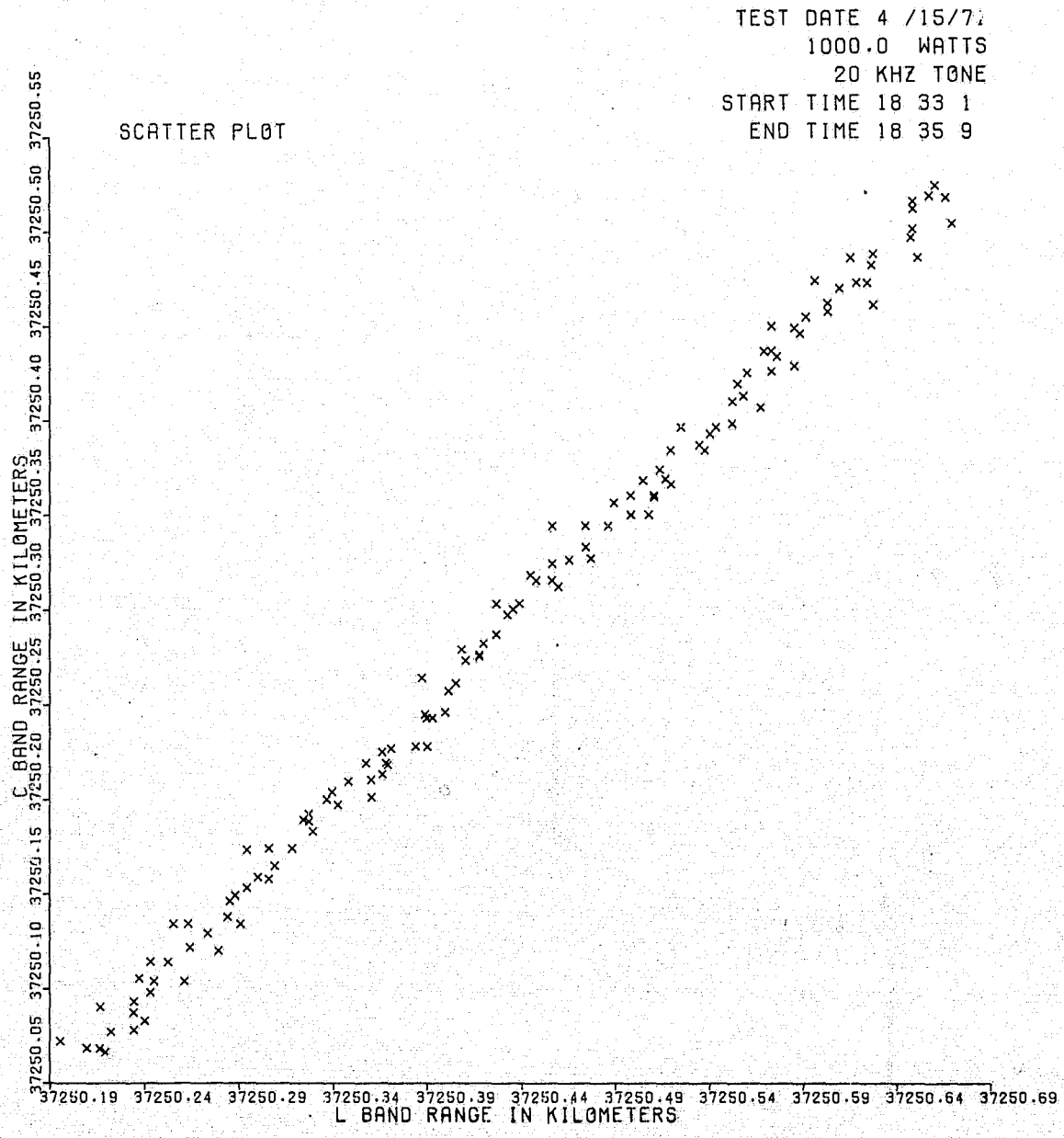

Figure 5.3 C-Band Range Versus L-Band Range (Example 1)

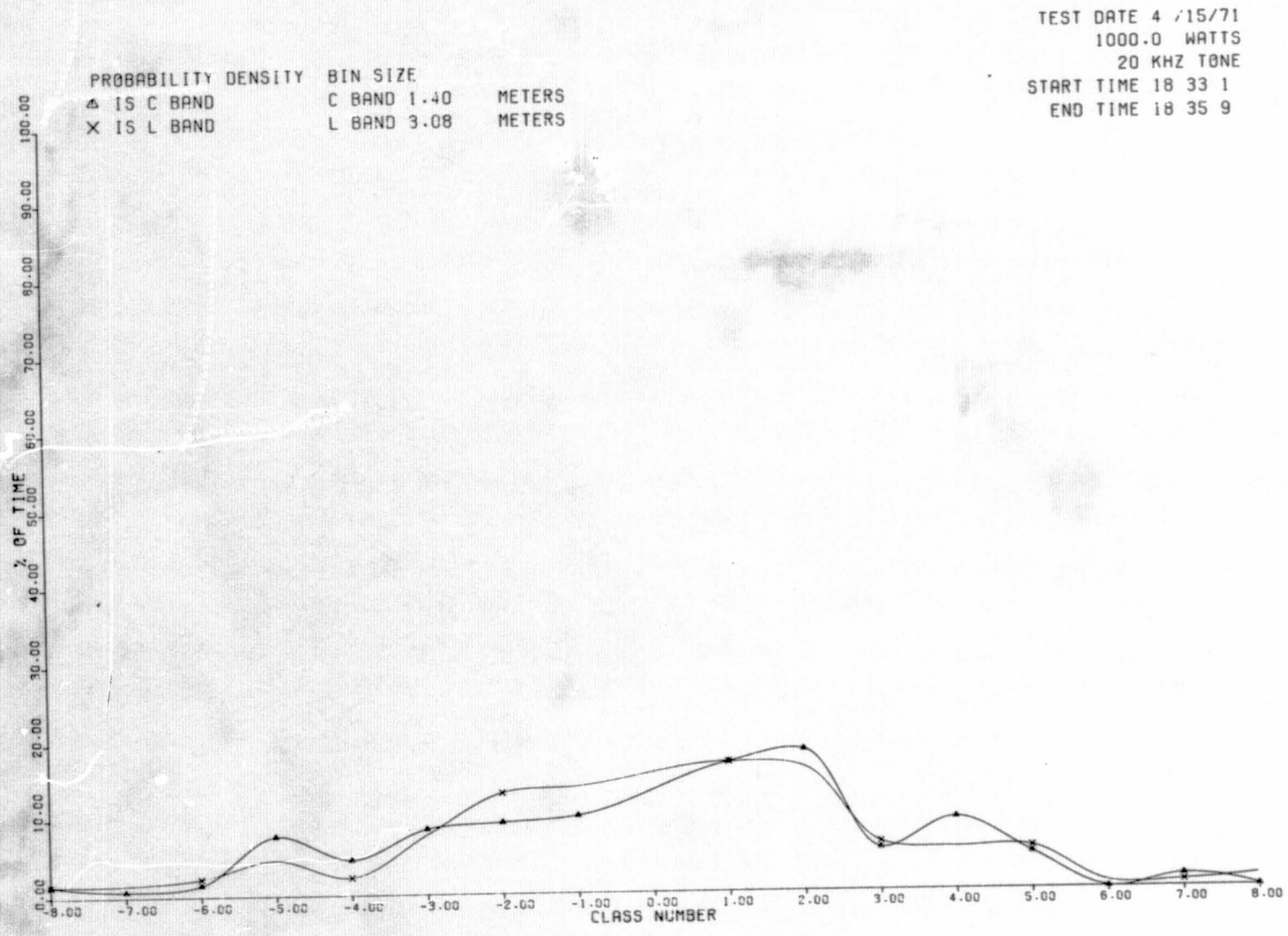

Figure 5.4 Probability Densities of C-Band and L-Band Ranging Errors (Example 1)

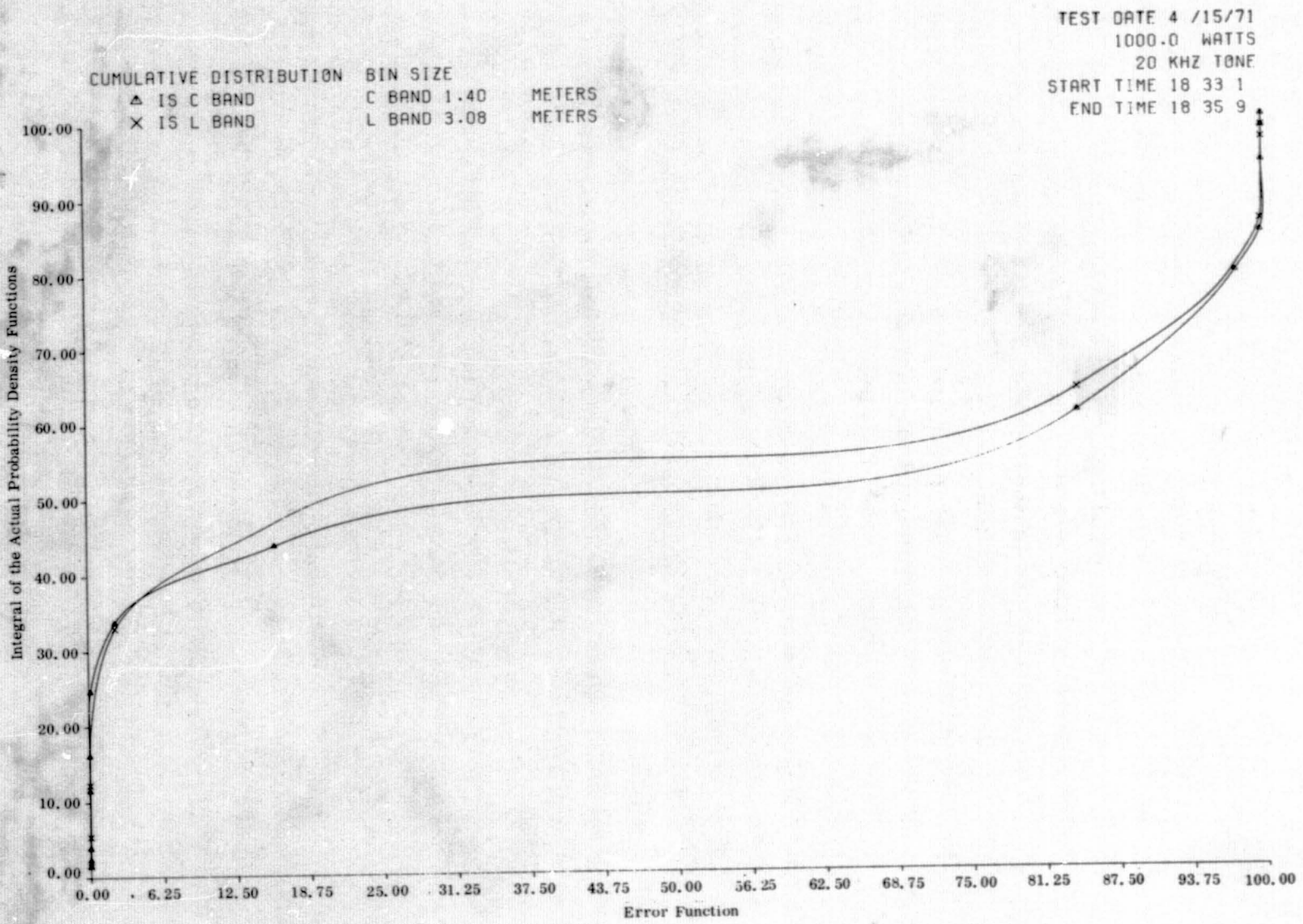

Figure 5.5 Cumulative Distributions of C-Band and L-Band Ranging Errors

while those shown in the table are:

$$\sigma_C = 3.97 \quad \text{meters}$$

and

$$\sigma_L = 8.72 \quad \text{meters}$$

This indicates that the computed correlation functions are correct.

Both the L and C-band error signals show periodic components, but the basic frequency of these components are on the order of 1/5 Hz. Further, the periodic component is less than 10% of the correlation spike, indicating that this 1/5 Hz periodic error signal must be at least 10 dB below the random errors in rms power. The 1/5 Hz frequency component in the L-band autocorrelation of the error has been identified as the 20-second time constant in the ranging demodulator. The periodic component in the C-band autocorrelation of the error is probably generated from the digital sampling rate of the ranging signal. The random nature of the errors causes small sidelobes to occur at the sampling rate, and the 10-dB figure is a measure of loss in error pattern correlation for L-band range signals.

The crosscorrelation function of figure 5.2 shows no peaks at levels in excess of those that would be generated by crosscorrelating two statistically independent data streams. This indicates that the errors during this 2-1/2 minute test interval were not caused by common ionospheric propagation anomalies or equipment problems common to both ranging systems. This also indicates that spin modulation was not a common error source for the L-band and C-band ranging measurements and that there were no unstable tones from the tone generator in the ATSR equipment.

The scatter plot of C-band range versus L-band range shown in figure 5.3 indicates good range tracking at both the L-band and C-band carrier frequencies. Using a best fit line, the range at L-band appears to be 140 meters longer than the range at C-band. The worst case peak-to-peak variability in range is approximately 40 meters, indicating that, except for the zero offset caused by the error in the "zero set" at calibration, the range signals should not vary more than $\pm$ 20 meters with respect to each other. Figure 5.4 is a graphical display of the range error probability density distributions for this test interval. The first significant observation is that at both L-band and C-band the errors are not "normally" distributed about the offsets. The C-band range errors have a major peak at class number 2 (2 x 1.4 = 3.8 meters), or 3.8 meters longer than the mean error. They also exhibit minor peaks at class

numbers +4 and -5, or range errors of 5.6 meters and -7 meters. Since a wavelength at 20 kHz is 15 kilometers, these subsidiary peaks are not caused by locking in the wrong phase (a 180° phase error is a 3.75 kilometer range error). There are either error sources which do not produce normally distributed errors, or a number of "normally" distributed sources, which contribute to the C-band ranging errors.

The L-band range error probability density distribution shows that the range errors ranging from -9.24 meters to +6.16 are equally probable. Beyond this error interval, the L-band error probability density is comparable to the C-band error density. With the limited data used in accumulating these density functions, it would appear that the error distributions at the two frequencies are the same except that the L-band error density function is approximately twice as wide as the C-band error density function. Even the sidelobes exhibited in figure 5.4 may be caused by truncating the data set.

The cumulative range error distributions shown in figure 5.5 verify the hypothesis that the actual error distributions are the same. However, the errors in the L-band range data are about twice the size of the C-band range errors. The distributions are very flat across the range between 25% of all errors and 75% of all errors, indicating that errors within these bounds are equally likely. The extremely sharp tails, above 90% and below 10% of all data, are certainly due to the limited sample set. Limiting the set to a finite number of points always causes these sharp tails, which are due to the extreme values in the sample set (maximum negative range error and maximum positive range error) for the test interval.

In summary an analysis of the statistical presentations for this test interval has revealed the following:

1) The L-band range data contained a random error component that has four times the power in the C-band error data.
2) There appears to be some intersymbol influence in the digitized L-band range data. This component was small, relative to random errors.
3) There are no observable propagation anomalies, at either frequency, that contribute to the range errors, during the test interval.
4) A periodic frequency component exists in the L-band ranging measurements due to the 20-second time constant of the range demodulator.

A periodic frequency component also exists in the C-band ranging measurements, which is probably due to the signal sampling rate of the ATSR system.

Satellite spin is not causing ranging errors at either the L-band or the C-band carrier frequencies.

5) Both L-band and C-band error distributions were similar, and show that there was more than one normally distributed error source in both. However, the L-band error peak covers an error range that was about three times as large as the error range for the C-band data.

6) Limited sampling distorted the cumulative probability distributions.

7) The range errors were not biased, other than an offset in the initial zero calibration, indicating that the "best fit" ranges were not biased.

8) The mean range to the spacecraft, as measured at L-band, was 140 meters longer than the C-band range to the spacecraft due to the previously mentioned zero set calibration error. This could easily be removed by the initial "zero set" calibration.

5.3.2 Example 2: A Case Where the L-Band C/N_o is Low at Both the Spacecraft and the Receiving Ground Terminal.

Figures 5.6 through 5.10 are plots derived from a ranging test run on 4/27/71, with 16 watts of L-band power transmitted from the earth station to the spacecraft. This is a condition where the C/N_o in the ranging receiver is low because the transmitted power from the earth station will not saturate the S/C transponder.

The autocorrelation function, figure 5.6, shows that the power in the error component of the L-band data is 50 times that in the C-band data, because the L-band ranging system is operating near its threshold. There are no significant sidelobes in this function, other than those caused by the sampling rate, so spin modulation is not introducing a periodic error. The random sidelobes in the L-band autocorrelation function of the range errors range data are significantly larger than they were in example 1 because of the increase in the random error power at L-band.

The crosscorrelation function of the C and L-band range error is essentially zero for all τ, figure 5.7. This shows that the L-band errors are not correlated with the C-band errors, thereby ruling out the possibility that some of the L-band errors are caused by propagation anomalies during this test interval.

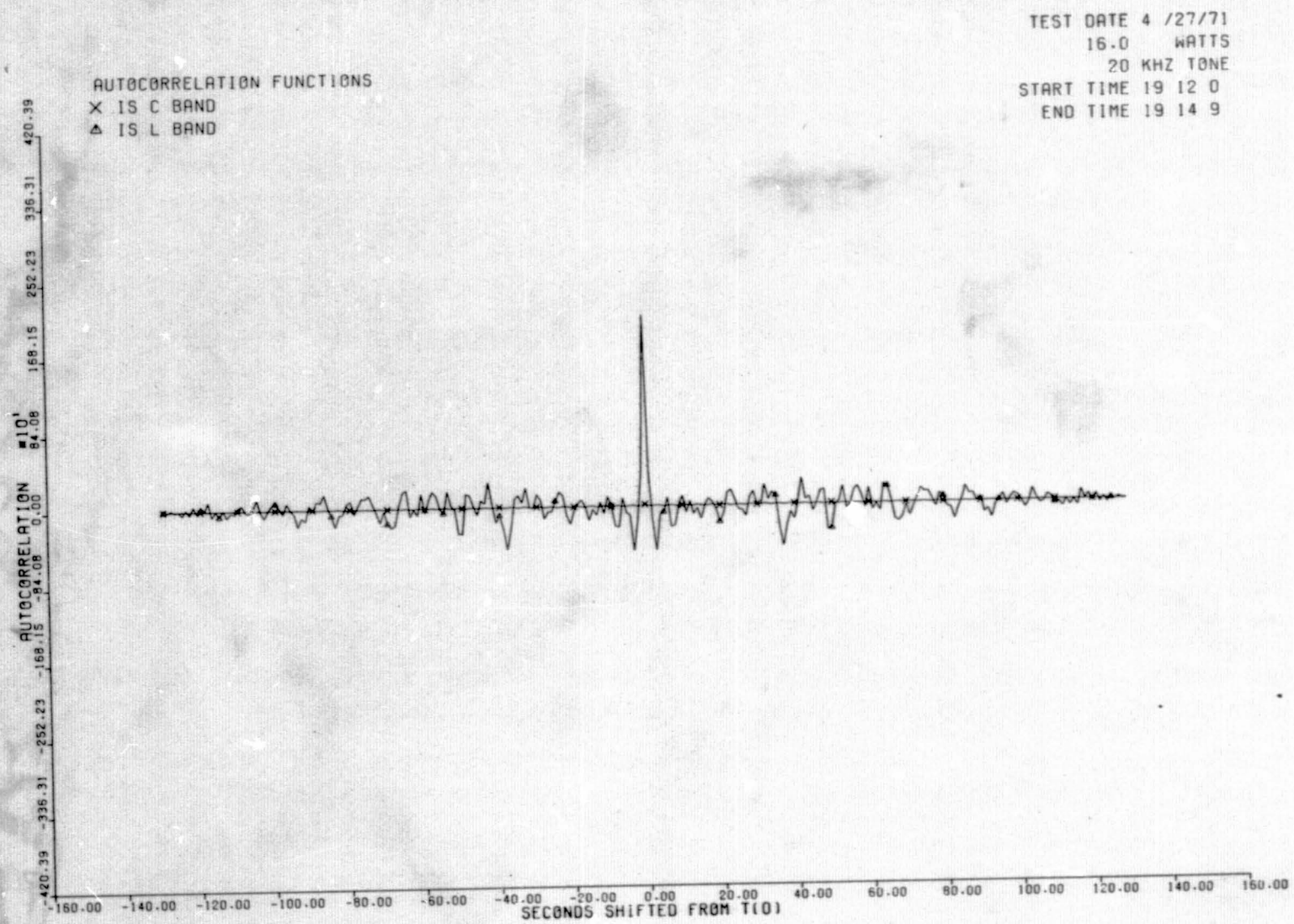

Figure 5.6 Autocorrelation Functions of C-Band and L-Band Ranging Errors (Example 2)

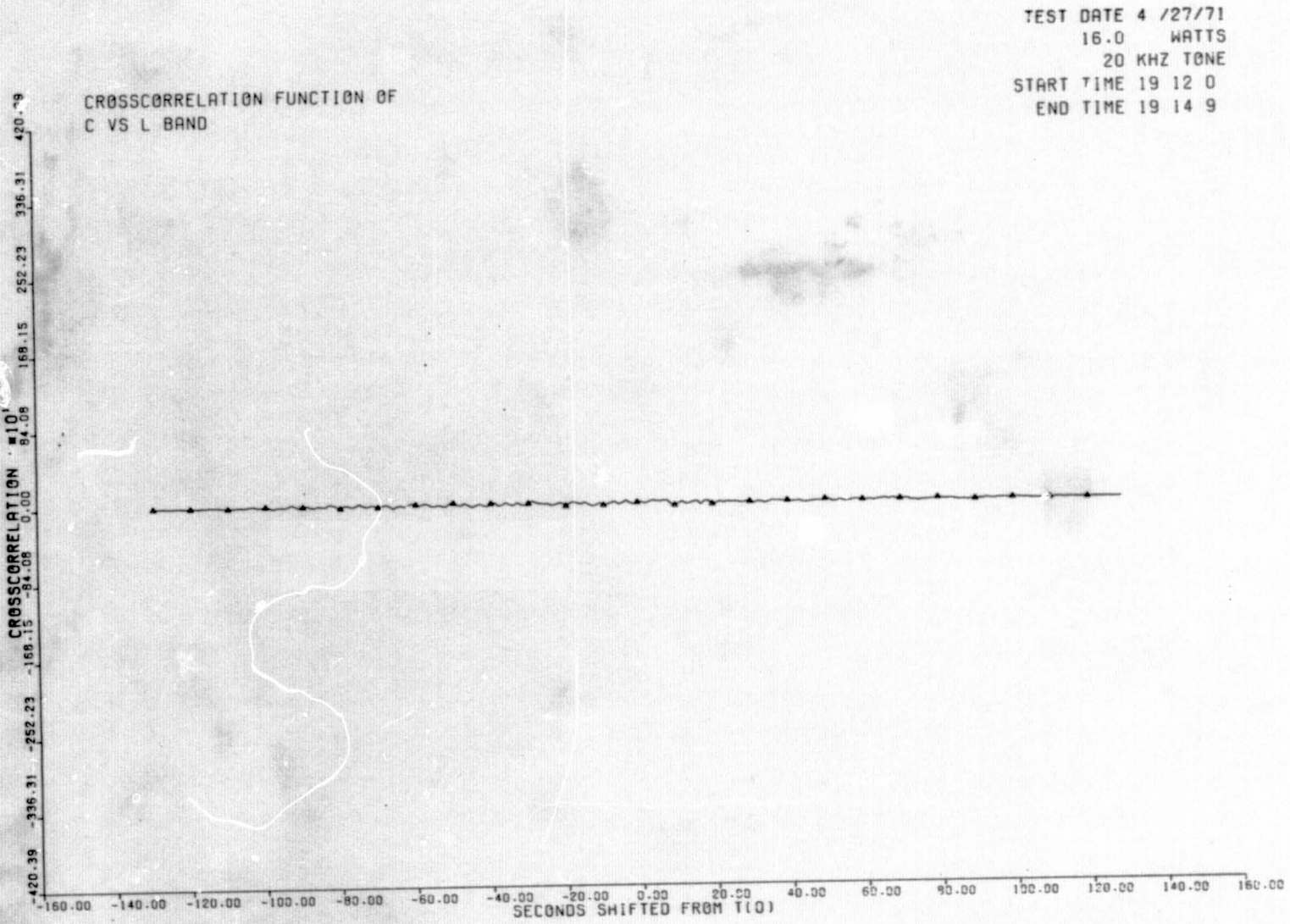

Figure 5.7 Crosscorrelation Function of C-Band With X-Band Ranging Errors (Example 2)

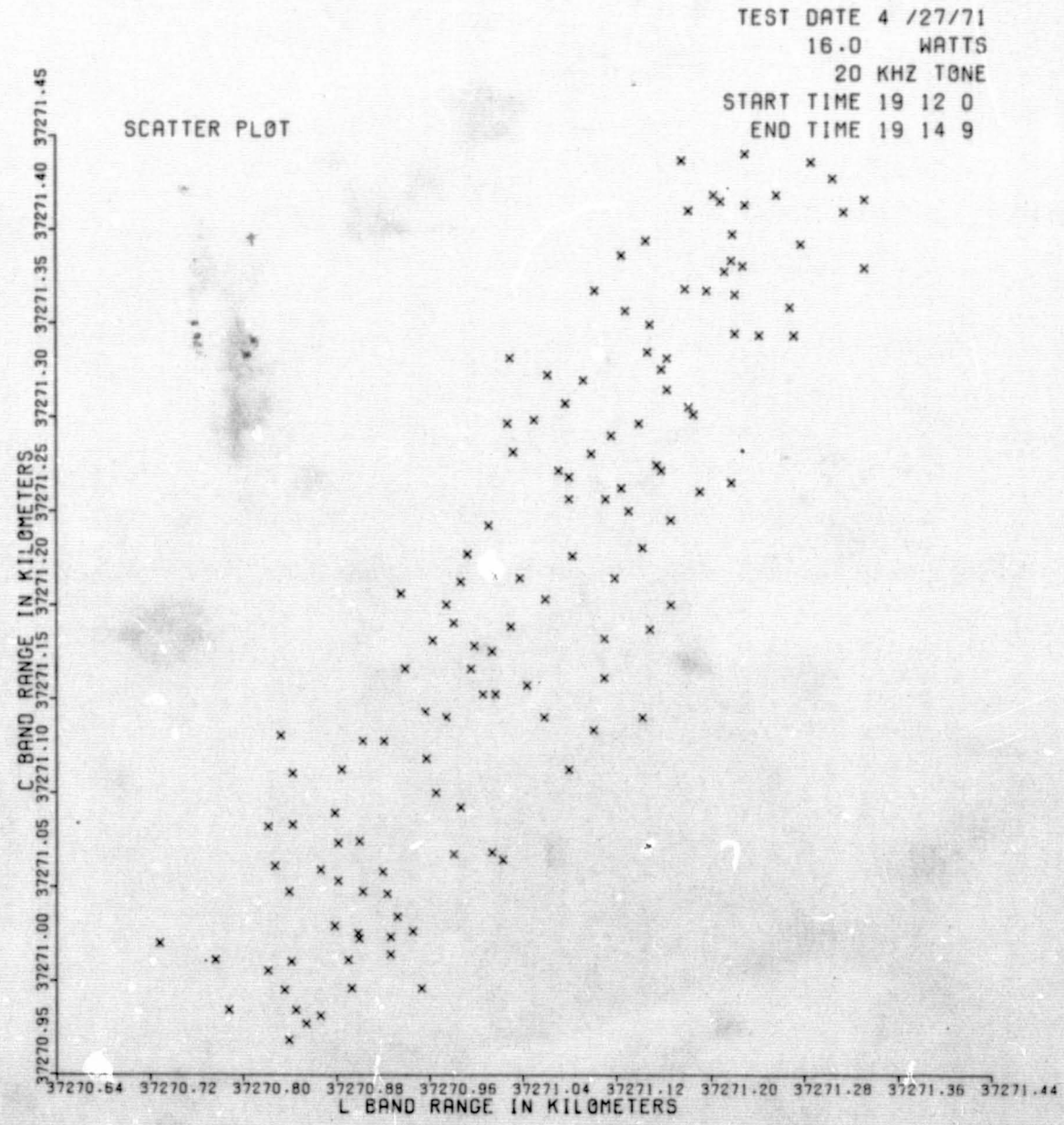

Figure 5.8 C-Band Range Versus L-Band Range (Example 2)

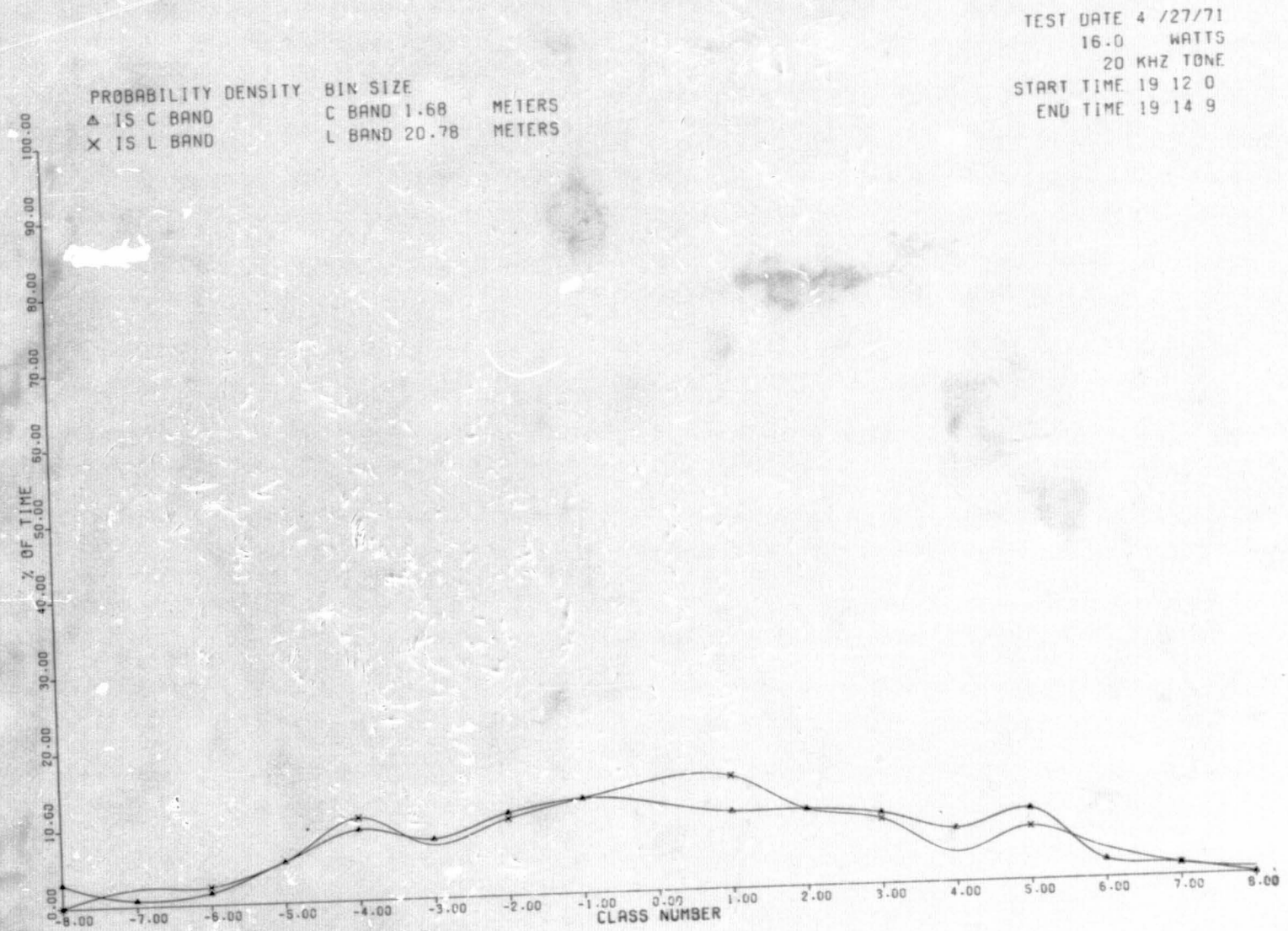

Figure 5.9 Probability Densities of C-Band and L-Band Ranging Errors (Example 2)

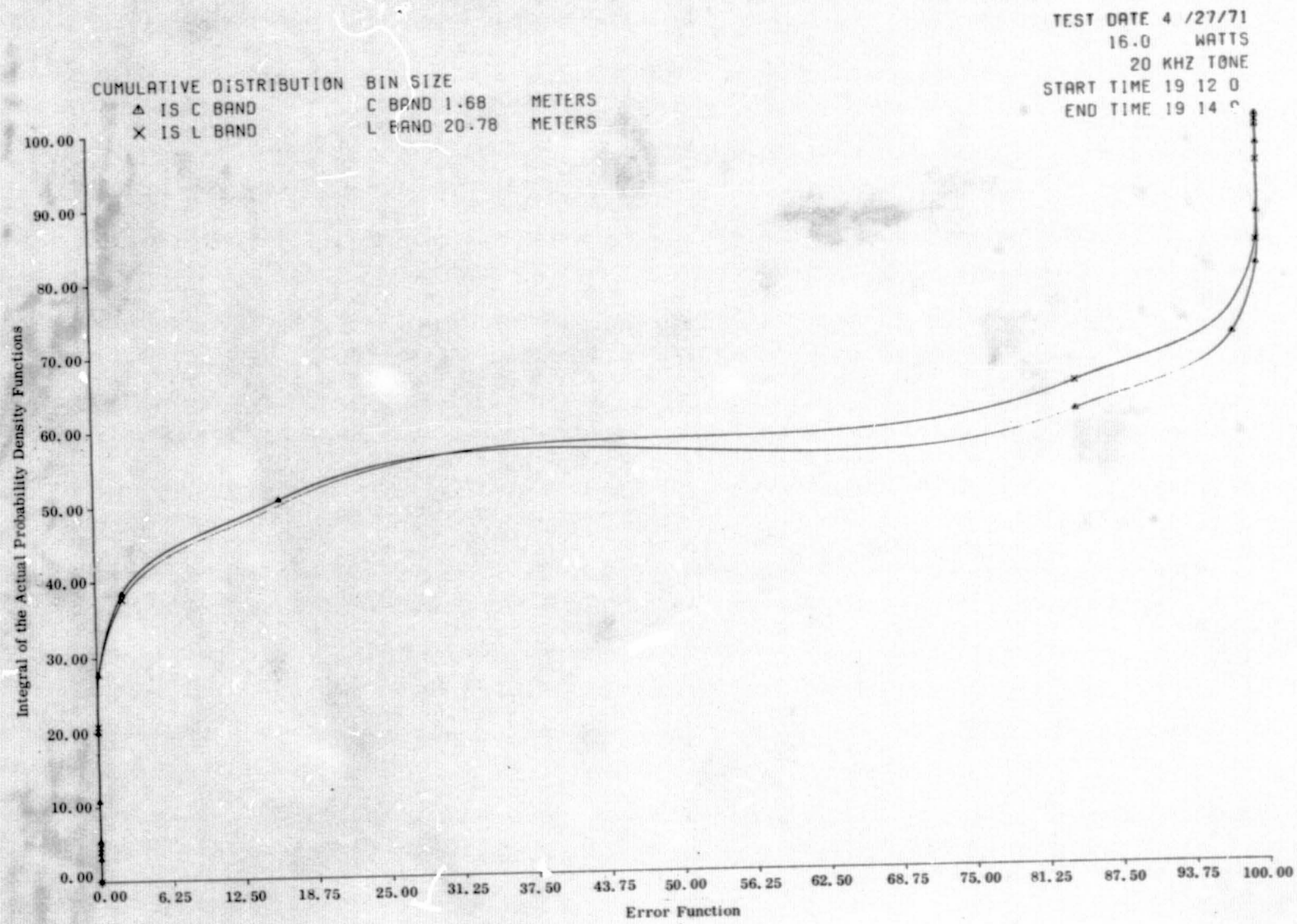

Figure 5.10 Cumulative Distributions of C-Band and L-Band Ranging Errors (Example 2)

The scatter plot, figure 5.8, illustrates how the spread of data about the best line increases as the received C/N_0 decreases. This is equivalent to saying that the correlation coefficient is less than it was in example 1, or the L-band range data is noiser than it was. Peak-to-peak variations of almost 200 meters can be seen in the range data, as compared with the peak-to-peak variations of 40 meters shown in example 1.

A best fit to the scatter plot shows an equipment related problem. The L-band range at low C/N_0 is approximately 130 meters less than the range at C-band, whereas it was 140 meters more at high C/N_0. This problem has been traced back to a defective analog shaping filter in the L-band ranging equipment and has been corrected.

The probability density curves, figure 5.9, show similar shapes for both the L-band and C-band errors. However, it must be remembered that a single bin represents a 20-meter range error at L-band, while it represents only 1.7 meters at C-band. If the L-band bin size were made 1.7 meters, then the density functions would show equally likely L-band errors over a range of ± 8 bins (± 12.5 meters), with peaks at the end of the density function for all L-band errors outside this range.

The peaks in bin numbers -4, 1, and 5 seem to be characteristic of all density functions, regardless of C/N_0. Conversely, if one made the C-band bin size 20 meters, which is equal to the plotted L-band bin size, all the C-band data would fall in bin 0. The C-band errors would then look normally distributed, with a variance much smaller than that for the L-band data.

This peaking in selected bins indicates that, in data processing, there is a preferred error bin, probably because of how the data processing program was written. If one compares example 1 with example 2, the error density curves are similar, despite the change in scale from three meters/bin to 20 meters/bin from figure 5.4 to figure 5.9.

As would be expected, the cumulative error distribution (figure 5.10) at the two frequencies are similar, and they are similar to the distribution shown in figure 5.5 for example 1. However, in this case, the flat area in the middle of the distribution spans an L-band error range which is at least three times larger than that shown in example 1. The tails are due to limited sampling, while the curvatures at 30% and 80% may be caused by multimechanism error sources. The fact that there is more than one error mechanism and that errors near the mean range are not normally distributed, are shown in figure 5.9.

The principle conclusions of this analysis are:

1) Range bias reverses polarity as the signal to noise decreases, and the L-band range becomes shorter than the C-band range to the S/C. The cause of this was a defective active baseband filter in the demodulation channel of the L-band ranging receiver.
2) Processing techniques appeared to be generating peaks in the error density function which were independent of the bin width.
3) At 16 watts transmitted power, L-band range errors from -40 to +50 meters were nearly equally probable.
4) There were no observable range errors caused by the spinning of ATS-5, pulse lock, or propagation anomalies.

5.3.3 Example 3: Mode 1 Operation, Where the 20 kHz Range Tone in the L-Band Equipment is Not Coherently Related to the Range Tone in the ATSR C-Band Equipment.

During Mode 1 operation the L-band ranging tone is not readily available from the ATSR equipment, because the ATSR range tone frequency is 500 kHz and the L-band range tone frequency is 20 kHz. The run of 4/21/71, with 64 watts transmitted to the S/C at L-band is typical of such a situation, and will be analyzed to determine the effect of using non-coherent tone sources.

Before beginning the actual analysis, certain general effects should be expected. They are as follows:

1) If the L-band range tone frequency is stable at 20 kHz +0.1 Hz, and it is phased properly during setup, the range offset should increase by 0.5 part in 10^5, or about 160 meters.
2) If the L-band phase tracking system is locked 180^o out of phase with a 20 kHz tone derived from the ATSR equipment, the L-band range offset will change by about 3.75 Km. This is an error of $\lambda/4$ for the 20 kHz tone.
3) For the same C/N_o, the error noise power will be the same as that measured during Mode 5 operation if the tracking tone generator is stable. If it is not stable, the error noise power will be larger than that measured in Mode 5 operation.

4) An actual frequency offset of the L-band tone source from 20 kHz will cause a periodic component in the L-band error auto-correlation function. A phase offset will not cause periodic components in the L-band error autocorrelation function.

5) For the case of drifting phase, the error density function should be flat over the drift range or show peaks at the maximum excursion.

Reference is made to the range error autocorrelation function, figure 5.11, and table 4.2. The large spike at $\tau = 0$ in the L-band data is due to a sum squared error power which is four times as large as that observed during Mode 5 operation at the same C/N_o (See Table 4.1, for April 22, 1971). At this noise level, any possible intersample influence is masked by the random error components in the range signal and the periodic components introduced by the tone source providing the L-band modulation. The larger spike at $\tau = 0$, and the larger standard deviation shown in table 4.2, both indicate that random phase modulation of the external tone generator is causing half of the ranging error. The distinctive periodic component in the error autocorrelation function shows that the random phase modulation of the source is, partially, caused by a periodic component in the phase errors of the tone generator. These periodic components can probably be attributed to phase modulation of the tone generator and the 20-second time constant in the L-band ranging demodulator.

The crosscorrelation is essentially zero on the ordinate scale used in figure 5.12. This shows that, to the resolution offered in this figure, error sources are not correlated. The potential sources of correlated errors between the two ranging systems are propagation anomalies and the spinning of ATS-5. Figure 5.12 shows that neither propagation anomalies nor the spinning of ATS-5 is a significant contributor to the L-band ranging errors.

The scatter plot, figure 5.13 is similar to the one shown in figure 5.3 for example 1, except for the range offset (range bias error) and the slight scatter of points about the best fit line caused by the lower C/N_o. Peak-to-peak errors are on the order of 100 meters, as compared with the peak-to-peak errors of 40 meters shown in example 1. Further, the zero offset is such that the best fit C-band range is 3,700 meters longer than the best fit L-band range. In normal operation, the C-band range is 140 meters less than the L-band range. This would indicate that either the L-band range tone is 180^0 out of phase from nominal zero or that

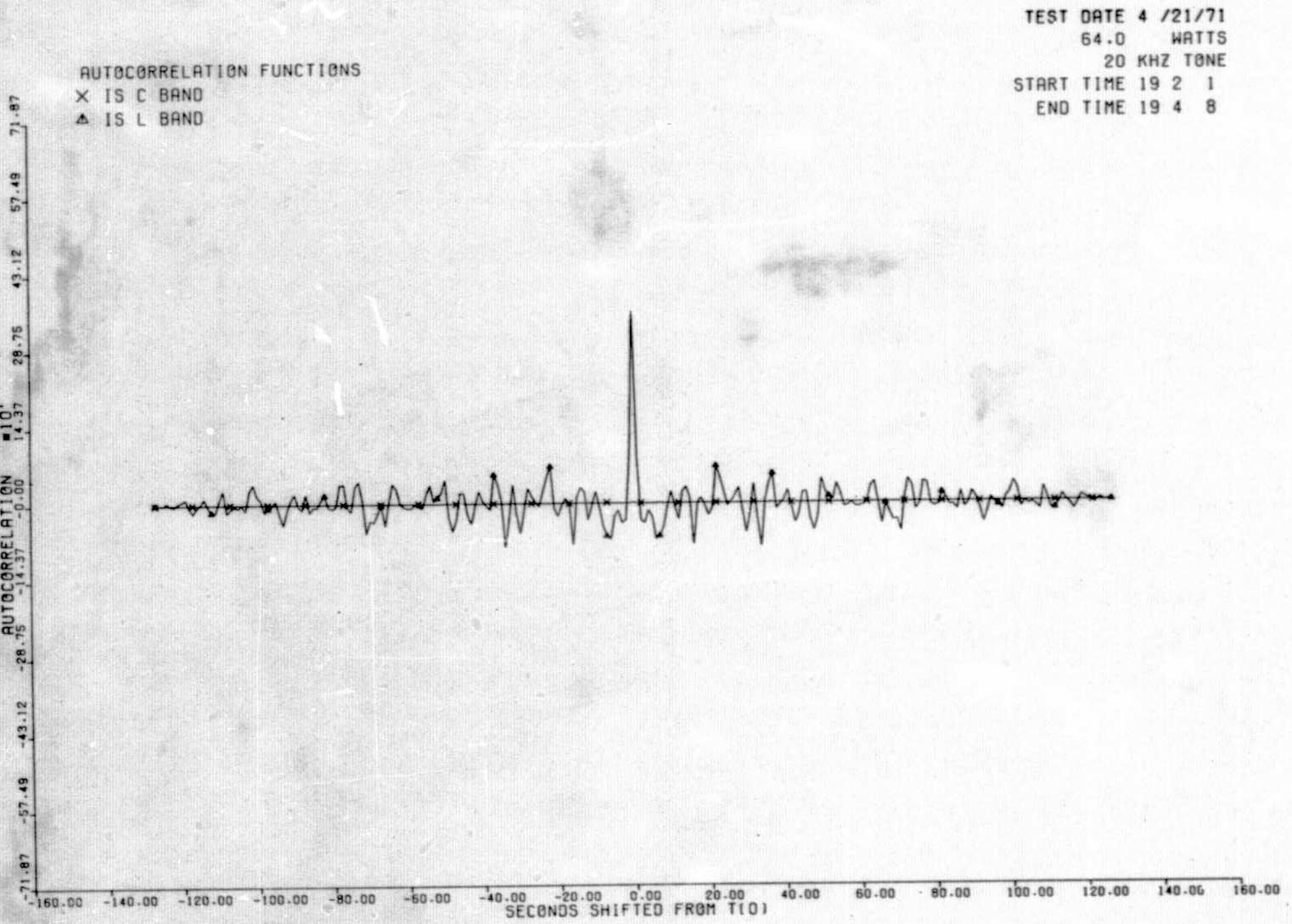

Figure 5.11 Autocorrelation Functions of C-Band and L-Band Ranging Errors (Example 3)

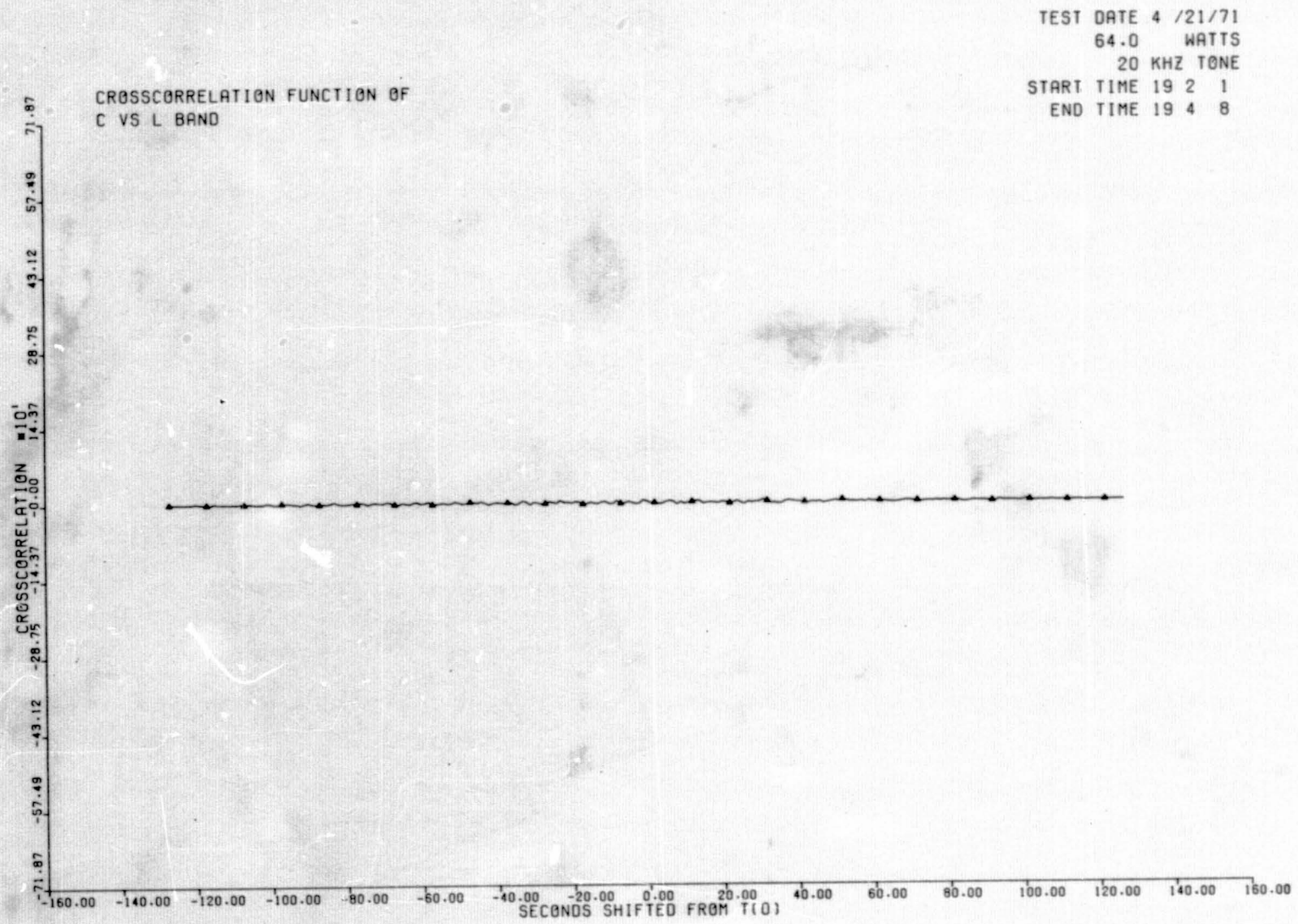

Figure 5.12 Crosscorrelation Functions of C-Band and L-Band Ranging Errors (Example 3)

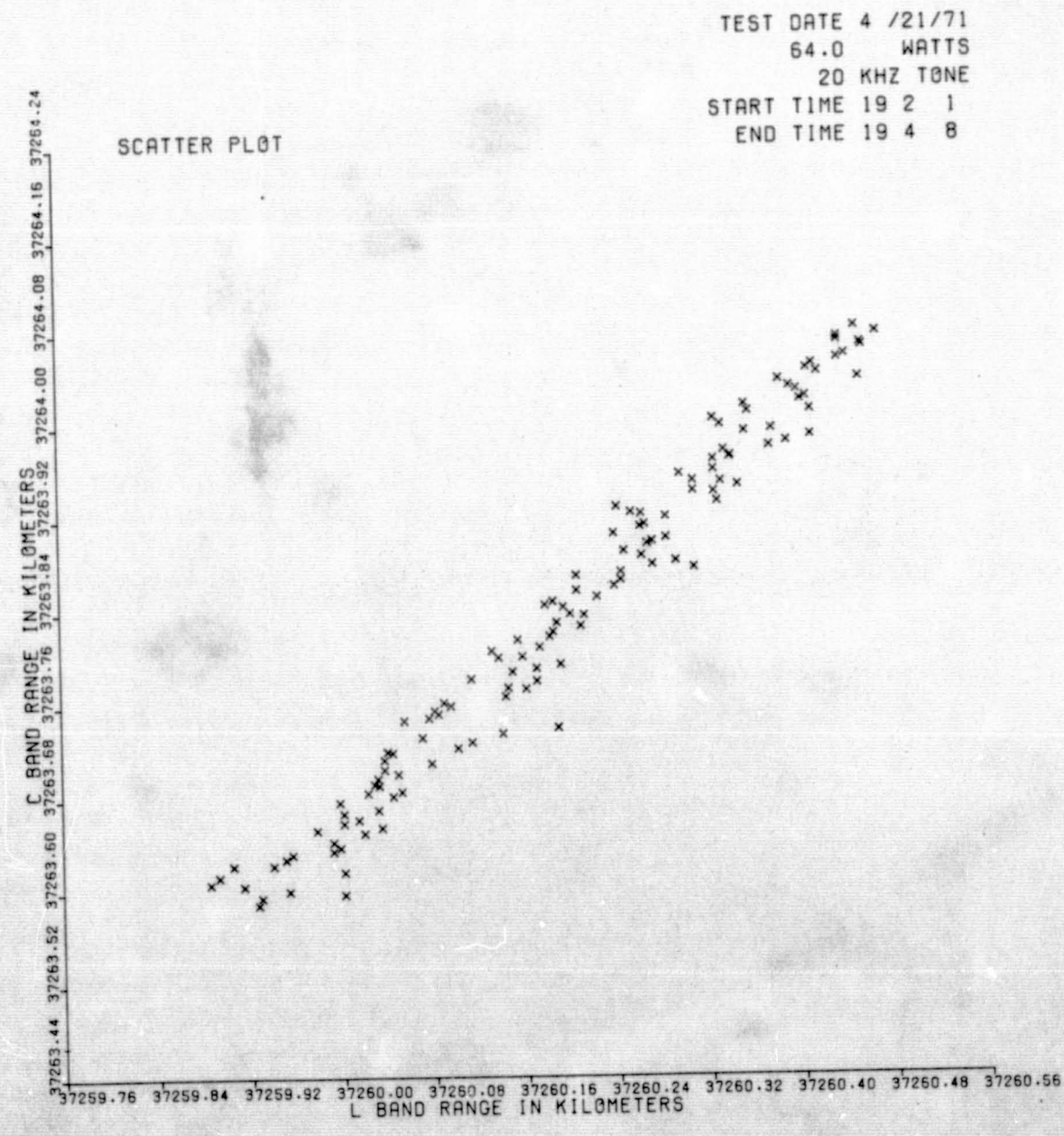

Figure 5.13 C-Band Range Versus L-Band Range (Example 3)

the processing equipment has generated a false set of lanes. If it is a phase offset problem, then it is associated with the zero set procedures used during equipment alignment. At any rate the externally generated tone can be said to have more noise power than the ATSR range tone, and it is stable to better than 1 part in 10^5 in phase during a run. The frequency stability of the ATSR system was 2.7 parts in 10^7.

The error density functions and the cumulative error distributions, figures 5.14 and 5.15, have the same shapes as those shown in figures 5.4 and 5.5 for example 1. Note that the density curves are plotted on different scales, an L-band error bin, or [illegible]s, being 12 times as wide as a C-band error bin. The densities within bins -8 and +8 are so close to those for example 1 that it is suspected that the error densities shown in figures 5.4 and 5.14 are caused, to some extent by the data processing programs.

5.4 CONCLUSION CONCERNING STATISTICS OF RANGING ERRORS

By way of three illustrative examples, it has been demonstrated how various statistical information concerning range errors has been obtained. These statistics are, of course, for specific time intervals and say nothing about "all time intervals." Except for the physical phenomenon of signal multipath (which was not within the scope of this experimental effort), various signal levels, signal to noise conditions, and system configurations were created and range errors resulting from these conditions statistically analyzed on a short term basis.

Under best L-band signal conditions it was found that the average rms range error precision was approximately $\pm$ 20 meters. The theoretical signal to noise ratio for a time jitter of 131.2 nanoseconds corresponding to the $\pm$ 20 meter range error is 34.8 dB for the 20 kHz ranging tone and agrees well with the design resolution capability of the L-band ranging equipment. The magnitude of the auto correlation function at $\tau = 0$ indicated that the rms range error was 8.7 meters for L-band measurements. This would indicate a better than average signal to noise ratio for maximum power conditions. This variation in S/N ratio is attributed to slight antenna pointing errors.

Of the specific time intervals examined, no evidence was found of ranging errors caused by propagation anomalies common to the C-band, L-band, or VHF carrier frequencies.

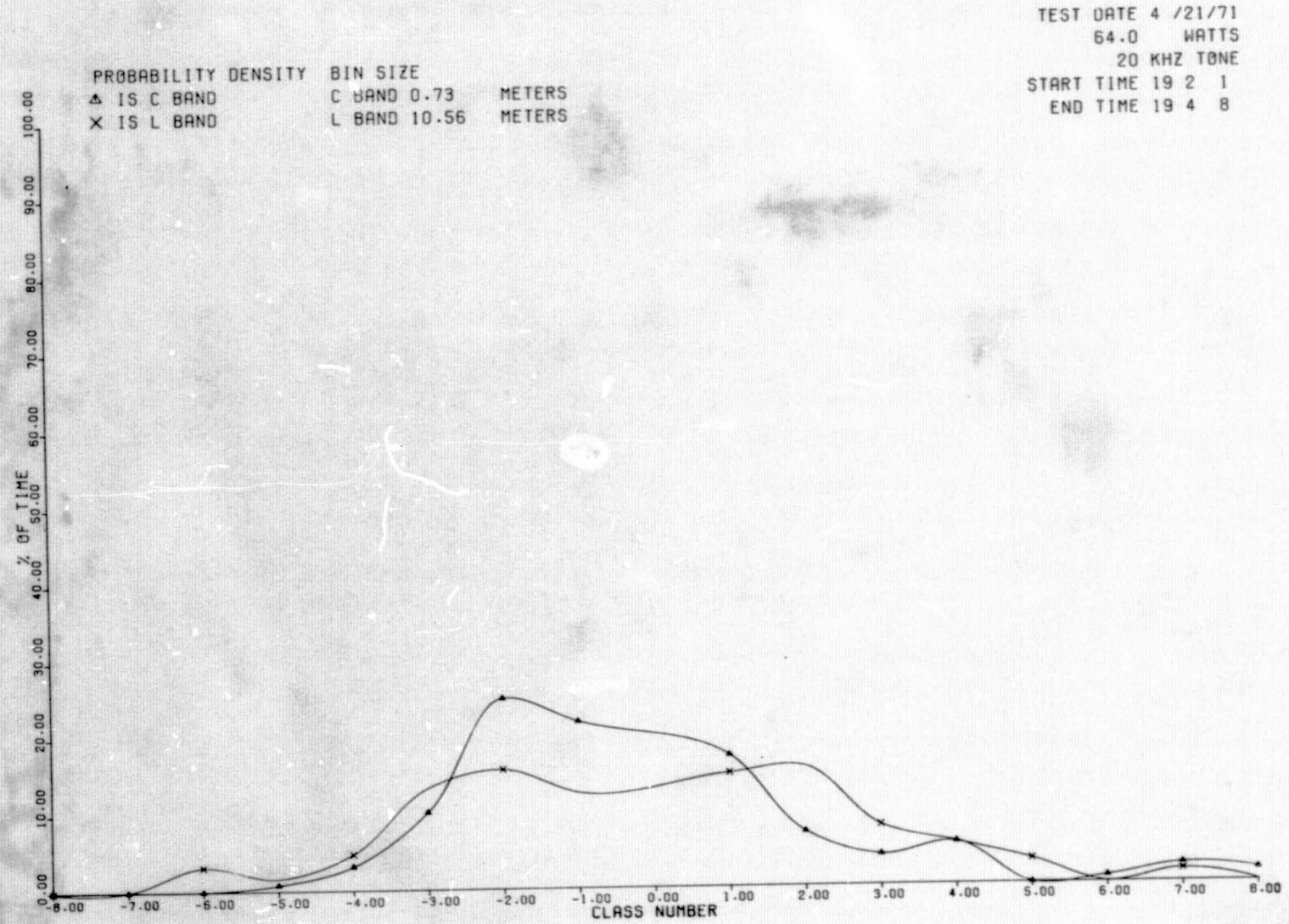

Figure 5.14 Probability Densities of C-Band and L-Band Ranging Errors (Example 3)

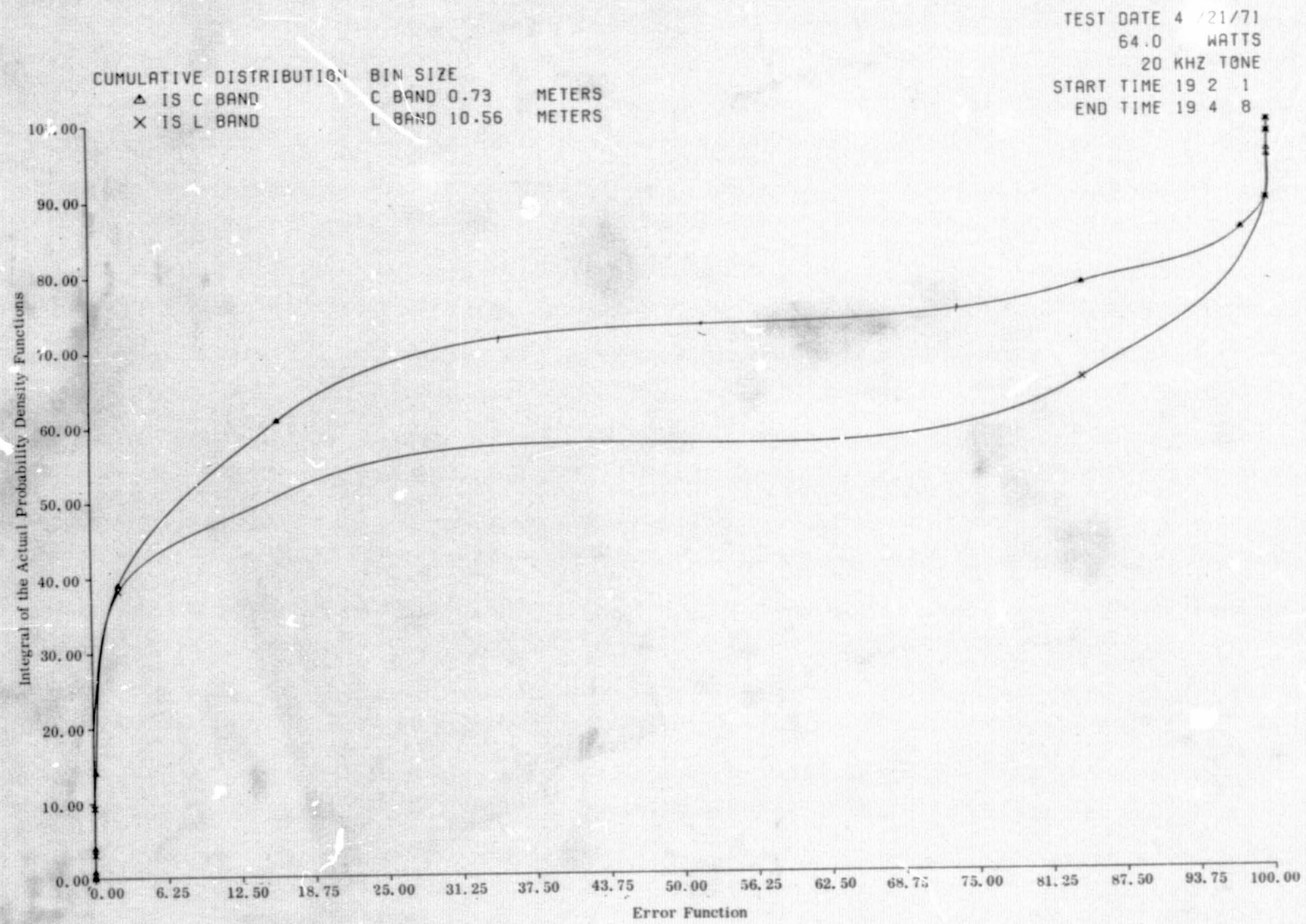

Figure 5.15 Cumulative Distribution of C-Band and L-Band Ranging Errors (Example 3)

SECTION 6

MOJAVE GROUND STATION ANTENNA LAYOUT

The antennas at the Mojave ground station are physically separated from each other by a distance that can make an appreciable error in the simultaneous ranging measurements. This section is an analysis of the station antenna layouts and the path geometry for this series of experiments.

Figure 6.1 is a layout drawing of the Mojave ground station showing the positions of the various antennas used in this experiment with respect to each other and to the operations building. The exact locations of the three antennas are listed in the table of this figure. The fourth entry in the table is the location of the Mojave station used in the Goddard orbit determination program. That position is given in the determination program as 116.888° longitude and 35.332° latitude - geodetic (35.150° latitude is used here while the corresponding geocentric latitude must be used in the position location experiment). The coordinates listed in the table were used to locate the points for the antennas in the station layout and to calculate the distances represented by the dotted lines shown in this figure. At this latitude, one second of latitude is 30.865 meters and one second of longitude is 25.237 meters. The distance between the C-band antenna and the L-band antenna is 139 meters and between the C-band antenna and the VHF antenna is 136 meters. The ephemeris station location shows the center of this station to be 25 meters east and 40 meters north of the VHF antenna.

6.1 SIMULTANEOUS RANGING

6.1.1 L-Band and C-Band to ATS-5

The station layout depicted in figure 6.2 shows the condition for simultaneous ranging with L-band and C-band to the ATS-5 satellite. The ATS Satellite Acquisition Tables for Mojave state the ATS-5 azimuth as being approximately 160° and the elevation as 47.5° from Mojave. These are the pointing angles for the two antennas. The two arrowed lines in the upper layout labeled "to ATS-5" are the plan view of the radiation paths at 160° azimuth from each antenna. Since the satellite is at such a distance, these lines can be considered parallel. If a perpendicular line (dotted line in the figure) is drawn from the C-band antenna point to the L-band radiation line, the distance (x) from this intercept to the L-band antenna is calculated

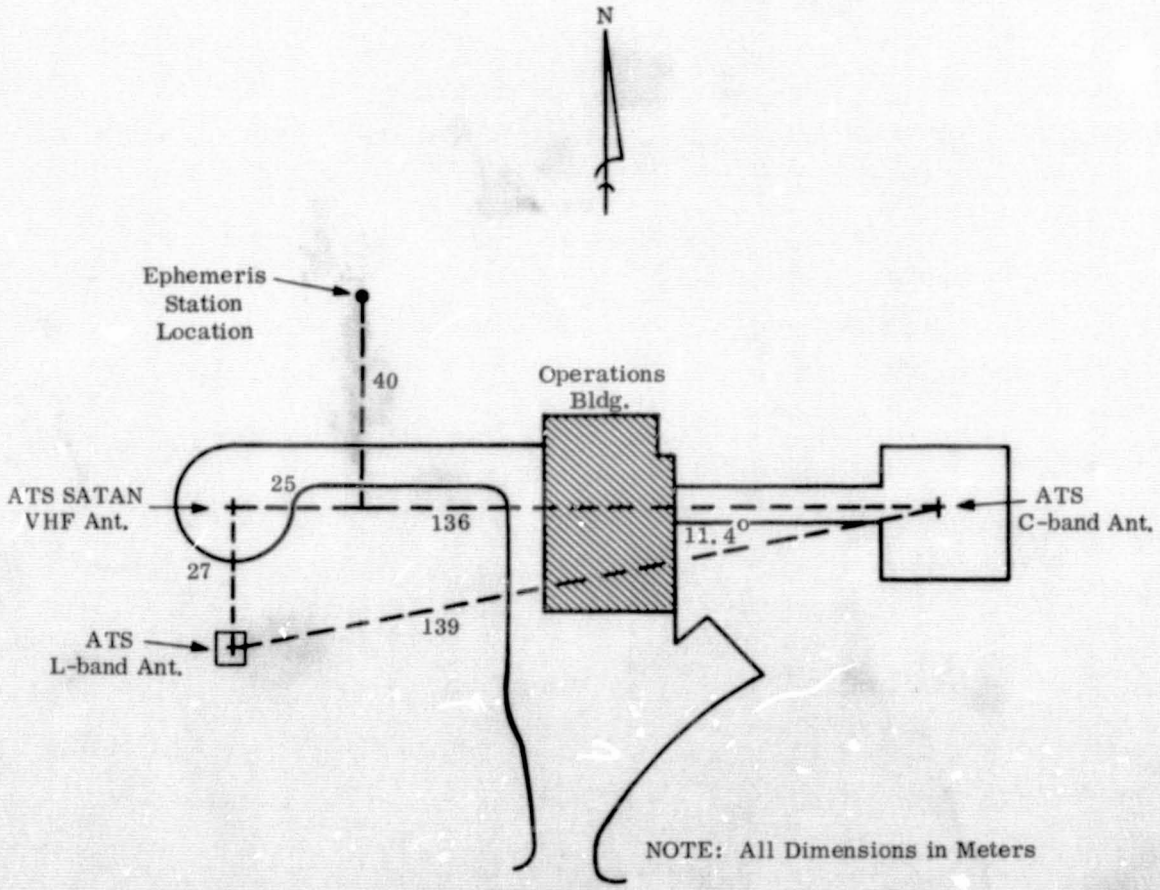

MOJAVE ANTENNA LOCATIONS

L-band Antenna	35° 19' 53.083"	116° 53' 17.613"
C-band Antenna	35° 19' 53.973"	116° 53' 12.243"
VHF Antenna	35° 19' 53.973"	116° 53' 17.612"
Ephemeris Station Center	35.332° 35° 19' 55.200"	116.888° 116° 53' 16.800"

At Mojave: 1 second of latitude = 30.865 Meters
1 second of longitude = 25.237 Meters

Figure 6.1 Mojave Ground Station Antenna Layout

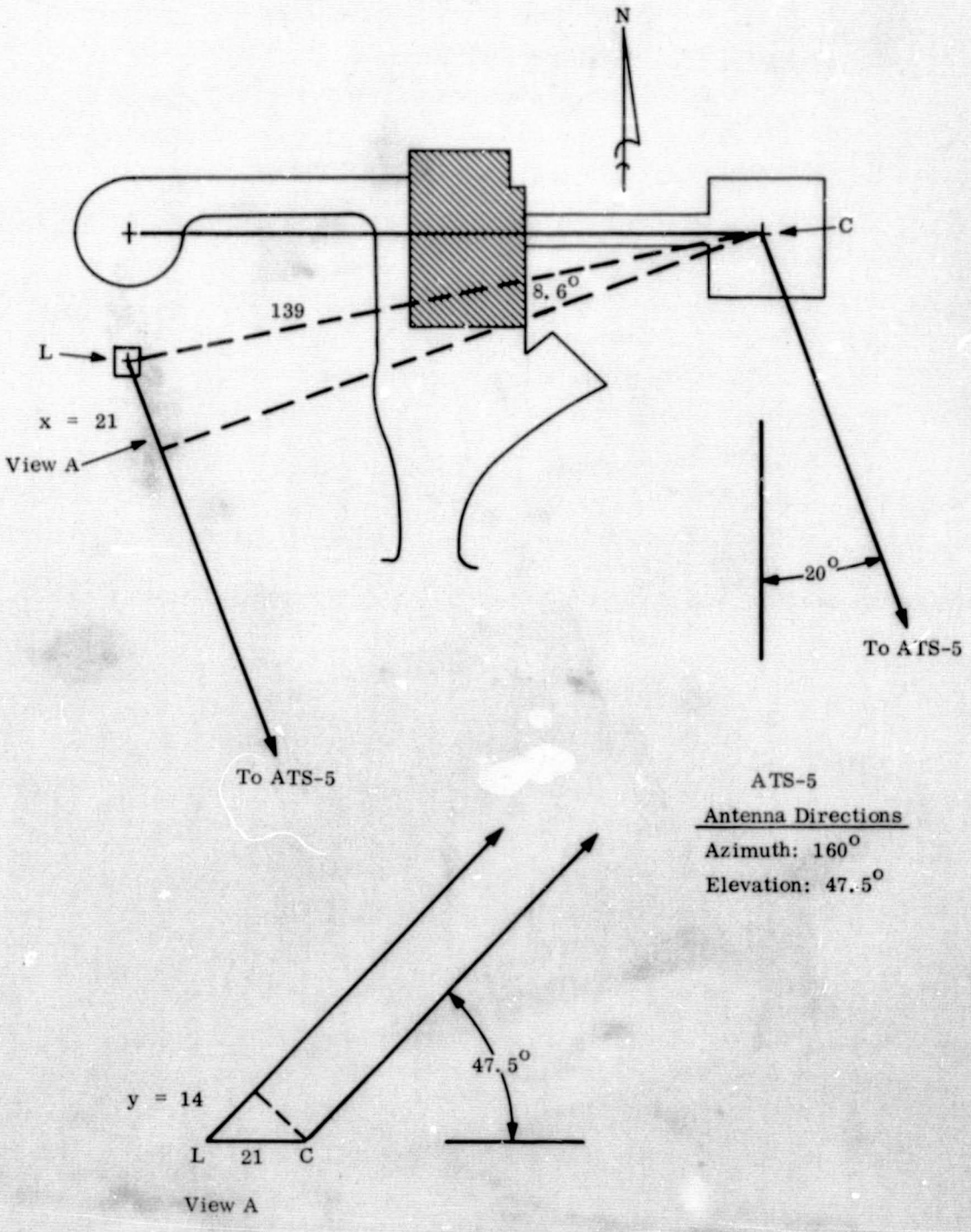

Figure 6.2 Simultaneous L-Band and C-Band Ranging to ATS-5

to be 21 meters. This means that on the ground the L-band antenna is 21 meters further away from the satellite than C-band antenna. The lower figure labeled "View A," is a side view of the radiation paths at the plane labeled "View A" in the upper figure. This shows the antenna elevation angles of 47.5° to the ATS-5 satellite and the distance of 21 meters is along the ground. If a perpendicular line is drawn from the C-band antenna to the L-band radiation line, the distance (y) from this intercept to the L-band antenna is 14 meters. From this location and path geometry, it is seen that the range to the ATS-5 satellite is 14 meters longer from the L-band antenna than it is from the C-band antenna.

6.1.2 C-Band and VHF to ATS-1

Figure 6.3 is a station layout for the simultaneous ranging to the ATS-1 satellite with C-band and VHF. In this figure the antenna pointing angles are approximately 227.5° in azimuth and 36.7° in elevation. Again, the two arrowed lines in the upper figure are the radiation paths at an azimuth of 227.5° toward the antenna. The C-band antenna for this layout is calculated to have an x distance of 100 meters along the ground beyond the VHF antenna. The side view (View A) showing the antenna elevation angles of 36.7° calculates the y distance to be 80 meters. Therefore, from this path geometry it is seen that the VHF range to the ATS-1 satellite will be 80 meters shorter than the C-band range to this satellite.

6.1.3 C-Band and VHF to ATS-3

The antenna layout for the simultaneous C-band and VHF ranging to the ATS-3 satellite is shown in figure 6.4. The antenna pointing angles are approximately 117° in azimuth and 27.2° in elevation. Similarly, from this path geometry the VHF antenna is shown to have an x distance behind the C-band antenna of 120 meters along the ground and a y distance of 107 meters. The VHF ranging to the ATS-3 satellite, therefore, will be 107 meters longer than the C-band ranging.

6.2 POSITION LOCATION

6.2.1 C-Band and L-Band Ranging

In the position location experiment, the data reduction computer program located, for each satellite, the precise point in space that was described by the ephemeris data obtained from the Goddard orbit determination program. This point was then used as the center of a sphere with the measured range data as the radius. The intersection of this sphere along the earth describes a circle. Assuming that the two measured rangings are precise the circle will pass back through the antenna location points.

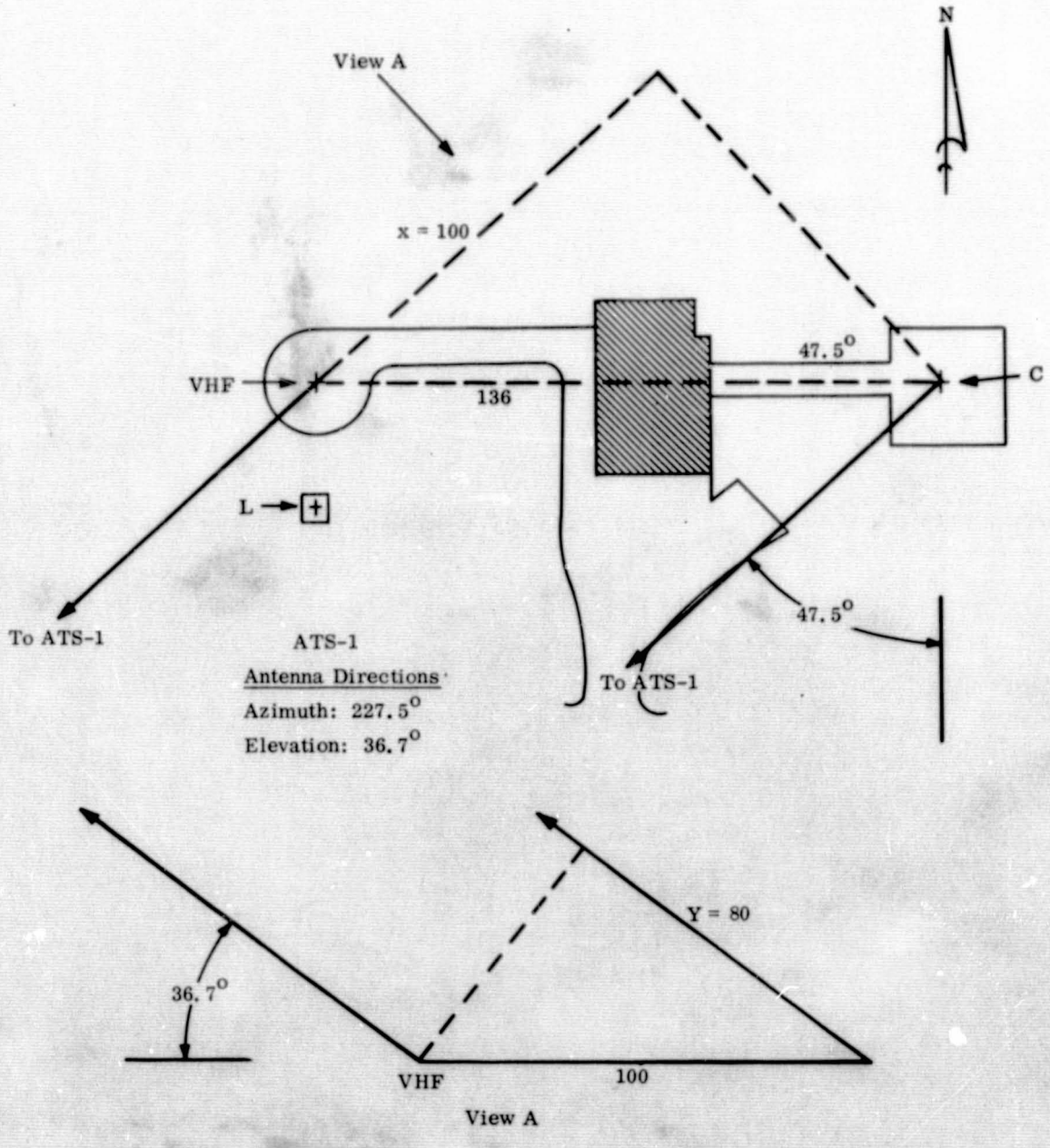

Figure 6.3 Simultaneous C-Band and VHF Ranging to ATS-1

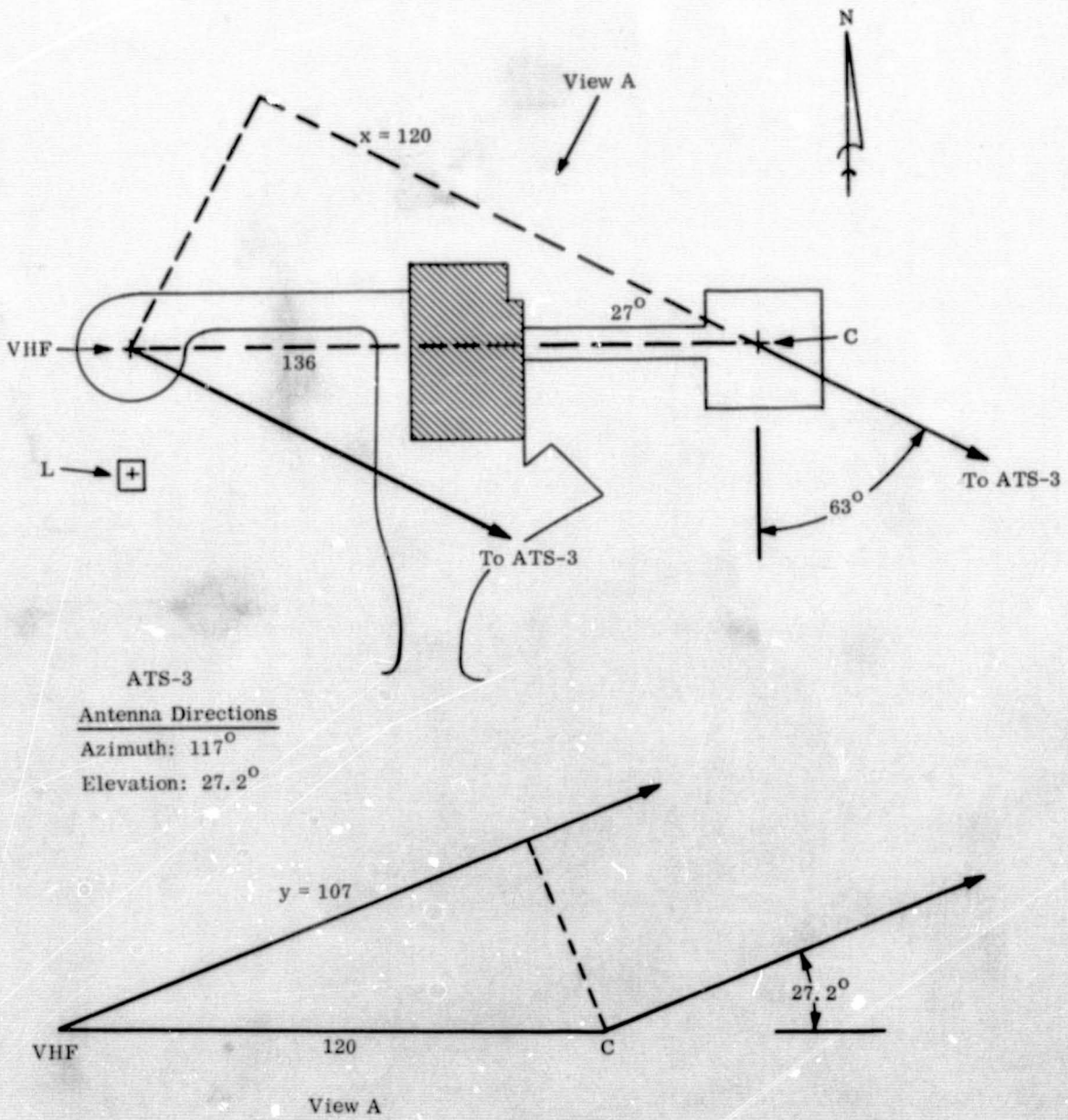

Figure 6.4 Simultaneous C-Band and VHF Ranging to ATS-3

The layout in figure 6.5 depicts the L-band antenna radiating in the direction of ATS-5 and the C-band antenna radiating toward ATS-1. Each dotted line represents a portion of an arc which would be drawn using the satellite as the circle center. Since the radius is extremely large, this arc is essentially a straight line perpendicular to the direction of radiation. As stated before, these lines assume that the two rangings are precise, causing the circle to pass through the antenna location. The intersection of these two arcs will be the "position location" obtained from these two rangings. If the measured ranging is shorter than the corresponding ephemeris data, the radius will not reach the antenna point, thus causing the arc to be drawn in front of the antenna. Conversely, if the measured ranging is longer, then the radius overshoots the antenna point, causing the arc to be drawn beyond the antenna. The ephemeris station location as shown in this layout plan is used as the target point in the position location data reduction program. This target point is shown to be 100 meters from the ranging intersect points in this figure.

6.2.2 C-Band and VHF Ranging

The position location diagram for the condition where the C-band system ranges to ATS-1 and the VHF system ranges to ATS-3 is shown in figure 6.6. This figure shows that the two arcs from the rangings intersect considerably north of the ground station. The distance from the target to this intersect is 60 meters to the northeast.

Figure 6.7 reverses the conditions, showing the C-band system ranges to ATS-3 and the VHF system ranges to ATS-1. This time the two arcs from these rangings cross south of the station. This point is 151 meters southeast of the ephemeris target location.

These examples are presented not to determine a position correction value but to illustrate that minor built-in errors will exist in the position location data reduction program due to factors such as the antenna separation, the "shifted" ephemeris station target location, or the cyclic nature of the ephemeris data. They must all be considered in the analysis of position location data.

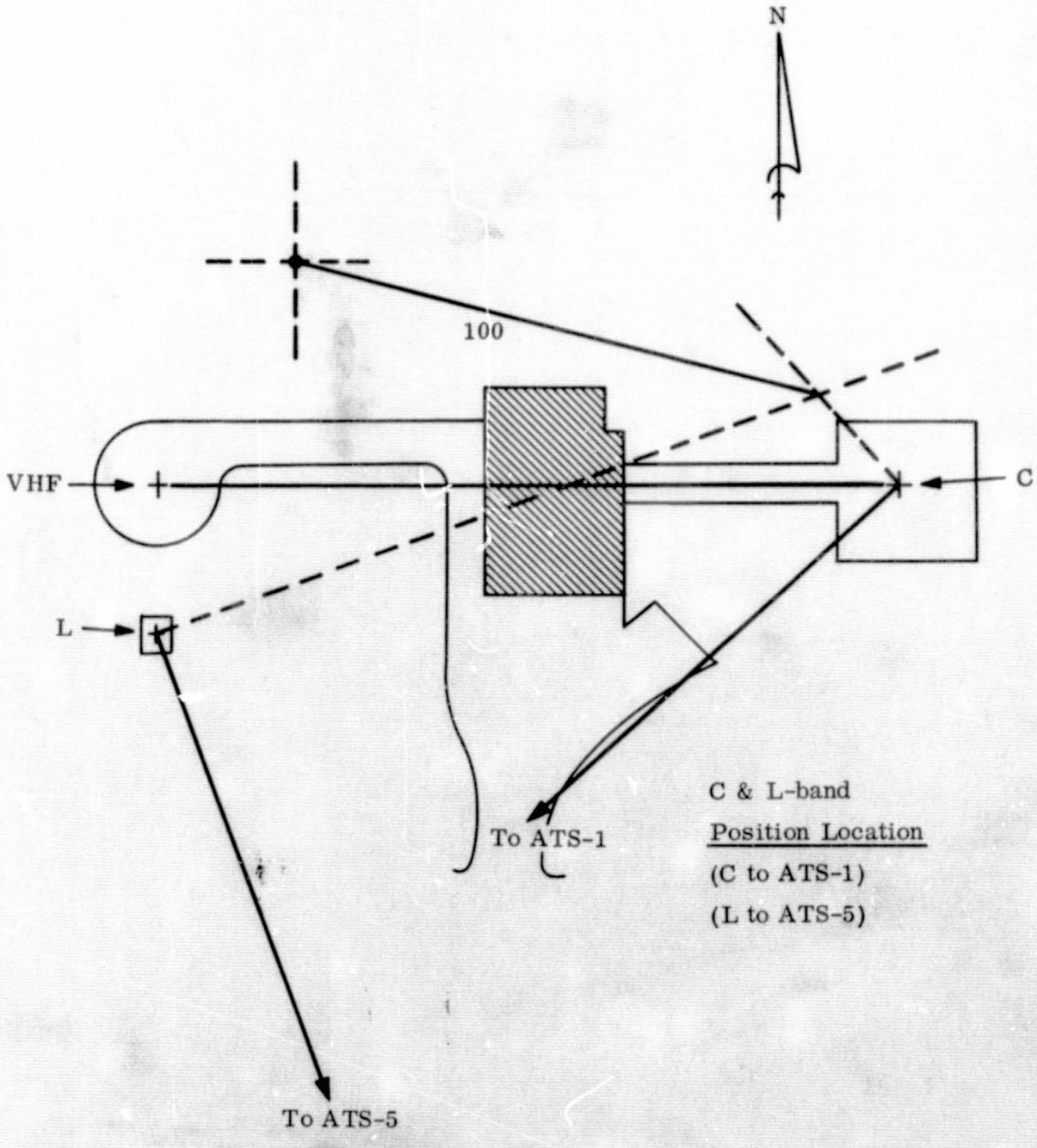

Figure 6.5 Position Location: C-Band to ATS-1 and L-Band to ATS-5

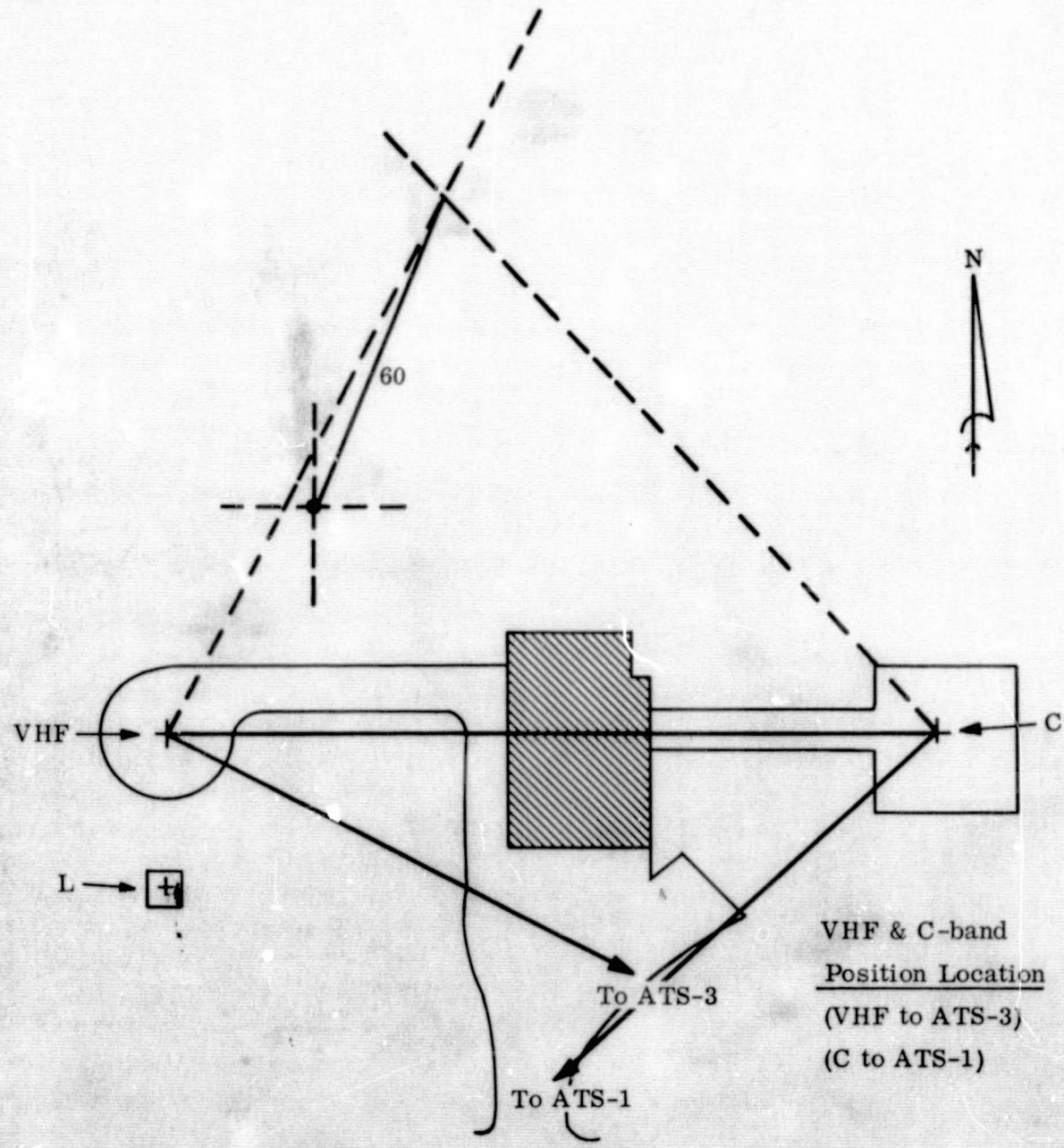

Figure 6.6 Position Location: C-Band to ATS-1 and VHF to ATS-3

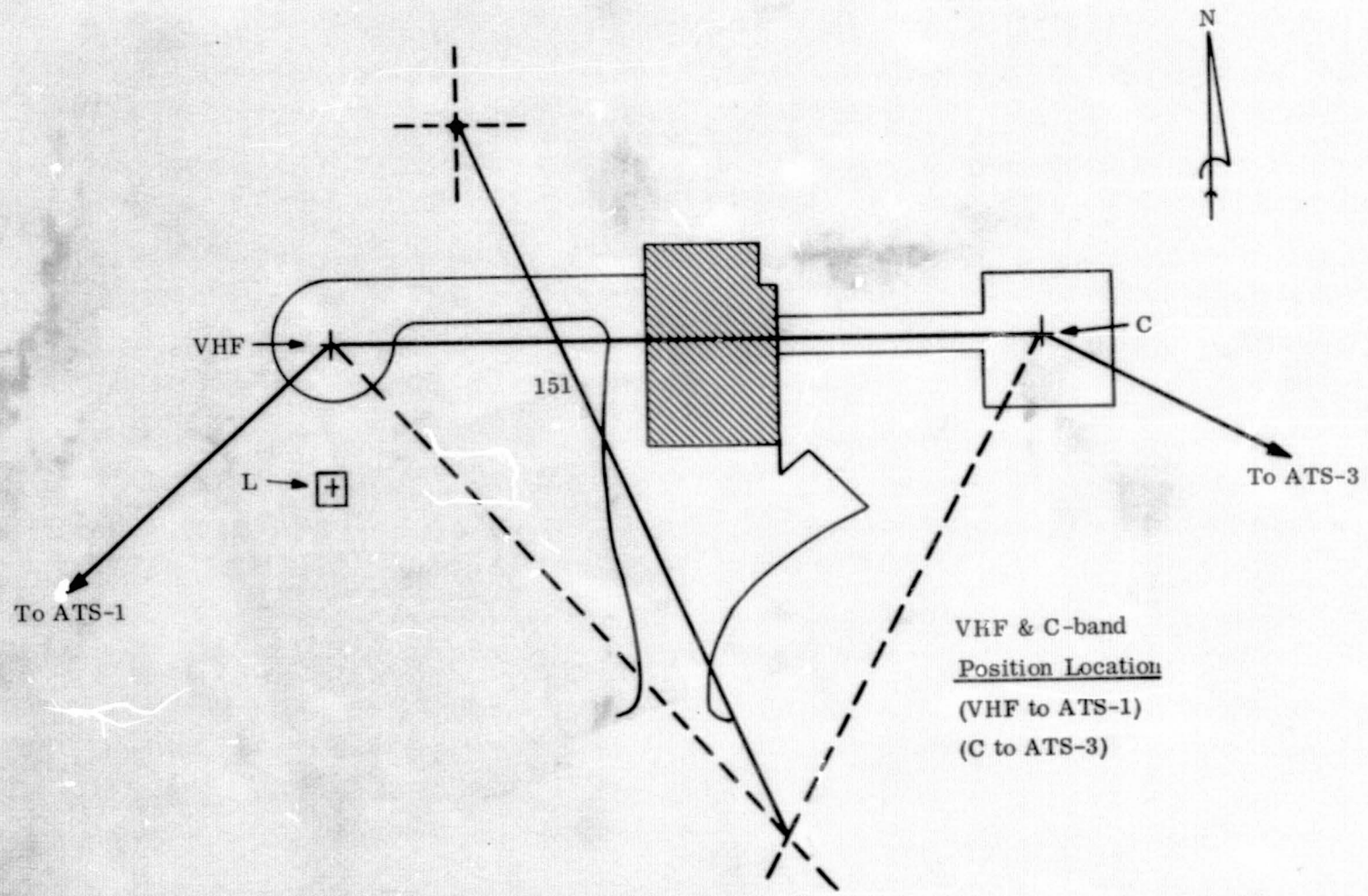

Figure 6.7 Position Location: C-Band to ATS-3 and VHF to ATS-1

GLOSSARY

Ambiguity - An ambiguity exists in the C-band range measurement to a synchronous satellite because the round trip range to the satellite exceeds the wavelength of the lowest tone used in measuring this range. Since the range measurement is actually accomplished by making a phase comparison on the returned tone, it is not possible for the ranging equipment to determine which cycle of the returned tone is being compared. Consequently, since the actual round trip range to the spacecraft exceeds the wavelength of the 8 hertz tone (125,000 microseconds) in the ATSR equipment, an ambiguity exists. To resolve this, the knowledge that the round trip range to a synchronous satellite is in the order of 250,000 usec must be used. A typical ATSR range measurement is 123,030 usec. It is therefore obvious that the range measurement lies in the second 8 hertz lane; and that 125,000 usec, corresponding to one 8 hertz wavelength, must be added to the measured range, giving 248,030 usec as the actual range.

An ambiguity exists in the L-band range measurement which is similar to the C-band ambiguity, except that the range tone frequency is either 4 or 20 kHz, corresponding to an ambiguity lane width of 250 usec and 50 usec respectively. To resolve the L-band ambiguity it is necessary to use either the C-band range or the ephemeris range to determine the number of ambiguous lanes.

S/N - Signal-to-Noise Ratio

S/C - Spacecraft

C/N_o - Carrier-to-Noise Ratio per Unit of Bandwidth

Mercury Geoid - This is a particular model for the shape of the earth, giving the radius of the earth as a function of latitude. This information is required for station position location by means of ranging to two satellites.